

THE UNIVERSITY OF NOTTINGHAM

**DEPARTMENT OF ELECTRICAL AND
ELECTRONIC ENGINEERING**



**Synchronisation of vascular ultrasonic scans
with heart activity using ECG signals**

By

Omer Faruk Bener, BEng

Thesis submitted to the University of Nottingham for the
degree of Master of Philosophy

November 2010

SUPERVISOR

Dr. Alexander Kalashnikov

CO-SUPERVISOR

Dr. Barrie Hayes-Gill

Abstract

Diagnosis, monitoring and curing of various vascular abnormalities can be linked to measurements of wall thicknesses of blood vessels. However, use of echo ultrasonic signals for these measurement is complicated by the low level of reflections from the vessels (1-2% from the incident energy), which results in considerable noise. Since the changes in thickness to be monitored are very small, this requires operation of ultrasonic scanners at high sampling frequencies, much higher than 50–100 MHz sampling frequencies that are used by contemporary ultrasonic scanners. That is because the resolution of the measured thickness is dependent on the time domain resolution of the recorded echoes; the latter is determined by the sampling frequency. An additional issue is the variability in the blood vessel wall thickness depending on the phase of the heart activity. Several studies show that these variations with a cycle time of around one second result in the same changes as building atherosclerosis for one year.

The objective of the study was to develop an instrument that would allow recording of ultrasonic A-scans that are synchronised with the heart activity and that would allow improved accuracy of wall thickness measurements. Using an electronics point of view, the objective was met by the simulation, construction, programming and testing of an ECG monitor that triggers ultrasonic scans. The FPGA design of an existing high accuracy ultrasonic A-mode scanner was modified to allow interfacing of this monitor. Ultrasonic scans were taken with different transducers and transducer attachments (“shoes”) using various settings of the scanner. The scans were then analysed using dedicated Matlab programs.

Overall, the design proved to be successful – it allowed repeatable records to be obtained at the same stage of heart activity. However, reliable and unambiguous detection of the artery walls (especially the back wall) was achieved only sporadically within the time available for in vivo experiments.

Acknowledgements

I would first like to thank my supervisor Dr. Alexander Kalashnikov for his guidance and invaluable contribution throughout this entire research project, not only for making this work possible, but also for his support in my life, like a friend, whenever I needed it. I would also like to thank my co-supervisor, Dr. Barrie Hayes-Gill, for his guidance and support throughout the whole scope of the project.

I would like to also thank to all my colleagues in the UDSP group who were helpful in my work in different ways throughout the time. I am especially grateful to Dr. Vladimir Ivchenko who has helped me in the development of the FPGA software at the initial steps. I would like to also thank all the technicians on the 9th floor, who have always provided me help for finding right components and also gave me advice on some ideas I had on different parts of the project.

I would also like to thank Valerie Pinfield for arranging those UDSP group meetings, where useful discussions took place on everyone's projects. I am also thankful for Prof. Richard Challis for his advice. I would like to thank all my friends who have been there for me and who helped me to believe in myself for achieving my goals. Finally, I would like to thank my family for the things they have sacrificed for me, as well as for all their support and belief they have given me. I would also like to thank my sisters for the love and kindness they have given me all the years.

Table of Contents

<u>Contents</u>	<u>Page</u>
1) <u>Introduction</u>	8
1.1) Ultrasonic Medical Imaging.....	8
1.2) Vascular Medicine and atherosclerosis.....	16
1.3) Using the ECG signal for medical imaging.....	30
1.4) Proposed Solution.....	37
1.5) Why wireless?.....	42
1.6) References.....	43
2) <u>Prototyping the ECG monitor</u>	56
2.1) Introduction.....	56
2.2) Instrumental Amplifiers.....	57
2.2.1) AD624.....	57
2.2.2) AD620.....	58
2.2.3) INA326.....	59
2.2.4) INA118.....	60
2.2.5) AD623.....	60
2.3) Which amplifier to choose?.....	61
2.4) Simulation of the amplifiers.....	62
2.5) Prototyping of the instrumental amplifiers.....	63
2.6) Testing of the amplifiers on a veroboard.....	65
2.6.1) Potential divider for testing the amplifiers in sinusoidal mode.....	65

2.6.2) Supply Voltage Source.....	65
2.6.3) AD624 testing.....	68
2.6.4) AD620.....	69
2.6.5) INA326.....	71
2.6.6) ECG pads.....	73
2.6.7) Connecting the ECG electrodes to the ECG monitor.....	74
2.6.8) Filters.....	75
2.7) Digital Filter.....	78
2.8) Power Supply.....	81
2.9) Selection of a microcontroller capable of RF communications..	83
2.10) Voltage Reference.....	84
2.11) References.....	85
3) <u>Development of the PCB for the ECG monitor with RF</u>	
<u>communication</u>	89
3.1) Introduction.....	89
3.2) Schematic of the front end of the system.....	89
3.2.1) Instrumental Amplifier.....	90
3.2.2) Input connectors.....	91
3.2.3) Active Low Pass Filter.....	92
3.2.4) Power Supply.....	93
3.2.5) Reference Voltage.....	94
3.2.6) rfPIC.....	95
3.2.7) Test Points.....	96
3.3) Final Schematic.....	96
3.4) Printed Circuit Board of the front end.....	96

3.5) References.....	98
4) <u>Programming, prototyping and testing the ECG monitor on a veroboard</u>.....	99
4.1) Changes to the development plan.....	99
4.2) The veroboard featuring the rfPIC development module.....	99
4.2.1) ICD header.....	100
4.2.2) RS-232.....	100
4.2.3) 5V powered RS232 transceiver.....	100
4.2.4) Board connectors.....	101
4.2.5) Regulators.....	101
4.3) Testing of the development veroboard.....	102
4.4) Programming the microcontroller.....	103
4.4.1) Main Program (wrap.asm).....	103
4.4.2) Initialisation Program (init.asm).....	106
4.4.3) Subroutines (subr.asm).....	108
4.4.4) Interrupt Service Routine (isr.asm).....	109
4.5) Testing the program with the rfPIC microcontroller.....	112
4.6) Development of a PIC16F688 veroboard module	115
4.7) Testing the PIC16F688 module.....	117
4.8) References.....	120
5) <u>Operation of the ultrasonic instrument and its modification for external triggering</u>.....	122
5.1) Operating the ultrasonic instrument.....	122
5.2) Changes to the design of the ultrasonic instrument.....	129

5.3) Testing the ultrasonic instrument with the external trigger mode...	136
5.4) References.....	137
6) <u>In vivo experiments</u>	138
6.1) Locating the CCA.....	138
6.2) Setting the analogue front end.....	139
6.3) Taking ultrasonic Scans.....	141
6.4) Designing a new buffer for the 20MHz transducer.....	154
6.5) Scanning the CCA with the new buffer.....	157
6.6) Considerations on use of Automated Gain Control (AGC) to improve clarity of ultrasonic scans.....	158
6.7) Taking the ECG triggered ultrasonic scans in vivo.....	160
6.8) Cardiovascular Disease Risk Assessment Protocol.....	164
6.8.1) Questionnaire.....	166
6.8.2) Ultrasonic Scan.....	166
6.8.3) Data Reporting.....	167
6.8.4) Interpretation.....	168
6.8.5) Recommendations.....	168
6.9) References.....	169
7) <u>Discussion and Conclusions</u>	173
8) <u>Future Work</u>	177

9) <u>Appendix</u>	178
9.1) Questionnaire form enquiring about ECG.....	178
9.2) Schematic of the 4 TH order Bessel 20Hz Low Pass Filter.....	180
9.3) Schematic of the 4 TH order Bessel 40Hz Low Pass Filter.....	181
9.4) Schematic of the front end that will be used for PCB.....	182
9.5) Error Rule Check Report for the front end schematic.....	183
9.6) Schematic of the front end that will be used for veroboard....	184
9.7) Glossary.....	185

Chapter 1 - Introduction

1.1 Ultrasonic medical imaging

Ultrasound is an imaging technique that uses high pitched inaudible sound frequencies. These frequencies are generated and transmitted to obtain reflections from a structure in order to give an internal view of it. Many different applications today use ultrasound, ranging from industrial to chemical and medical uses. The approximate frequency ranges corresponding to ultrasound, and the applications related to the frequencies being used are shown in fig 1.1:

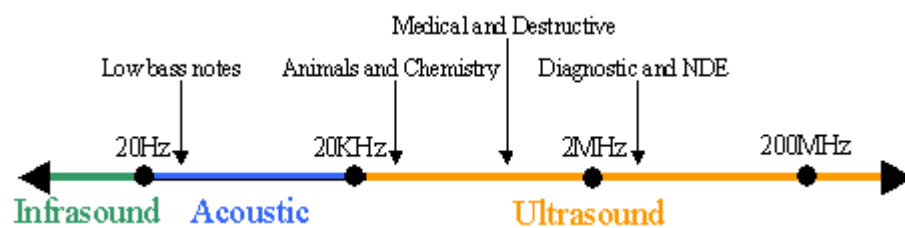


Figure 1.1: Diagram showing the applications of various ultrasound frequencies [1.1]

The non-destructive evaluation (NDE) is used to find flaws in order to assess the quality of a component during the manufacturing process, or to service an operational object to find if there are any cracks due to intense use. These types of tests are common in various industrial companies. The frequencies used for these applications typically range from 2 to 10 MHz, but lower frequencies are also used to examine less dense materials such wood and concrete. In contrast, medical ultrasonic applications usually use frequencies ranging from 2 to 20 MHz, where the operating frequency would depend on the body part being diagnosed. The most common applications of

medical sonography are related to obstetrics. However, medical sonography is used in many other medical departments such as Cardiology, Endocrinology, Gastroenterology, Gynaecology, Ophthalmology, Urology, Vascular, Intravascular, Biopsy and Histology. Typical scans provide images of the heart, liver, muscles, eye, gallbladder, arteries, veins, fine needle aspirations, masses and lymph nodes. The UK Department of Health estimates that the number of non-obstetric medical sonography scans accounts for 65% of the total number of ultrasonic scans taken [1.2]. Although many other types of medical imaging are available for the assessment of different parts of the body, such as Magnetic Resonance Imaging (MRI), nuclear medicine or a Computed Axial Tomography (CAT), ultrasound medical imaging is preferred in many cases (fig 1.2).

Advantages	Disadvantages
- It offers a real time imaging where the sonographer can select the most important areas for diagnosing and can keep a copy.	- Ultrasound is not powerful enough to go through bones
- It can be used for many different applications since it shows the structures of organs, which makes it very flexible	- Unlike CAT and MRI scans there is no scout imaging so it is harder to determine the desired area.
- Compared to the other types of imaging, it is less expensive. The instrument is also smaller and portable.	-Accuracy depends on the experience and skills of the sonographer: an accurate image requires a highly experienced sonographer
- No known long term side effects or any discomfort caused to the patient	- The penetration depth is limited and it could be harder to image patients who are obese.

Figure 1.2: Advantages and disadvantages of ultrasound imaging in
medicine

An important advantage of the ultrasonic scans, shown in fig 1.2, is the absence of any known long-term side effects. In the medical field, ultrasound is considered not to present any risks to the patient [1.3] and is called a safe test since the patient is not exposed to harmful radiation. However, some physiological effects are possible, such as inflamed sensations, heating of soft tissues [1.4], or cavitation in human body liquids exposed to intense ultrasound radiation. The long-term effects of these factors are not yet known [1.5]. Nevertheless, medical ultrasonography is used as a check-up to detect any abnormal conditions that would put either the mother or the baby at risk during pregnancy. Medical experts would rather take the risks resulting from a possible harm produced by ultrasonic radiation in order to identify any abnormal conditions [1.6].

Ultrasound is also used for therapy, treatment and hygiene. In physical therapy (therapeutic ultrasound), ultrasound with frequencies 1 – 3 MHz is used to create waves with high water or low protein content. These waves then bounce off bone and cartilage, as these waves are absorbed mostly by the connective tissue: ligaments, tendons and fascia [1.7]. This speeds up the healing process of injured muscle tissues and joints.

Ultrasound used in drug delivery applications is termed Acoustic Targeted Drug Delivery [1.8]. The frequencies used for these applications are within 1 – 10 MHz. This method is mostly used in cancer treatments, such as tumour treatment. When a tumour is removed by surgical methods, first of all the drug-encapsulated wafer needs some time to react. Due to the complications that exist while removing the tumour cells in surgery [1.9], Acoustic Targeted Drug Delivery can help in speedy delivery of the drug, resulting in a decrease

in the time needed for it to react [1.10]. This method has been applied successfully in chemotherapy where its application reduced both time and risk. This method was also found more efficient for treatment of infected areas [1.11].

Both therapy and treatment fall under the same procedures, termed Therapeutic Ultrasound and include a number of different treatments [1.12]. Ultrasound in the range 20 - 40 kHz can also be used for hygienic purposes with dental and surgical instruments, eliminating dirt by mechanically breaking it off of surfaces. Ultrasound is also used for the elimination of bacteria for medical and industrial purposes, as a way of disinfecting waste undergoing disposal.

This project will focus on ultrasonic medical imaging. The inaudible sound waves are created at frequencies greater than 20 kHz by mechanical oscillations of piezoelectric crystals. These waves can be focused using an acoustic lens and by changing the signals applied to the ultrasonic transmitters. This focusing helps to improve both axial and radial resolution. Different types of transducers include linear, curvilinear and phased array transducers. All of these will have different uses because not every part of the body is easily accessible using any single type of transducer.

Newer technology uses phased arrays while the older ones used an acoustic lens to focus the wave being sent. A water-based gel is used as an interface between the transducer and the body, because most of the energy would be reflected back to the transducer if no acoustic impedance-matching was used. After propagating a water-based gel, the waves travel through different objects of the body and are reflected back at the interfaces between

objects with different acoustic impedances. The receiver of the ultrasonic waves converts these reflected waves into electrical signals. In the pulse-echo mode, the same transducer is used first for transmission, then for reception. The ultrasonic instrument determines the wave propagation time and the amplitude of the reflected waves. This information is then plotted on a display, with different colours assigned to different amplitudes. Usually a greyscale imaging is used for amplitudes of the reflected waves, but some newer technologies use colour imaging.

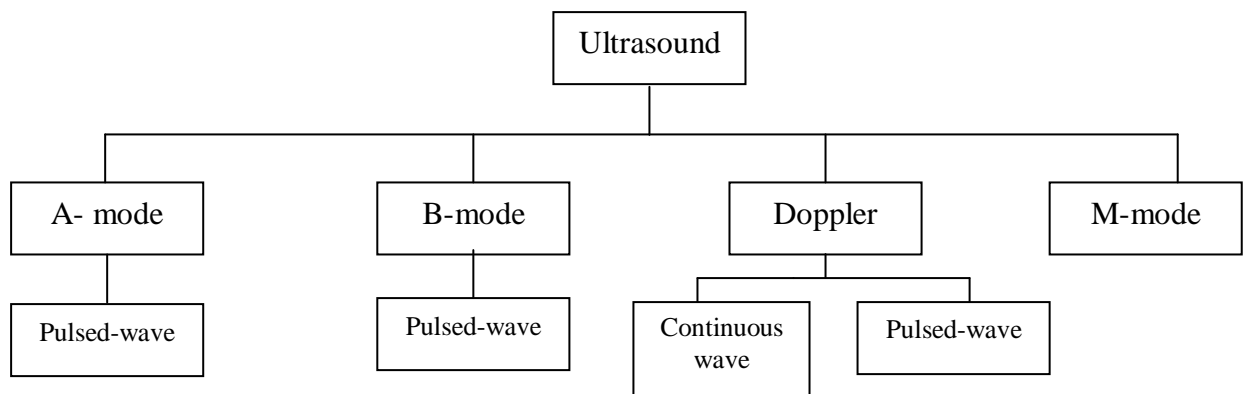


Figure 1.3: Classification of medical ultrasonic imaging

Fig.1.3 presents four distinctive types of medical ultrasonography:

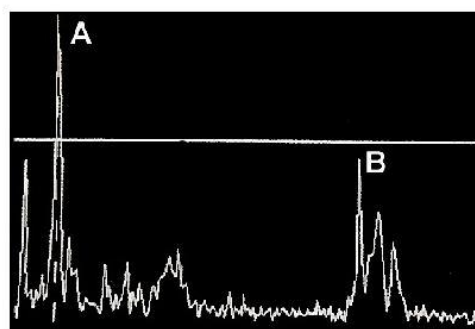


Fig 1.4: A-mode ultrasonic scan [1.13]

A-mode: This is the most basic type of ultrasonic scanning. Its basic principle is a single transducer that is placed on the body and the waveform from the transducer then forms an image on the screen. Fig.1.4 shows reflections at points A and B. Time delay between these two points can be converted into the distance in that medium, using ultrasonic velocity.

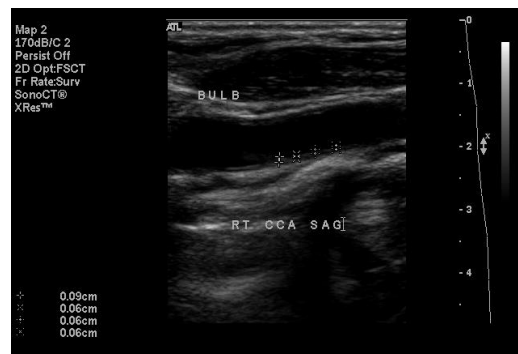


Figure 1.5: B-mode ultrasonic scan [1.14]

B-mode: B-mode is not appreciably different from the A-mode, since in the B-mode an array of transducers is used to scan a specific area of the body. This can then be viewed as a 2D-image (fig.1.5). The B-scan is, in fact, a number of A-scans combined and plotted onto the screen, thus making this scan easier to analyse. B-mode scans are the predominantly form used for medical imaging at present.

Doppler: There are two further subdivisions of this method: continuous and pulsed wave. Continuous wave (CW) usually takes into account the phase shift between the transmitted and received waves, whereas the delay between the transmitted and received pulses is of interest in the pulsed wave method. Doppler ultrasound helps to determine blood flow velocity and its direction.

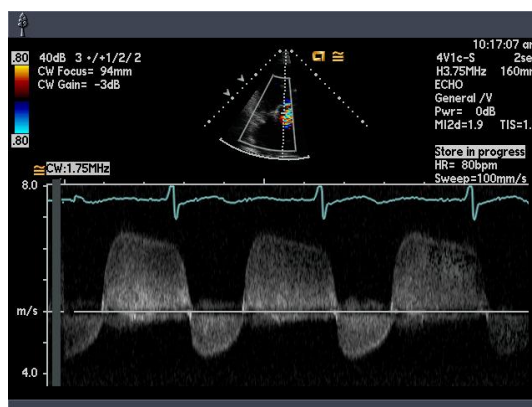


Figure 1.6: CW Doppler ultrasound scan for detection of aortic stenosis and insufficiency [1.15]

Two piezoelectric elements (the transmitter and receiver) operate continuously in the Doppler CW mode. The advantage of this mode is that it can detect very high flow velocities, as is seen in the lower portion of fig.1.6. The disadvantage of this method is the difficulty in detecting of the point of origin. An ECG is frequently superimposed onto the Doppler CW scans (as indicated in fig. 1.6) to identify what is happening at any point in the cardiac cycle.

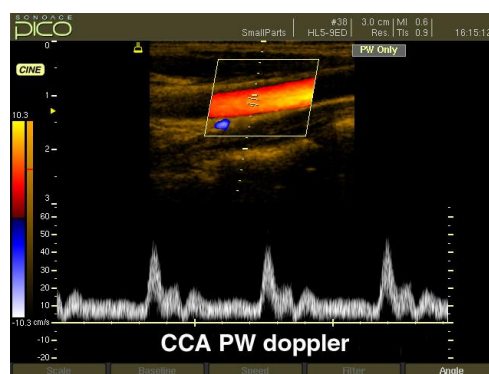


Figure 1.7: Diagram showing the Common Carotid Artery on a pulsed wave (PW) Doppler ultrasound [1.16]

For a pulsed wave (PW) the same piezoelectric element is used for transmitting and receiving. The common carotid artery (CCA) can be seen at

the top of the diagram fig.1.7 where a PW gate is shown. The sonographer can control the gate (making it larger or smaller, or even lower or higher) to view the point of interest. The PW Doppler scan shows the direction and velocity of the flow (lower portion of fig.1.7). The direction of the flow can also be identified by considering the gate colour. Pulse waves are used more frequently than are continuous waves in contemporary medical ultrasound imaging.



Figure 1.8: Cardiac M-mode ultrasound [1.17]

M-mode: Just as B-mode is formed from a combination of A-mode scans, the M-mode is formed from a combination of B-scans taken one after another and updated quickly on the screen. M-mode allows sonographers to see movement over time (it is called M-mode because it shows motion), and the parameters of the motion can be measured as necessary. At first, a B-mode scan is taken, as shown in the upper portion of fig.1.8. The sonographer then chooses the line of interest on the B-mode scan as shown in the upper part of fig.1.8. Once the line of interest is chosen, the system will show the structures either moving to or away relative to that line (fig.1.8). The ECG signal is frequently superimposed underneath the scan to allow the sonographer to relate the scan to the heart activity.

1.2) Vascular medicine and atherosclerosis

The prevalence of diabetes mellitus is increasing worldwide due to sedentary life quality, obesity and diet habits. Consequently, the complications of diabetes, especially atherosclerosis, are increasing. Detection of early signs of atherosclerosis is crucial for reducing cerebrovascular accidents and hence for providing patients with early stage medical and/or surgical treatment, if necessary.

The main method for the early detection of atherosclerosis in diabetic patients is the measurement of intima media thickness (IMT) of the artery wall. If atherosclerotic disease is detected early in diabetic patients, further development of carotid stenosis and stroke can be prevented.

The human body consists of many different blood vessels that form from arteries and veins, as shown in figure 1.9. Blood flow through each of these blood vessels is different and will depend on the age of the person [1.18].

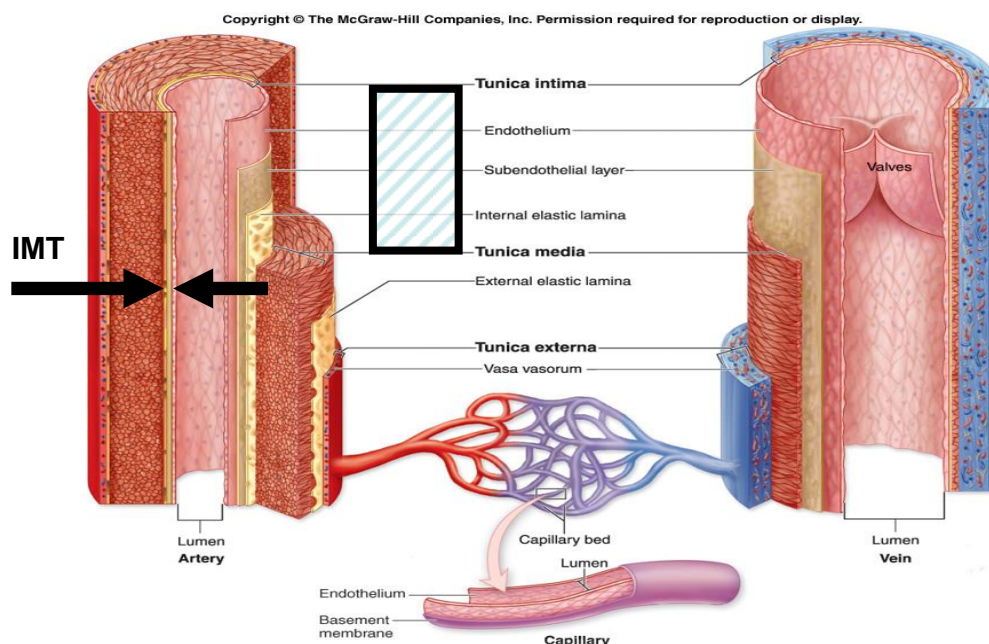


Figure 1.9: Diagram showing the arteries and veins in a human body

[1.20] with the intima media thickness (IMT) annotated

Eight different arterial lesion types [1.19] occur, which can be divided into two groups (fig 1.10): early stage lesions 1-3 and advanced lesions (4-8).

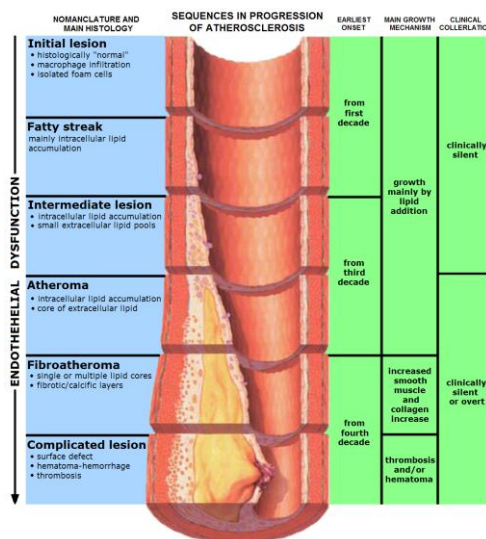


Figure 1.10: The developmental stages of arterial lesions [1.21]

As the lesion progresses, the wall thickness increases and the lumen cross-sectional area narrows. Early lesions and even advanced lesions can be clinically silent until a heart attack. The risk for lesion development depends on both modifiable and non-modifiable factors. Non-modifiable risk factors include those such as age, gender, genetic factors, race and environment that cannot be corrected. In contrast, the modifiable risk factors that include smoking, high blood pressure, stress, obesity, diabetes mellitus and physical inactivity can be influenced by changing eating habits, by exercising and by undergoing medical treatment.

While guidelines for detection of silent myocardial and lower limb ischemia are well established, data on screening asymptomatic carotid lesions remain scarce. The ADA (American Diabetes Association) [1.22] recommendations for detection of silent myocardial ischemia agree on the following criteria: age and presence of another macroangiopathic disease as

two additional cardiovascular risk factors (CVRF). They disagree, however, on two other criteria, namely duration and type of diabetes. The SFC/ALFEDIAM (French Cardiology Society/French-speaking Association for the Study of Diabetes and Metabolic Diseases) [1.23] recommends carotid ultrasonography screening for patients with myocardial or lower limb atherosclerosis and for patients whose cardiovascular risk is “particularly high”. Diabetic patients are subject to an increased risk of ischemic cerebral attack. According to a recent SFC report [1.24], the risk in diabetic patients is two to five times higher than that in the general population. (For the general population, the prevalence is 1 per thousand patients [1.27].) In studies that include diabetic patients without known macroangiopathy, the increased risk was even higher, at over 6.2 per thousand patients according to the Collaborative Atorvastatin Diabetes Study (CARDS) [1.25] or 5 per thousand patients according to the UK Prospective Diabetes Study (UKPDS) [1.26]. In addition to the classical CVRFs, several predictive factors for ischemic cerebral attacks were identified in [1.28], namely triglyceride levels, blood sugar and HbA1c.

The outcome of these strokes differs between diabetic and non-diabetic patients: the diabetic patients are more handicapped, particularly by lower limb deficits and dysarthria [1.29]. Therefore, the detection of carotid lesions in diabetic patients is even more important for improving life expectancy and quality of life. However, this type of screening would be costly, since the prevalence of diabetes is constantly increasing worldwide. Therefore it is necessary to establish criteria that can define the category of patients who are particularly at risk of ischemic cerebral attack as well as those who would

hopefully benefit from medical or surgical management with the aid of this development.

Reduction of the costs of ultrasonic scanners would directly reduce the screening costs. The cost of screening would be reasonable if the relative risk reduction provided by screening is 37% or more and if the cost of ultrasound screening is less than \$300 [1.30]. According to Whitty et al [1.31], screening for asymptomatic carotid stenosis would be beneficial only when the prevalence of severe stenosis is more than 20%. According to Derdeyn [1.32] (in a study mostly on secondary prevention), in patients with more than 20% prevalence of a 60%-stenosis, a one-time screening program is most cost-effective. Yin [1.30] recommends one-time screening, which is superior to 5 yearly screenings, considering quality of life and cost. In asymptomatic patients undergoing currently recommended therapy [1.33], the natural progression of median carotid stenosis shows no changes within 4 years. Therefore, it is unnecessary to repeat investigations when optimal medical care is applied.

Carotid IMT was initially reported to increase the relative risk (RR) of cardiovascular disease [1.34] in a non-diabetic population. Bernard et al [1.35] studied patients with type 2 diabetes mellitus (T2DM) and with at least 1 additional CVRF. They concluded that carotid IMT was a marker of cardiovascular risk in 5 years. According to Hayashi et al [1.36], measurement of the carotid IMT was a reliable prognostic indicator of heart attack, cerebral stroke or carotid atheroma in T2 diabetes patients. IMT measurements, which are reliable and reproducible, are also correlated with the results of myocardial scintigraphy in patients screened for silent

myocardial ischemia [1.37]. In type 2 diabetic patients, duration of diabetes [1.38], age and smoking duration [1.39], early nephropathy [1.40] and renal failure [1.41], cardiac neuropathy [1.42], and even post-prandial hypertriglyceridemia [1.43] appear to increase the IMT. Nagata et al [1.44] suggested type 2 diabetes to be a major risk factor of cerebral lacunas and carotid arterial plaque, independent of hypertension. De Angelis et al [1.45] studied the prevalence of carotid stenosis in cerebrovascular disease-free type 2 diabetic patients. Diabetic patients were three times more likely to develop carotid stenosis than the non-diabetics. Decades of silent arterial wall alterations precede vascular clinical events, which then reflect advanced atherosclerotic disease.

The first morphological abnormalities of arterial walls can be visualized by B-mode ultrasonography. This high-resolution, non-invasive technique is one of the best methods for the detection of early stages of atherosclerotic disease, because it is rapidly applicable, readily available and demonstrates the wall structure with better resolution than any other similar technique (e.g., magnetic resonance imaging, such as including the adventitia in the IMT results, as shown in fig. 1.11) [1.46].

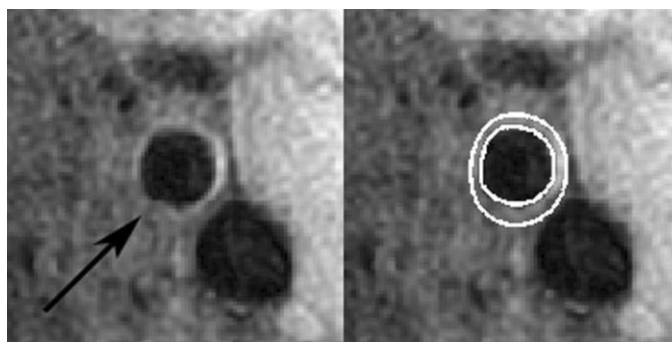


Fig 1.11: Diagram showing IMT calculation of CCA using MRI [1.47]

This is because the IMT reflects not only early atherosclerosis, but also nonatherosclerotic compensatory enlargement with largely medial hypertrophy as a consequence of smooth muscle cell hyperplasia and fibrocellular hypertrophy. This differentiation is important because epidemiological studies have shown that wall thickening, as depicted by ultrasonographic measurements of IMT, are different from atherosclerotic plaque in terms of localization, natural history, risk factors and predictive value for vascular events [1.46].

The Mannheim Carotid Intima-Media Thickness Consensus (2004–2006) recommends the following definitions for ultrasound characterization of IMT and atherosclerotic plaque:

1) The IMT is a double-line pattern visualized by echotomography on both walls of the CCAs in a longitudinal image. It is formed by two parallel lines, which consist of the leading edges of two anatomical boundaries: the lumen- intima and media-adventitia interfaces. The IMT can be seen in figure 1.4;

2) Plaque is a focal structure encroaching into the arterial lumen of at least 0.5 mm or 50% of the surrounding IMT value.

These definitions allow classification of the vast majority of carotid lesions observed with ultrasound. Carotid examination includes visualization of common, internal and external carotid arteries (CCA, ICA and ECA respectively). The CCA can be assessed in nearly every patient. In contrast, successful examination of the internal carotid artery and of the carotid bulb

depends both upon the anatomical topography of the patient and on the sonographer's expertise.

The following observations are related to the IMT measurements:

1) Measurement of IMT is most convenient in a region free of plaque, where the double-line pattern is observed. In this region, the measurements are easier to perform, are more accurate, are reproducible and can be standardized by computerized analyses.

2) IMT can be measured in the CCA, at the bulb and at the origin of the internal carotid artery.

3) The IMT values obtained from different sites of the carotid arteries should be documented separately [1.46].

Standard equipment for IMT measurements includes a high-resolution B-mode system operating preferentially with linear ultrasonic transducers at a frequency of about 7 MHz. Appropriate depth of focus (e.g., 30–40 mm), an optimal frame rate of 25 Hz (or at least greater than 15 Hz) and appropriate gain settings (that introduce minimal intraluminal artefacts) are recommended to obtain the best image quality. Logarithmic gain compensation should be around 60 dB deep. It must be adjusted to obtain a symmetrical brightness on near and far walls, decreasing, if necessary, the gain in the middle part of the waveform to avoid intraluminal artefacts.

Carotid IMT scanning and reading protocol recommendations (European Society of Cardiology Guidelines) [1.46] are as follows:

- The arterial wall segments should be assessed in a longitudinal view, strictly perpendicular to the ultrasound beam, with both walls clearly

visualized in order to achieve diameter measurements. Lateral probe incidence is recommended as it offers the best view in the middle field, where the resolution is known to be greater than in the near or far field. A horizontal display of the arterial image is also recommended to obtain the optimal interfaces between blood and vascular structures, on the longest possible segment. The localization of the end of the CCA is necessary to help in repositioning during the follow-up;

- IMT should be measured preferably on the far wall. This is because the IMT values from the near wall depend in part on gain settings and are less reliable. If taken on the near wall, IMT should be measured separately from IMT of the far wall;

- Along a minimum of 10 mm length of an arterial segment, a high-quality image acquisition is required for serial reproducible measurements. Due to vessel tortuosity, IMT measurement could only be possible at a shorter vessel segment, especially in the carotid bifurcation or the ICA bulb;

- Adventitia-to-adventitia diameter and intraluminal diameter of CCA must also be measured, as IMT is significantly correlated with the arterial diameter;

- Each vascular laboratory must perform periodical quality control of their equipment (phantom scans) and reliability studies of scans and measurements for ultrasonographers and readers. The intraclass correlation coefficient should be evaluated for intra- and interobserver variability, both for IMT and plaque measurements.

The available epidemiological data indicate that increased IMT (at or above 1 mm) represents a risk of myocardial infarction and/or cerebrovascular disease [1.48].

The presence of increased carotid IMT in one individual with intermediate cardiovascular risk would be expected to lead to his classification into the high-risk category and thus would influence the aggressiveness of risk factor modifications [1.48]. Various non-invasive markers of early arterial wall alteration are currently available, such as arterial wall thickening and stiffening, endothelial dysfunction and coronary artery calcification [1.49]. Among these, the IMT of large artery walls, especially the carotid, can be assessed by B-mode ultrasound in a relatively simple way and this measure is safe, inexpensive, precise and reproducible [1.50]. However, the measurement of IMT in the distal common carotid artery suffers from the inability to assess whether IMT represents atherosclerosis (intimal thickening) or vascular hypertrophy (medial thickening), or both. The reason is that ultrasonography cannot distinguish between intimal thickness and medial thickness in the IMT measurement because of insufficient axial resolution. Therefore, the IMT, when measured in the distal common carotid artery, free from intrusive atherosclerotic plaque, should be considered as a marker of early arterial wall change rather than as a surrogate for atherosclerosis [1.48]. The type of reading of the IMT value (i.e., automatic versus manual) also influences reproducibility. The automatic measurement clearly has better reproducibility than operator-dependent manual measurement [1.48].

Since the IMT is now increasingly used for detecting early alterations of the arterial walls, it is of major clinical relevance to define the threshold values beyond which the IMT may be considered as abnormally high. Thus, ultrasonographic diagnosis of “increased” IMT in one individual at risk for atherosclerosis might help to better stratify the risk of the patient [1.51].

The “normal” values of carotid IMT are highly dependent on the methodology used for its measurement. These values are established on the basis of the histogram of IMT values for a general healthy population [1.52, 1.53]. The “normal” IMT values are strongly influenced by age and sex [1.52]. The upper normal limit for the IMT is frequently set at the 75th upper percentile of the IMT distribution. However, since the IMT is considered as a candidate marker of cardiovascular risk [1.50], the normal value should be interpreted in terms of increased risk rather than in terms of statistical distribution within a population. Epidemiological studies should contribute to definition of the threshold of the IMT above which the cardiovascular risk begins to increase sharply. The epidemiological data currently available indicate that an IMT value at or above 1 mm at any age is associated with a significantly increased risk of myocardial infarction and/or cerebrovascular disease [1.46].

A close correlation of the IMT with a number of cardiovascular risk factors was demonstrated in [1.54]. Traditional risk factors, such as male sex [1.55], ageing [1.55], being overweight [1.55], elevated blood pressure [1.56], high blood cholesterol [1.57], diabetes and insulin resistance [1.58] and cigarette smoking [1.59] positively correlated with the carotid IMT in observational and epidemiological studies in patients from cardiovascular risk

groups and from the general population. Among the traditional risk factors, hypertension appears to have the greatest effect on IMT, probably via medial hypertrophy, which is a process specifically related to this disease [1.57]. Cumulative effects of classical risk factors on IMT were shown by a positive relationship between the multifactorial Framingham risk score and the carotid IMT [1.60]. New or emerging risk factors have also been tested with regard to their relationship with the carotid IMT [1.61]. Some of these studies have demonstrated a consistent association with the increased IMT, such as various lipoproteins [1.61], psychosocial status [1.62], plasma viscosity [1.63] and hyperhomocysteinemia [1.64]. Carotid IMT has also been found to be associated with cardiovascular alterations or organ damage [1.65]; specifically: (i) in the brain with white matter lesions assessed by magnetic resonance imaging [1.66]; (ii) in the heart with angiographically assessed coronary artery disease [1.67].

All of the relationships of the IMT to cardiovascular risk factors and organ damage indicate that increased IMT may be considered as a comprehensive measure of the alterations caused by multiple risk factors over time on the arterial walls. The extensive use of the IMT in medical literature highlights the major role it currently plays as a biomarker in clinical research [1.48]. The Kuopio Ischaemic Heart Disease (KIHD) Study of middle-aged healthy Finnish men showed that a carotid IMT of 1 mm was associated with a two-fold greater risk for acute myocardial infarction over 3 years [1.68]. The Atherosclerosis Risk in Communities (ARIC) study in several US communities showed that a carotid IMT of 1 mm was associated with an increased risk ratio of coronary event over a period of 4-7 years (a risk ratio

of approximately 2 and 5 in 45-64 year old men and women, respectively) [1.69]. The CHS Study in elderly US subjects showed that a carotid IMT of 1.18 mm was associated with a four-fold greater risk for combined acute myocardial infarction and stroke over 6 years [1.70]. The Rotterdam Study in elderly Dutch subjects showed that each difference of 0.16 mm in IMT was accompanied by a risk ratio of 1.4 for acute myocardial or stroke over 3 years [1.71]. In addition, studies in secondary prevention, in particular the Cholesterol Lowering Atherosclerosis (CLAS) study [1.72] in patients with established coronary artery disease, showed that for each 0.03 mm increase per year in common carotid IMT, the relative risk for any coronary event was 3.1. All of these studies demonstrate that increased IMT is a powerful predictor of coronary and cerebrovascular complications regardless of the method and the site of measurement, including the distal common carotid far wall IMT.

However, the predictive power appears less strong for IMT measured only in the distal common carotid than for IMT measured at multiple extracranial carotid sites. This supports the idea that the common carotid artery alone may not be the most appropriate segment to study if the objective is to predict atherosclerotic-related complications [1.48].

A number of trials have tested the effects of lipid lowering drugs (statins) on the carotid IMT, while other trials have tested the effects of various calcium antagonists [1.73]. The outcome of all of the above trials (i.e., the IMT measured at multiple carotid sites, frequently including plaque in the bifurcation or internal carotid) can be considered as a surrogate of atherosclerosis. Therefore, when a drug (such as pravastatin, atorvastatin,

amlodipine or ramipril) demonstrates a beneficial effect on the IMT progression, the drug can be inferred to exert an antiatherosclerotic effect on the carotid walls [1.48]

These trials on the common carotid IMT highlight three main observations. First, the measurement of the IMT in the far wall of a CCA free of atherosclerotic plaque allows a perfect image to be obtained of the two echogenic lines that define the IMT. Therefore, these two lines can automatically be detected using computerized edge detection program. This automatic measurement considerably improves the precision and reproducibility and therefore allows demonstration of a significant difference in the IMT progression between both treatments using a relatively small sample size. The CCA is the site of earlier lesions, which are not necessarily atherosclerotic in nature when compared to the more advanced lesions in the bifurcation or internal carotid arteries [1.48].

The IMT-INSIGHT trial has found the same incidence of events following nifedipine and diuretic treatment, whereas the IMT progression was different between both treatments. The reason is that the common carotid IMT reflects a very early preintrusive lesion and its short-term change cannot be translated into atherothrombotic complications whose mechanisms involve advanced atherosclerotic lesions. Nevertheless, a common carotid IMT change is likely to indicate the incidence of clinical complications in the long term, but further trials of longer duration are required to validate this hypothesis. The carotid diameter change may passively modify wall thickness by stretching the artery wall due to the non-compressibility of the arterial wall mass [1.48].

Since the carotid IMT is a marker of early arterial wall change, caused by atherosclerosis and/or vascular hypertrophy, detection of this change by B-mode ultrasonography might be of substantial value in diagnosis of high cardiovascular risk. This detection may lead to the decision to treat at-risk patients with drugs or by correcting modifiable risk factors [1.51].

Before proposing routine measurement of the IMT in clinical practice, several existing limitations must first be resolved. These include standardization of measurement methods (including the site and the method of analysis of the IMT measurement) and precisely defining the threshold for the IMT above which the risk of cardiovascular event can be considered to substantially increased for a given individual [1.74].

The IMT assessed by B-mode ultrasound in superficial large arteries, especially the carotid, is of major relevance with regard to the following points [1.51]:

- (i) Reflection of multiple risk factors;
- (ii) Mirror of atherosclerotic burden and/or index of cardiovascular growth, particularly in hypertension;
- (iii) Predictor of subsequent events;
- (iv) End point for therapeutic trials.

Identifying the presence of increased IMT in the carotid arteries of one individual with intermediate cardiovascular risk would be expected to lead to his/her classification in the high risk category and thus to influence the aggressiveness with which risk factor modification would be performed [1.51].

1.3) Using the ECG signal for medical imaging

An Electrocardiogram (ECG) is a graphical presentation of the heart activity over time. It is recorded by placing electrodes on the human body at certain points, and then measuring the potential difference between the electrodes caused by the depolarisations and repolarisations of the heart. The graphical presentation of the ECG can be interpreted, so that normal and abnormal rhythms of the heart can be detected and diagnosed [1.75]. Traditionally, these graphical presentations were produced on ECG graph paper. Today, ECG machines are compact electronic systems capable of automatic interpretation [1.76].

The signals picked up from the human body are typically 0.1 – 5 mV, with the bandwidth between .05 and 130Hz [1.77]. Simple heart monitoring uses frequencies up to 30Hz, whereas, in some cases (e.g., intensive care monitoring), the frequencies of interest increase up to 1 kHz [1.78].

The graphical presentations of the heart activity are usually called “leads” in medical terms. The word “lead” in electrical terms means the actual wire connected to an electrode placed at a particular location of the human body. The leads can be both bipolar (the potential difference between two electrodes is of interest) and unipolar (the potential of the electrode is related to the electrical ground).

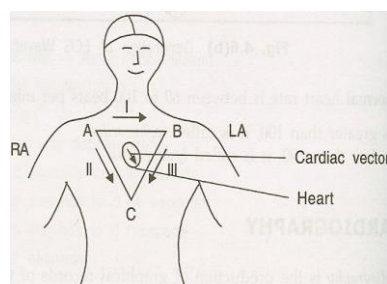


Figure 1.12: Frontal Plane ECG electrode placement [1.79]

The first type, bipolar limb lead frontal plane ECG, is depicted in fig. 1.12. It consists of a plane vector with three axes at an angle to each other. This plane (triangle) is derived from Einthoven's triangle, where electrodes are placed on the patient's body at the positions A, B and C for measuring the corresponding vectors I, II and III, as shown in fig.1.12. Although the recordings from any two leads are sufficient for a simple examination, more information can be obtained because the third electrode is easily added. These leads are the first 3 leads of the conventional 12 lead ECG.

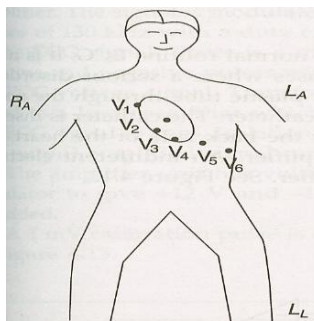


Figure 1.13: Transverse Plane ECG electrode placement [1.79]

Another type of lead measurement is the transverse plane ECG, which is also known as the V lead measurement (fig. 1.13). The leads are unipolar here. An additional three leads are added at the back of the patient, and an extra ground lead would be added if the complete 12 lead ECG were required. Four main steps in heart activity are reflected in the ECG signal.

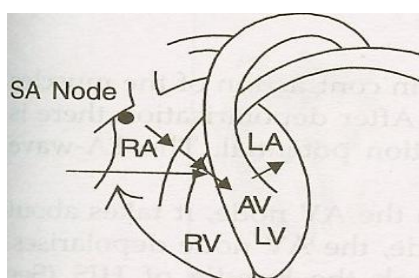


Figure 1.14: P wave generation [1.79]

The P wave is generated first. This results from the depolarisation of the Sino Atrial node (SA node) (fig 1.14). The SA node is usually known as the primary pacemaker and the P wave travels to the Atrioventricular node (AV node). The AV node, also known as the secondary pacemaker, is where the blood flows from the right and left atrium into the right and left ventricle by opening of the tricuspid and bicuspid valves, respectively. The corresponding electrical activity is represented as a P wave on the ECG signal, having an amplitude of about 0.25mV. This usually takes around 0.11 seconds. Changes in the width and shape of the wave indicates a change in depolarisation.

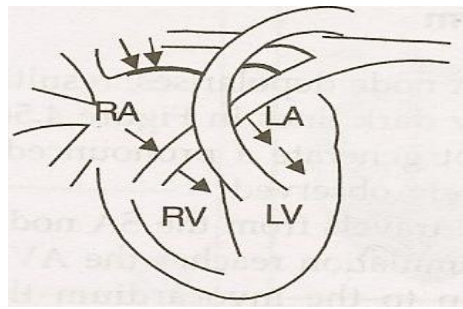


Figure 1.15: PR interval generation [1.79]

The following PR interval consists of the AV node acting as a delay (fig. 1.15), which controls the blood flow from the atrium to the ventricle. It can be seen at the PR interval on the ECG signal, where it usually takes from 0.12 to 0.2 seconds, starting from the beginning of the P wave. If the delay time taken is greater than 0.2 seconds, the first degree heart block occurs as a sign of coronary artery disease. Some PR intervals show conditions that are more advanced, such as the second and complete heart block. A delay smaller than 0.12 seconds indicates Wolff-Parkinson-White syndrome.

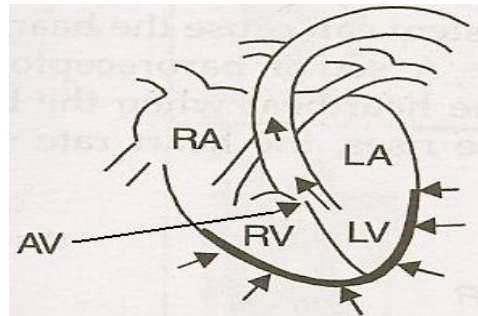


Figure 1.16: QRS complex generation [1.79]

The subsequent QRS complex is known as the ventricular depolarisation (fig. 1.16). The electrical impulse that travelled to the AV node is propagated to the myocardium and muscles of the ventricles by the bundle of HIS and the Purkinje conducting system. This results in a contraction of the muscle and causes pumping of the blood. The bundle of HIS splits into two branches, where the left and the right branches activate the left and right ventricles, respectively. Consequently, the ejected blood flows in two directions. The blood in the left ventricle flows towards the aorta while the blood in the right ventricle flows to the lungs and to the pulmonary artery. The QRS complex is similar to the P wave in that they both represent depolarisations. The QRS complex looks steeper than the P wave because heart activities in this complex are much faster compared to those of the P wave. The QRS complex typically takes from 0.06 to 0.10 seconds, starting from the end of the PR interval. The peak value of the R wave is around 0.25mV. This value can be useful in identifying the correct disease state, such as myocardial infraction, cardiac arrhythmia, ventricular hypertrophy and some others.

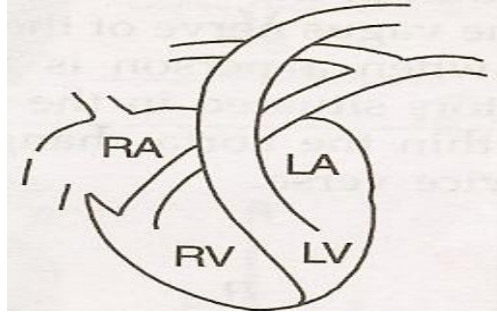


Figure 1.17: T wave generation [1.79]

Finally, the T wave represents the stage where the heart muscles relax before initiating the next heart cycle (fig. 1.17). The SA node creates the corresponding electrical activity. This stage is usually called the late diastole. The T wave duration can vary from patient to patient. The amplitudes of T wave are positive in most of the leads; a negative wave indicates coronary ischemia.

The complete ECG signal is shown in fig 1.18.

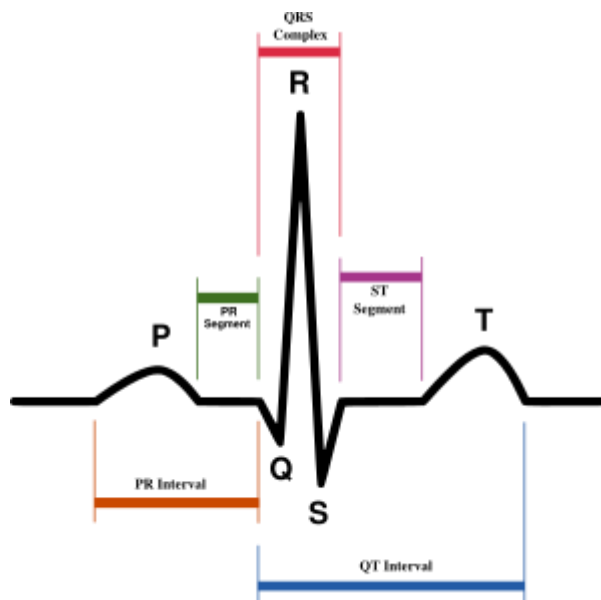


Figure 1.18: The complete ECG signal [1.80]

The U wave, which has not yet been discussed, is usually present in most ECG traces (50-75%). It can be thought of as arising from inexplicable

sources. The inverted U wave seen can be a sign of myocardial ischemia [1.81].

The QT interval is measured from the beginning of the QRS complex until the end of the T wave. The QT interval varies from patient to patient and from time to time, depending on the heart rate of the patient. It can take from 0.35 to 0.44 seconds.

The RT segment connects the QRS complex to the T wave, and normally takes from 0.08 to 0.012 seconds. The length of the segment may not be as important as is its curvature. If this segment is curved downwards, remains flat or takes a shorter time than usual, then it can be an indication of coronary ischemia.

The next segment is the ST segment, from the beginning of the QRS complex until the apex of the T wave, also referred to as the absolute refractory period (no longer than 0.8 seconds). If this segment takes more than 0.8 seconds and if an increase in the isoelectric line (known as the baseline of the ECG voltage) is also present, then it could be a sign of myocardial infarction.

The final segment is the PR segment. The PR segment shows how atrial polarisation is occurring.

The ECG can be used for many applications, e.g., it can be used on its own for monitoring the cardiac cycle or for diagnostics of heart problems. It can also be used, along with other examinations, to allow comparisons of different examinations to better diagnose a particular condition. In some medical applications, ECG gated machines are used to examine different diseases [1.82, 1.83]. However, these triggering systems are not yet common

in the field of IMT measurement. In the present project, the ECG signal will be used as the trigger for the ultrasonic instrument that measures the IMT. The advantage of this type of automated system is that the IMT measurement can be obtained at a particular stage in the cardiac cycle. Performing an ultrasonic screening program on diabetic patients by experienced radiologists, combined with ECG, could help to identify patients at risk of developing carotid stenosis and stroke. It could also help to establish recommendations for screening and management of carotid atheroma in diabetic patients, especially those who show signs of ischemic heart disease in ECG.

Blood pressure varies during the cardiac cycle (fig 1.19).

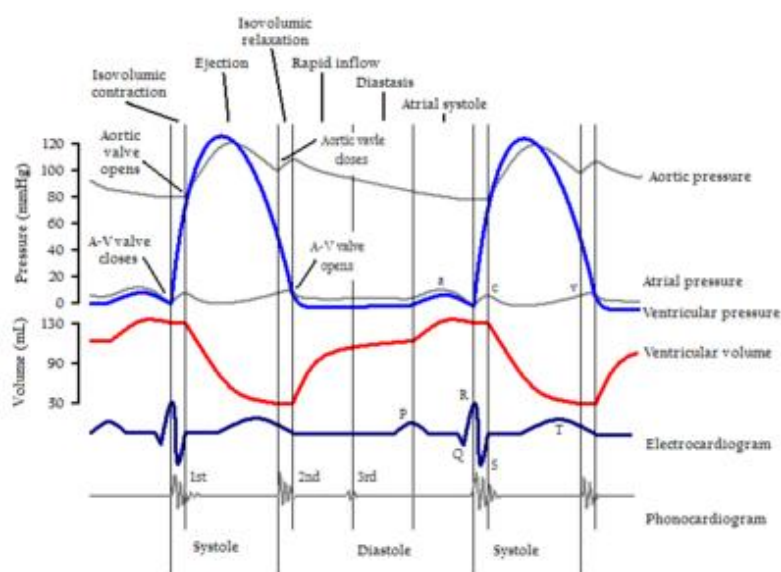


Figure 1.19: The in vivo ECG with the different pressures created by the arteries [1.84]

Different blood pressures result in different values for IMT measurements. The largest value corresponds to the least blood pressure in the arteries. This pressure is caused by a number of different physical and physiological factors. Physical factors include, e.g., pushing the transducer too deep into the skin, resulting in different IMT measurements.

Physiological factors include pressure variations during either systolic or diastolic parts of the cardiac cycle (fig. 1.20).

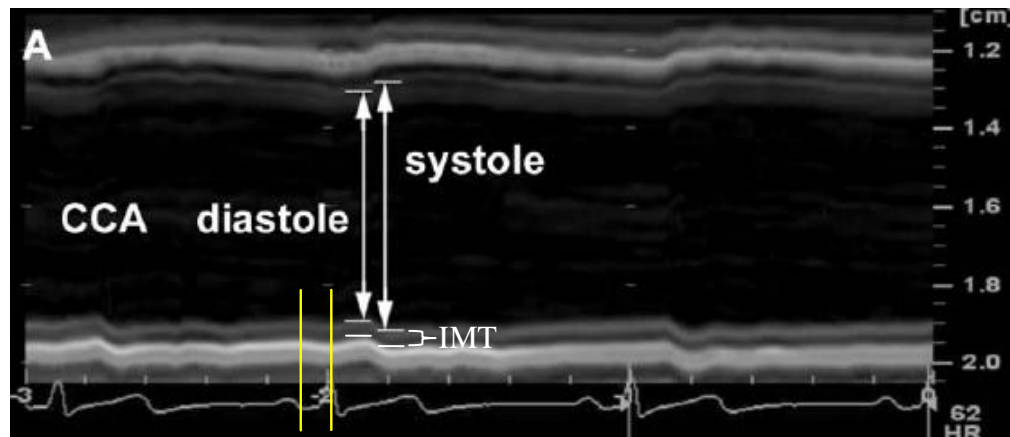


Figure 1.20: M-mode ultrasonic scan of the CCA showing different CCA diameter and IMT values depending on the heart activity [1.85]

After the QRS complex, the heart pumps a bolus of blood up the carotid artery via the aorta, as the aortic pressure increases. A delay occurs as this bolus propagates from the heart, up the artery and past the point of analysis in the neck (shown by the vertical markers in fig.1.20). Once the bolus has passed and the carotid artery settles, there is a still period until the next bolus passes. When the carotid artery has settled, the IMT measurement can be taken. Depending on the heart rate of the patient (slow, normal, fast or even irregular), the time that the carotid artery is static will change, so an appropriate delay is required.

1.4) Proposed Solution

Diagnosis, monitoring and curing of various vascular abnormalities could be performed using ultrasonic measurements of the blood vessels. These measurements are complicated by the low level of reflections from the blood

vessels (1-2% from the incident energy [1.86]) that results in reduction of the signal-to-noise ratio (SNR).

Reliable measurement of the carotid IMT presents a substantial technical challenge because of the small size of the object (661 μm on average for the carotid IMT [1.87]) compared to the wavelength of the ultrasonic waves (around 250 μm for the 6 MHz operating frequency). In addition, the IMT varies both short term with the heart activity (up to 25 μm per heart cycle [1.87]) and long term (up to 80 μm per year [1.88]). Therefore, in order to detect any pathology or any trend, ultrasonic scans must be taken in sync with the heart activity, and they need to provide a resolution in the micrometer range. Since the changes in thickness to be monitored are very small, this requires operation of ultrasonic scanners at high sampling frequencies, much higher than 50–100 MHz sampling frequencies that are used by contemporary ultrasonic scanners. The measurement resolution of the scans largely depends on the sampling frequency of the ultrasonic echoes. If this frequency equals 100 MHz (a typical value for present day advanced instruments), the echo samples are taken every 10 ns (10^{-8}s). During that time, ultrasound propagates $10\text{ ns} \times 1540\text{ m/s} = 15\text{ }\mu\text{m}$ (the ultrasound velocity for human tissues was taken from [1.86], and this figure agrees well with data from the Kaye & Laby tables [1.89]). Substantial improvements to the pixel size of conventional ultrasonic scan limits could be achieved by using significantly higher sampling frequencies. On the other hand, improvements in axial resolution for ultrasonic measurements can be achieved by using higher operating frequencies of the transducer. The downside of this approach is that the ultrasound attenuation notably increases with frequency; therefore echoes

from only close range will be available for further analysis.

These two issues (low SNR of the echo signal and need for high sampling frequency) can be addressed by using a novel architecture for ultrasonic instruments developed in the Applied Ultrasonics Laboratory of Nottingham University. An additional issue is the variability of the blood vessel size, which depends on the phase of the cardiac cycle. Several studies have shown that these variations with a cycle time of around one second result in the same changes as building atherosclerosis over a period of one year.

The present research will focus on building an instrument that takes ultrasonic scans at the required time instant, determined on an ECG diagram, and then testing and experimenting with the resulting instrument.

Primary objectives

- Develop an ultrasonic medical instrument for carotid IMT measurements with a resolution of 10 μm
- Develop medical instrumentation that synchronizes ultrasonic scans with the heart activity monitored by the ECG
- Integrate the above developments in a low cost portable medical instrument capable of taking A-mode scans

Design outcomes

- Self-contained ultrasonic instrument capable of taking A-mode scans *in vivo* with a sampling frequency above 1 GHz
- An add-on device that monitors the patient's ECG and triggers an ultrasonic scan at a desired phase of the heart activity
- An integrated instrument that uses a conventional ultrasonic transducer for A-mode scans

Experimental evidence of success

- *In vivo* A-mode scans
- Consistent A-mode scans taken *in vivo* at the same phase of the heart activity in a space of several minutes
- A-mode scans synchronized with *in vivo* heart activity

The development will enable accurate monitoring of the carotid IMT to detect any trends (e.g., related to progression of disease or to an effect of some treatment) within a short time of observation. This will enable further advances in cardiovascular disease detection and faster development of novel medicines.

The new system

The new proposed system will consist of the following three parts:

- Front end
- Processing
- Back end

Front End

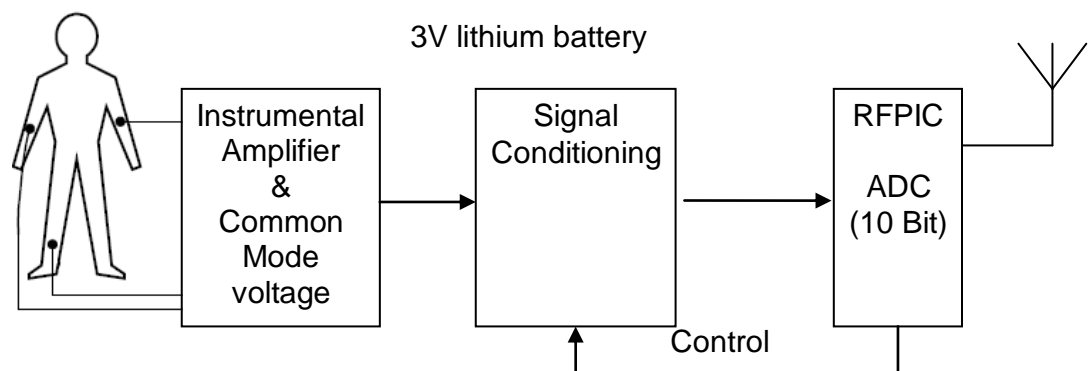


Figure 1.21: Diagram showing the front end of the system under development

The ECG signal is acquired from the patient (fig 1.21). Safety of the patient is of primary importance because, in case of malfunction, a high voltage risk can occur to the patient. A battery-operated device can eliminate this risk [1.90]. In addition, to eliminate the possibility of high voltage appearance via communication wires, a wireless link can be employed.

Processing

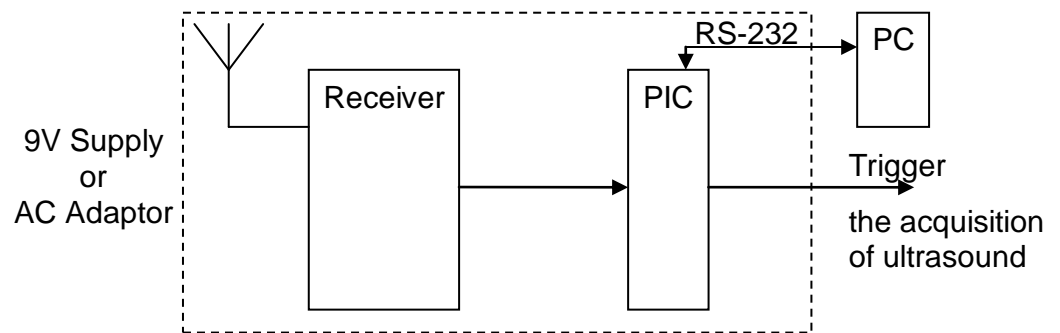


Figure 1.22: Diagram showing the receiver end of the system

When the transmitter sends the data acquired from the patient, they will be received by the receiver and then used to trigger the ultrasound machine for the IMT measurement (fig.1.22). A 9V battery supply for the receiver seems to be a better choice than an AC adaptor because it produces less noise. This receiver also offers communication over an RS-232 interface, which simplifies debugging and allows logging of the received data on a PC.

Back End

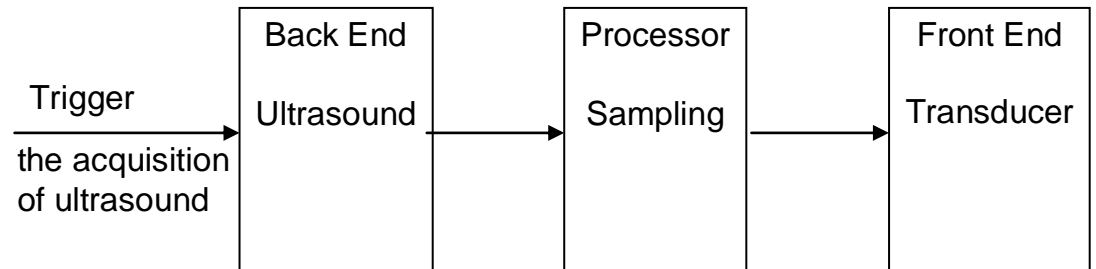


Figure 1.23: Diagram showing the ultrasound end of the whole system

The back end (fig 1.23) includes the ultrasonic instrument that sends and receives ultrasonic signals via a transducer. Small changes in IMT will require a better time domain resolution, which will be achieved with a sampling frequency of around 1GHz.

1.5) Why wireless?

Today, many electronic devices provide wireless communications. This allows people unrestricted mobility as there are no connecting wires. The wireless systems that are used in hospitals should not cause interference to sensitive instruments located in the close vicinity. Wireless ECG monitors can be built using a number of different microcontrollers [1.91]. Of these options, the rfPIC from Microchip uses a radio frequency that does not require licensing. In addition, an evaluation board for the rfPIC was available from the EEE department, making it a logical choice. After the signal from the patient is picked by the electrodes, it needs to be amplified by an instrumental amplifier. The rfPIC then converts the signal using a built in 10-bit ADC, and transmits the digital data obtained to the receiver.

1.6) References:

- [1.1] Rough diagram of sound frequency scale, showing ultrasound and some applications, 2007-01-11 01:04 LightYear,
http://en.wikipedia.org/wiki/Image:Ultrasound_range_diagram.png
- [1.2] Ultrasound, <http://en.wikipedia.org/wiki/Ultrasound>
- [1.3] AAPM/RSNA Physics Tutorial for Residents: Topics in US, B-mode US: Basic Concepts and New Technology, Nicholas J. Hangiandreou, PhD, Imaging & Therapeutic Technology, Radiographics. 2003; 23:1019-1033.
- [1.4] Ultrasound, <http://www.physiomontreal.com/Ultrasound.pdf>
- [1.5] Ultrasound Imaging, FDA Radiological Health Program, March 26 08,
<http://www.fda.gov/cdrh/radhealth/products/ultrasound-imaging.html>
- [1.6] About your Exam - Ultrasound Safety,
<http://www.aium.org/patient/aboutExam/safety.asp>
- [1.7] Electrotherapy and Tissue Repair,
<https://uhra.herts.ac.uk/dspace/bitstream/2299/1085/1/103740.pdf>
- [1.8] Acoustic targeted drug delivery in neurological tissue (A), George Lewis, Jr. and William Olbricht ,The Journal of the Acoustical Society of America -- November 2007 -- Volume 122, Issue 5, p. 3007,
<http://scitation.aip.org/getpdf/servlet/GetPDFServlet?filetype=pdf&id=JASMAN000122000005003007000003&idtype=cvips&prog=search>
- [1.9] Highlights of upcoming acoustics meeting in New Orleans, Jason Bardi, Acoustics and brain cancer - Acoustical Society of America,6-Nov-2007,
http://www.eurekalert.org/pub_releases/2007-11/aiop-hou110607.php

- [1.10] A phantom feasibility study of acoustic enhanced drug perfusion in neurological tissue, Lewis, G.K., Olbricht, W., Life Science Systems and Applications Workshop, 2007. LISA 2007. IEEE/NIH, 8-9 Nov. 2007, p 67-70, 978-1-4244-1813-8
- [1.11] Therapeutic Ultrasound, Tim Watson, Electrotherapy on the Web, 2000,<http://impulseo.pagespro-orange.fr/publications/therapeutic-ultrasound.pdf>
- [1.12] Therapeutic Ultrasound: A Promising Future in Clinical Medicine, Lawrence Crum, Michael Bailey, Peter Kaczkowski, Inder Makin, Pierre Mourad, Kirk Beach, Stephen Carter, Udo Schmiedl, Wayne Chandler, Roy Martin, Shahram Vaezy, George Keilman, Robin Cleveland, and Ronald Roy, ICA/ASA '98, Seattle WA, 2aBV2, June 23, 1998
- [1.13] <http://www.ob-ultrasound.net/sliceabd.html>, Accessed January 2010
- [1.14] <http://emedicine.medscape.com/article/1155193-overview>, Accessed January 2010
- [1.15] http://www.medical.siemens.com/webapp/wcs/stores/servlet/PSProductImageDisplay~q_catalogId~e - 3~a_catTree~e 100010,1007660,12761,1003854~a_langId~e - 3~a_productId~e 137961~a_storeId~e 10001.htm, Accessed January 2010
- [1.16] <http://www.medison.ru/uzi/eho267.htm>, Accessed January 2010
- [1.17] http://www.umiultrasound.com/ge_vivids6.html, Accessed January 2010

- [1.18] Ebrahim S, Papacosta O, Whincup P, Wannamathee G, Walker M, Nicolaides AN, Dhanjil S, Griffin M, Belcaro G, Rumley A, Lowe GDO. Carotid plaque, intima media thickness, cardiovascular risk factors, and prevalent cardiovascular disease in men and women: The British Regional Heart Study. *Stroke* 1999; 30:841-850
- [1.19] Intima-Media Thickness and Atherosclerosis: predicting the risk? Ed. P.-J Touboul, 1997, ch.1
- [1.20] Human Anatomy - Learning the Cardiovascular System - Chapter 23: Vessels and Circulation, Cynthia Herbrandson, http://academic.kellogg.cc.mi.us/herbrandsonc/bio201_McKinley/Cardiovascular%20System.htm
- [1.21] Stages of endothelial dysfunction in atherosclerosis, Maderibeyza, 12:05, 26 September 2007, http://en.wikipedia.org/wiki/Image:Endo_dysfunction_Athero.PNG
- [1.22] American Diabetes Association. Standards of Medical Care in Diabetes. *Diabetes Care* 2005; 28, suppl 1: S1-S71.
- [1.23] Charbonnel B, Bouhanick B, Le Feuvre C, et al. SFC/ALFEDIAM (French Cardiology Society/French-speaking Association for the Study of Diabetes and Metabolic Diseases) guidelines on the management of the diabetic patient seen by a cardiologist. *Arch Mal Coeur Vaiss* 2004; 97:229-49.
- [1.24] De Sèze J, Leys D. Les accidents vasculaires cérébraux chez le diabétique. *Sang Thromb Vaiss* 1997; 9:235-240.
- [1.25] Colhoun HM, Betteridge DJ, Durrington PN, et al. CARDS investigators. Primary prevention of cardiovascular disease with

atorvastatin in type 2 diabetes in the Collaborative Atorvastatin Diabetes Study (CARDS): multicentre randomised placebo-controlled trial. *Lancet* 2004;364:685-96.

- [1.26] UK Prospective Diabetes Study (UKPDS) group. Intensive blood glucose control with sulfonylureas or insulin compared with conventional treatment and risk of complications in patients with type 2 diabetes. *Lancet* 1998; 352:837-53.
- [1.27] Lemesle M, Milan C, Faivre J et al. Incidence Trends of ischemic stroke and transient ischemic attacks in a well-defined French population from 1985 Through 1994. *Stroke* 1999; 30:371-7.
- [1.28] Lehto S, Ronnema T, Pyorala K, Laakso M. Predictors of stroke in middle-aged patients with non-insulin dependent diabetes. *Stroke* 1996; 27:63-8.
- [1.29] Megherbi SE., Milan C., Minier D. et al. European BIOMED Study of stroke Care Group. Association between diabetes and stroke subtype on survival and functional outcome 3 months after stroke: data from the European BIOMED Stroke Project. *Stroke* 2003; 34:688-94.
- [1.30] Yin D, Carpenter JP. Cost-effectiveness of screening for asymptomatic carotid stenosis. *J Vasc Surg* 1998; 27:245-55.
- [1.31] Whitty CJ, Sudlow CL, Warlow CP. Investigating individual subjects and screening populations for asymptomatic carotid stenosis can be harmful. *J Neurol Neurosurg Psychiatry* 1998;64:619-23.
- [1.32] Derdeyn CP, Powers WJ. Cost-effectiveness of screening for asymptomatic carotid atherosclerotic disease. *Stroke* 1996; 27:1944-50.

- [1.33] Sleight SP, Poloniecki J, Halliday AW. Asymptomatic Carotid Surgery Trial collaborators. Asymptomatic carotid stenosis in patients on medical treatment alone. *Eur J Vasc Endovasc Surg* 2002; 23:519-23.
- [1.34] O'Leary DH, Polak JF, Kronmal RA, et al. The Cardiovascular Health Study Collaborative Research Group : Carotid-artery intima and media thickness as a risk factor for myocardial infarction and stroke in older adults. *N Engl J Med* 1999; 340:14-22.
- [1.35] Bernard S, Serusclat A, Targe F, et al. Incremental predictive value of carotid ultrasonography in the assessment of coronary risk in a cohort of asymptomatic type 2 diabetic subjects. *Diabetes Care* 2005; 28: 1158-62.
- [1.36] Hayashi C, Ogawa O, Kubo S, et al. Ankle brachial pressure index and carotid intima-media thickness as atherosclerosis markers in Japanese diabetics. *Diabetes Res Clin Pract* 2004; 66:269-75.
- [1.37] Boucher B, Cerisier A, Bouchou K, et al. Silent myocardial ischemia in type 2 diabetes. Predictive value of intima-media thickness. *Presse Med* 2002; 31:218-22.
- [1.38] Sigurdardottir V, Fagerberg B, Hulthe J. Preclinical atherosclerosis and inflammation in 61-year-old men with newly diagnosed diabetes and established diabetes. *Diabetes Care* 2004; 27:880-4.
- [1.39] Karim R, Buchanan TA, Hodis HN, Li Y, Mack WJ. The association of smoking and subclinical atherosclerosis in type 2 diabetes: modification by duration of diabetes. *Diabet Med* 2005; 22:81-7.
- [1.40] Nomura M, Kasami R, Ohashi M, Yamada Y, Abe H. Significantly higher incidence of carotid atherosclerosis found in Japanese type 2

diabetic patients with early nephropathy. *Diabet Res Clin Pract* 2004; 66(Suppl. 1):S161-3.

- [1.41] Ishimura E, Shoji T, Emoto M, et al. Renal insufficiency accelerates atherosclerosis in patients with type 2 diabetes mellitus. *Am J Kidney Dis* 2001; 38(Suppl. 1):S186-90.
- [1.42] Gottsater A, Ryden-Ahlgren A, Szilag B, et al. Cardiovascular autonomic neuropathy associated with carotid atherosclerosis in Type 2 diabetic patients. *Diabet Med* 2003; 20:495-9.
- [1.43] Teno S, Uto Y, Nagashima H, et al. Association of postprandial hypertriglyceridemia and carotid intima-media thickness in patients with type 2 diabetes. *Diabetes Care* 2000; 23:1401-6.
- [1.44] Nagata K, Sasaki E, Goda K, et al. Cerebrovascular disease in type 2 diabetic patients without hypertension. *Stroke* 2003;34 : e232-3; author reply e232-3.
- [1.45] De Angelis M, Scrucca L, Leandri M et al. Prevalence of carotid stenosis in type 2 diabetic patients asymptomatic for cerebrovascular disease. *Diabet Nutr Metab* 2003; 16:48-55.
- [1.46] Touboul PJ, Hennerici MG, Meairs S. Mannheim Carotid Intima-Media Thickness Consensus (2004–2006) *Cerebrovasc Dis* 2007; 23:75–80.
- [1.47] Underhill HR, Kerwin WS, Hatsukami TS, Yuan C. Automated measurement of mean wall thickness in the common carotid artery by MRI: A Comparison to Intima-Media Thickness by B-Mode Ultrasound. *J Magn Reson Imaging*, 2006; 24:379–387

- [1.48] Simon A, Gariépy J, Chironi G et al. Intima-media thickness: a new tool for diagnosis and treatment of cardiovascular risk. *J Hypertens* 2002; 20:159-169
- [1.49] Simon A, Megnien JL, Levenson J. Coronary risk estimation and treatment of hypercholesterolemia. *Circulation* 1997; 96:2449-2452.
- [1.50] Aminbakhsh A, Mancini GB. Carotid intima-media thickness measurements: what defines an abnormality? A systematic review. *Clin Invest Med* 1999; 4:149-157.
- [1.51] Greenland P, Abrams J, Aurigemma FP, Bond MG, Clark LT, Criqui MH, et al. Prevention Conference V: beyond secondary prevention identifying the high-risk patient for primary prevention: noninvasive tests of atherosclerotic burden; Writing Group III. *Circulation* 2000; 101: E16-E22.
- [1.52] Howard G, Sharrett AR, Heiss G, Evans GW, Chambless LE, Riley WA, Burke GL. Carotid artery intimal-medial thickness distribution in general populations as evaluated by B-mode ultrasound. ARIC Investigators. *Stroke* 1993; 9: 1297-1304.
- [1.53] Denarie N, Gariépy J, Chironi G, Massonneau M, Laskri F, Salomon J, et al. Distribution of ultrasonographically assessed dimensions of common carotid arteries in healthy adults of both sexes. *Atherosclerosis* 2000; 2:297-302.
- [1.54] Sharrett AR, Sorlie PD, Chambless LE, Folsom AR, Hutchinson RG, Heiss G, Szklo M. Relative importance of various risk factors for asymptomatic carotid atherosclerosis versus coronary heart disease

incidence: the Atherosclerosis Risk in Communities Study. *Am J Epidemiol* 1999; 149:843-852.

[1.55] Gariépy J, Salomon J, Denarie N, Laskri F, Megnien JL, Levenson J, Simon A. Sex and topographic differences in associations between large-artery wall thickness and coronary risk profile in a French working cohort: the AXA Study. *Arterioscler Thromb Vasc Biol* 1998; 4:584-590.

[1.56] Zanchetti A, Crepaldi G, Bond MG, Gallus GV, Ventura A, Mancia G, et al. Systolic and pulse blood pressures (but not diastolic blood pressure and serum cholesterol) are associated with alterations in carotid intima-media thickness in the moderately hypercholesterolaemic hypertensive patients of the Plaque Hypertension Lipid Lowering Italian Study. PHYLLIS study group. *J Hypertens* 2001; 19:79-88.

[1.57] Poli A, Tremoli E, Colombo A, Sirtori M, Pignoli P, Paoletti R. Ultrasonographic measurement of the common carotid artery wall thickness in hypercholesterolemic patients. A new model for the quantitation and follow-up of preclinical atherosclerosis in living human subjects. *Atherosclerosis* 1988; 3:253-261.

[1.58] Mykkänen L, Zaccaro DJ, O'Leary DH, Howard G, Robbins DC, Haffner SM. Microalbuminuria and carotid artery intima-media thickness in nondiabetic and NIDDM subjects. The Insulin Resistance in Atherosclerosis Study (IRAS). *Stroke* 1997; 9:1710-1716.

[1.59] Bolinder G, Noren A, de Faire U, Wahren J. Smokeless tobacco use and atherosclerosis: an ultrasonographic investigation of carotid intima

media thickness in healthy middle-aged men. *Atherosclerosis* 1997; 132:95-103.

[1.60] Persson J, Formgren J, Israelsson B, Berglund G. Ultrasound-determined intima-media thickness and atherosclerosis. Direct and indirect validation. *Arterioscler Thromb* 1994; 2:261-264.

[1.61] Skoglund-Andersson C, Tang R, Bond MG, de Faire U, Hamsten A, Karpe F. LDL particle size distribution is associated with carotid intima media thickness in healthy 50-year-old men. *Arterioscler Thromb Vacc Biol* 1999; 10:2422-2430.

[1.62] Matthews KA, Owens JF, Kuller LH, Sutton-Tyrrell K, Jansen-McWilliams L. Are hostility and anxiety associated with carotid atherosclerosis in healthy postmenopausal women? *Psychosom Med* 1998; 60:633-638.

[1.63] Lee AJ, Mowbray PI, Lowe GD, Rumley A, Fowkes FG, Allan PL. Blood viscosity and elevated carotid intima-media thickness in men and women: the Edinburgh Artery Study. *Circulation* 1998; 97:1467-1473.

[1.64] McQuillan BM, Beilby JP, Nidorf M, Thompson PL, Hung J. Hyperhomo-cysteinemia but not the C677T mutation of methylenetetrahydrofolate reductase is an independent risk determinant of carotid wall thickening. The Perth Carotid Ultrasound Disease Assessment Study. *Circulation* 1999; 99:2383-2388.

[1.65] Ebrahim S, Papacosta O, Whincup P, Wannamethee G, Walker M, Nicolaides AN, et al. Carotid plaque, intima media thickness, cardiovascular risk factors, and prevalent cardiovascular disease in men

and women: the British Regional Heart Study. *Stroke* 1999; 30:841-850.

- [1.66] Bots ML, van Swieten JC, Breteler MM, de Jong PT, van Gijn J, Hofman A, Grobbee DE. Cerebral white matter lesions and atherosclerosis in the Rotterdam Study. *Lancet* 1993; 341:1232-1237.
- [1.67] Crouse JR III, Craven TE, Hagaman AP, Bond MG. Association of coronary disease with segment-specific intimal-medial thickening of the extracranial carotid artery. *Circulation* 1995; 92:1141-1147.
- [1.68] Salonen JT, Salonen R. Ultrasonographically assessed carotid morphology and the risk of coronary heart disease. *Arterioscler Thromb* 1991;11:1245-1249.
- [1.69] Chambless LE, Heiss G, Folsom AR, Rosamond W, Szklo M, Sharrett AR, Clegg LX. Association of coronary heart disease incidence with carotid arterial wall thickness and major risk factors: the Atherosclerosis Risk in Communities (ARIC) Study, 1987-1993. *Am J Epidemiol* 1997; 146:483-494.
- [1.70] O'Leary DH, Polak JF, Kronmal RA, Manolio TA, Burke GL, Wolfson SK. Carotid-artery intima and media thickness as a risk factor for myocardial infarction and stroke in older adults. Cardiovascular Health Study Collaborative Research Group. *New Engl J Med* 1999; 340:14-22.
- [1.71] Bots ML, Hoes AW, Koudstaal PJ, Hofman A, Grobbee DE. Common carotid intima-media thickness and risk of stroke and myocardial infarction: the Rotterdam Study. *Circulation* 1997; 96:1432-1437.

- [1.72] Hodis HN, Mack WJ, LaBree L, Selzer RH, Liu CR, Liu CH, Azen SP. The role of carotid arterial intima-media thickness in predicting clinical coronary events. *Ann Intern Med* 1998; 128:262-269.
- [1.73] Salonen R, Nyssonen K, Porkkala E, Rummukainen J, Belder R, Park JS, Salonen JT. Kuopio Atherosclerosis Prevention Study (KAPS). A population-based primary preventive trial of the effect of LDL lowering on atherosclerotic progression in carotid and femoral arteries. *Circulation* 1995; 92:1758-1764.
- [1.74] Simon A, Gariépy J, Levenson J. [Is there a clinical future for echographic measurement of intima media thickness]? *Presse Med* 1999;28:1021-1022.
- [1.75] Heart Disease: A Textbook of Cardiovascular Medicine, Fifth Edition, Eugene Braunwald, Douglas P. Zipes, Peter Libby, p. 108, 1997
- [1.76] Atlas of cardiovascular monitoring, Jonathan B., M.D. Mark, Churchill Livingstone; 1st edition (January 15, 1998)
- [1.77] Measuring the ECG signal with a mixed analog-digital application-specific IC, Wolfgang Grossbach, Hewlett-Packard Journal, Oct, 1991, http://findarticles.com/p/articles/mi_m0HPJ/is_n4_v42/ai_11398513
- [1.78] ECG Front-End Design is Simplified with MicroConverter, Enrique Company-Bosch, Eckart Hartmann, Analog Dialogue, Volume 37, November 2003, p1-5
<http://www.analog.com/library/analogDialogue/archives/37-11/ecg.pdf>
- [1.79] Electronics in Medicine and Biomedical Instrumentation, Nandini K. Jog, 2006, 8120329260, p78-101

- [1.80] Schematic diagram of normal sinus rhythm for a human heart as seen on ECG, Atom cz,22:39, 13 January 2007,
<http://en.wikipedia.org/wiki/Image:SinusRhythmLabels.svg>
- [1.81] Conrath CE, Opthhof T. The patient U wave. *Cardiovasc Res* 2005; 67: 184-186
- [1.82] Festa A, D'Agostino R, Rautaharju P, O'Leary DH, Rewers M, Mykkänen L, Haffner SM. Is QT Interval a marker of subclinical atherosclerosis in nondiabetic subjects? The Insulin Resistance Atherosclerosis Study (IRAS). *Stroke* 1999; 30:1566-1571.
- [1.83] Hong C, Becker CR, Huber A, Schoepf UJ, Ohnesorge B, Knez A, Bruning R, Reiser MF. ECG-gated reconstructed multi-detector row ct coronary angiography: effect of varying trigger delay on image quality, *Radiology* 2001Sep; 220(3):712-7.
- [1.84] Picture of the cardiac cycle events occurring in the left ventricle.
February 14th, 2007, DestinyQx,
http://en.wikipedia.org/wiki/Image:Cardiac_Cycle_Left_Ventricle.PNG
- [1.85] Harloff A, Zech T, Frydrychowicz A, Schumacher M, Schöllhorn J, Hennig J, Weiller C, Markl M., Carotid intima-media thickness and distensibility measured by MRI at 3 T versus high-resolution ultrasound. *Eur Radiol.* 2009 Jun; 19(6):1470-9. Epub 2009 Feb 13.
- [1.86] Myers K and Clough A, Making sense of vascular ultrasound: a hands-on guide, Arnold, London, 2004.
- [1.87] Van Bortel LM. "What does intima-media thickness tell us?", Editorial comment, *J Hypertens* 2005; 23(1): 37-39.

- [1.88] Michele Cazaubon MD PhD, Lecture on Intima Media Thickness and Atherosclerosis, slide 6, available online
<http://www.pitt.edu/~super1/lecture/lec3281/006.htm>
- [1.89] R.C.Preston, “2.4.6. Medical ultrasonics”, Kaye & Laby tables of physical and chemical constants, available online at
http://www.kayelaby.npl.co.uk/general_physics/2_4/2_4_6.html
- [1.90] A portable ECG monitoring device with Bluetooth and Holter capabilities for telemedicine applications, Daniel Lucani, Giancarlo Cataldo, Julio Cruz, Guillermo Villegas, Sara Wong, Proceedings of the 28th IEEE EMBS Annual International Conference New York City, USA, Aug 30-Sept 3, 2006
- [1.91] Embedded Wireless Transceivers and Applications in Lightweight Wearable Platforms, Mathew Laibowitz and Joseph A. Paradiso, Responsive Environments Group, MIT Media Laboratory,
http://www.media.mit.edu/resenv/pubs/papers/2003-12-circuit_cellar5.1.pdf

Chapter 2 - Prototyping the ECG monitor

2.1) Introduction

There are two different types of ECG recording: the 3-lead ECG and the 12-lead ECG. The 12-lead ECG (consisting of V1-V6 and also the right leg electrodes in addition to the 3-lead ECG) is usually used to obtain detailed information about the heart. In the present study, the 3-lead ECG provided all the necessary information and thus was chosen over the 12-lead ECG.

The 3-lead ECG can be taken from the positions near to the heart or from each arm. In hospitals, it is preferred to take the ECG near the position of the heart because it is more accurate. Additionally, if the patient lies in a bed, the electrodes can be fixed more securely. Taking measurements from the arms could be inconvenient for both the medical personnel and the patient. These two types of electrode placements for ECG recording are shown in fig 2.1:

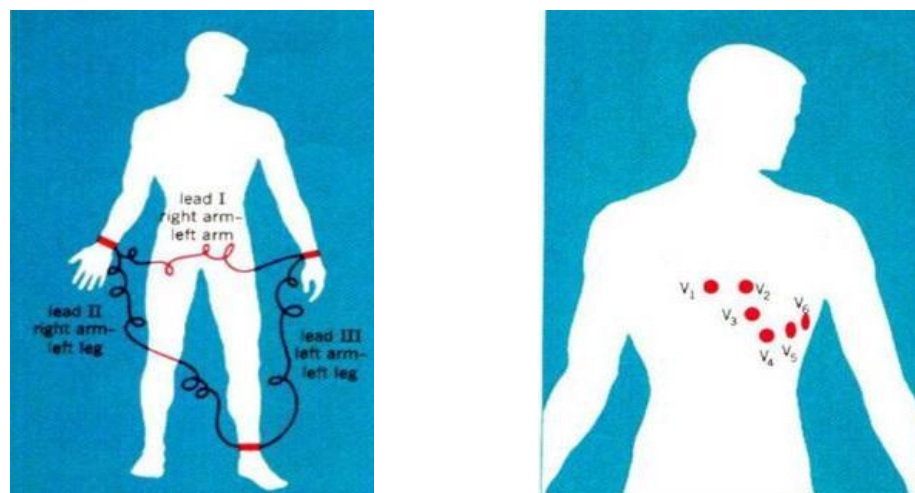


Figure 2.1: Different possibilities of connecting electrodes [2.1]

Both methods are acceptable for triggering ultrasonic scans, and in the developed device, the ECG is acquired from the wrists for simplicity.

The electrodes used in hospitals are designed for a single (disposable) use only. However, different types of electrodes such as clamps, chest straps and stick electrodes can be employed for testing.

A questionnaire form (Appendix A on page 178) was sent to doctors in different departments, such as cardiology, radiology and cardiovascular, to confirm that the decisions made for the development were correct and efficient.

2.2) Instrumental amplifiers

2.2.1) AD624

This instrumental amplifier was used for a final year project completed by Mr. Richard Waddington [2.2]. In his thesis, he analysed the feasibility of using a dsPIC for short time measurements of the heart rate. He used an AD624 instrumental amplifier for the ECG signal amplification.

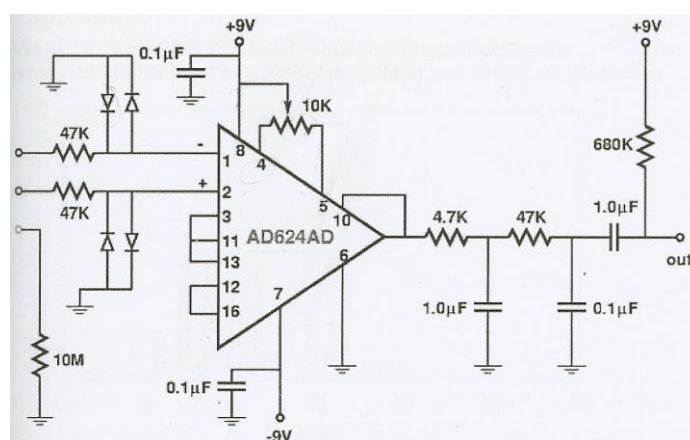


Figure 2.2: Schematic diagram of an ECG monitor
that uses AD624AD [2.2]

This circuit took the signal from two inputs (positive and negative inputs) and output the ECG of the patient. The third input was used as a neutral. The resistors in series provided protection to the patient. The diodes placed between the AD624 inputs and ground ensured protection of the AD624 from electrostatic discharges. The amplification process consisted of a single step. The circuit included a low pass filter at the output to eliminate unwanted noise. The schematic (fig 2.2) used bipolar leads because of configuration of its inputs.

2.2.2) AD620

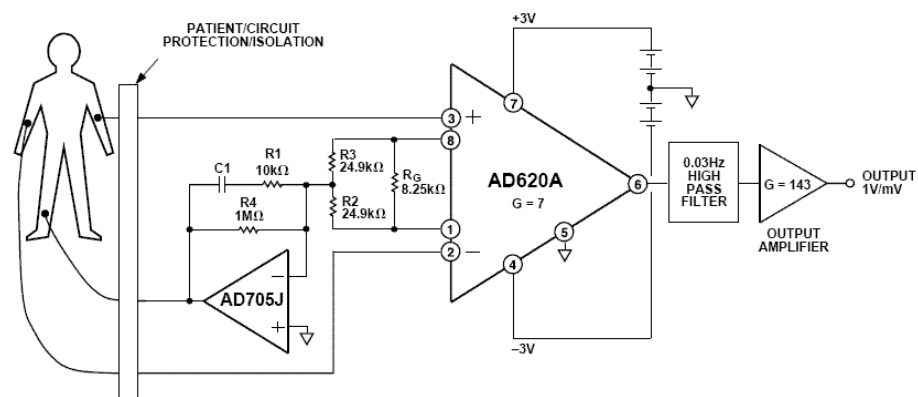


Figure 2.3: Schematic of the ECG monitor based on the AD620A [2.3]

The AD620 was one of the recommended low power and voltage ICs for ECG machines [2.4]. The schematic for the ECG monitor (fig 2.3) uses bipolar leads like the AD624 (fig.2.2), but the AD620 uses a two step amplification with high pass filtering in between.

The other difference is the use of the third electrode, which is connected to the leg and acts as a feedback. It is used for a common-mode rejection to decrease interference. Finally, this instrumental amplifier offers the choice of amplification gain by changing the value of the resistor R_G . The required value can be calculated using the gain formula provided in the datasheet.

2.2.3) INA326

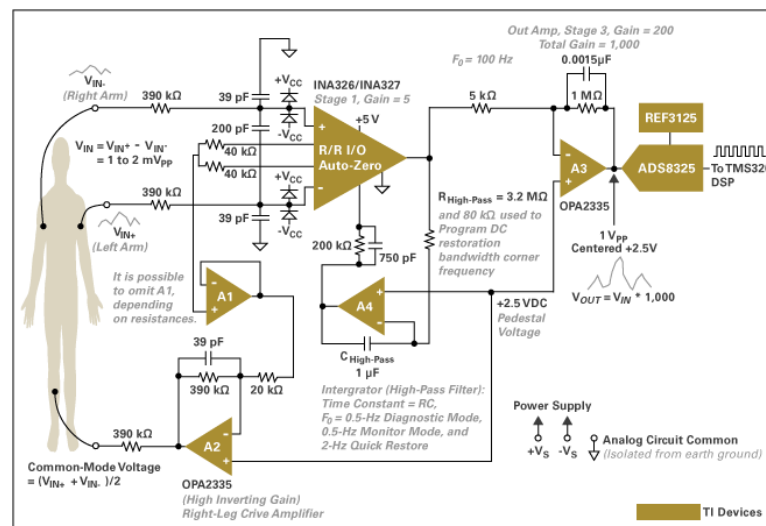


Figure 2.4: Schematic of the INA326 ECG circuit [2.5]

The circuit shown in fig.2.4 is similar to the AD620 instrumental amplifier because it also contains the leg driver op-amp and uses a two stage amplification with a filter between the stages. The circuit is more complex because of its unipolar power supply. Resistors of the same value are added at each input in series, which helps to protect the patient from being shocked in case of a serious hardware fault. The resistance differs from circuit to circuit and it is calculated depending on the circuit. The gain of this instrumental

amplifier can be set easily using the information provided in the datasheet [2.6].

2.2.4) INA118

This instrumental amplifier already had an example of an ECG monitor in its datasheet [2.7]. It was one of the instrumental amplifiers that had a SPICE model, which could be used to simulate the operation of the IC under various conditions.

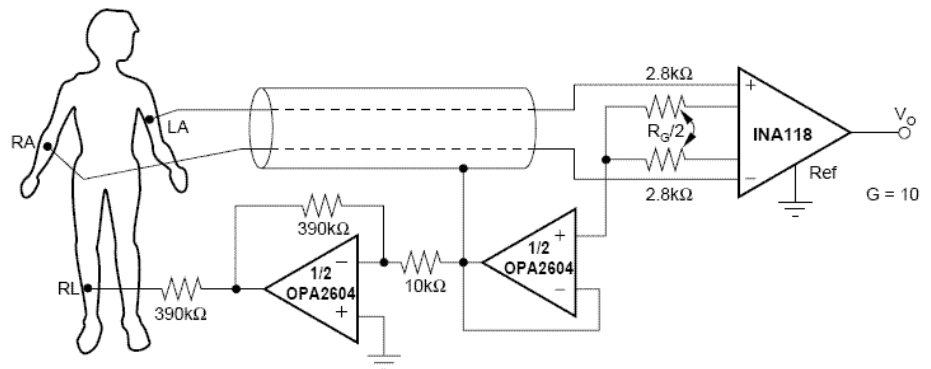


Figure 2.5: Schematic of the ECG monitor based on the INA118 [2.7]

The schematic for the INA118 (fig 2.5) is similar to the previous two schematics, as it uses a leg driver and a resistor to set the output gain. It uses single step amplification. No output filter is shown in fig.2.5 but one can be easily added to the output.

2.2.5) AD623

Another ECG monitor uses AD623 (fig.2.6, [2.8]).

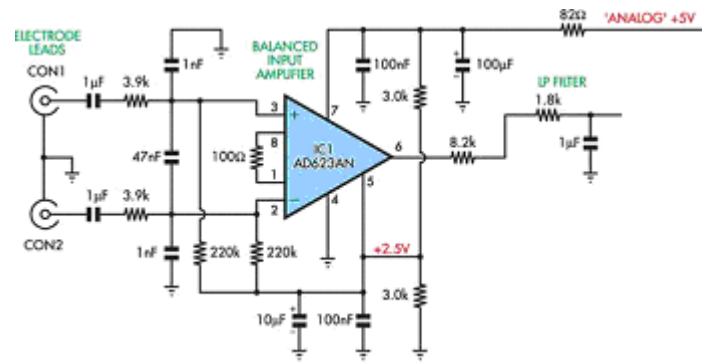


Figure 2.6: ECG monitor that uses the AD623 instrumental amplifier [2.8]

Only part of the complete schematic is presented in fig 2.6 to allow comparison of the different instrumental amplifiers in the same conditions. Two electrode inputs are shielded and series input resistors are also used to protect the patient. This was single step amplification and a low pass filter was used at the output to eliminate the unwanted noise.

2.3) Which amplifier to choose?

Fig.2.7 presents three ways of implementing an ECG signal amplifier.

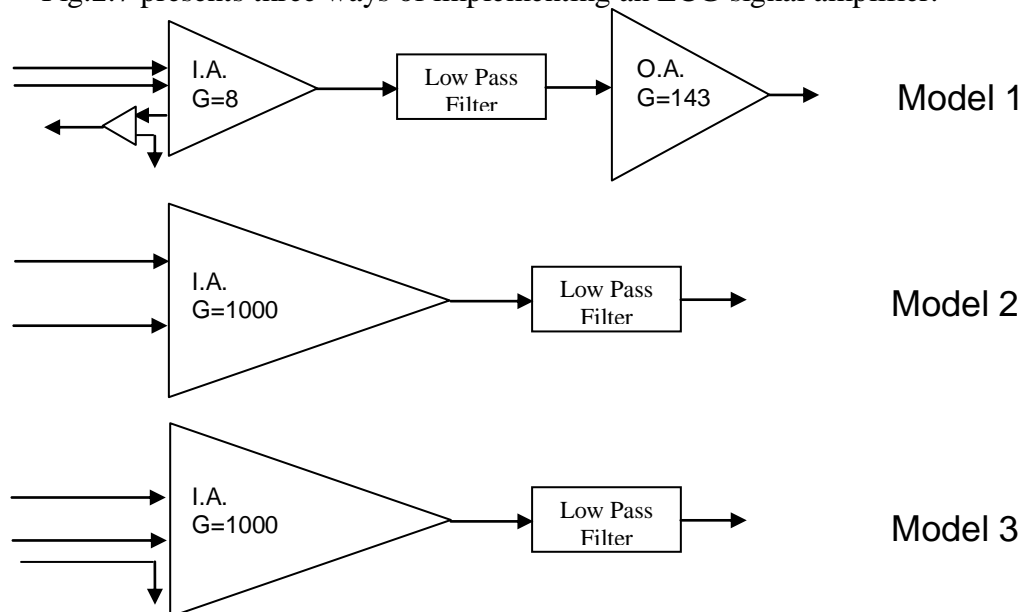


Figure 2.7: Block diagram of three options for the ECG signal amplifier

The advantages and disadvantages of these architectures are compared in fig 2.8.

Designs	Advantages	Disadvantages
Model 1	- Two step amplification has a lower noise when compared to single step amplification	- If the value of gain (G) is not well decided for both amplifiers then this will not give an accurate reading
Model 2	- Less circuitry and one step amplification is useful for simple ECG machines for experimenting	- There is no third electrode in the system.
Model 3	- It is better to have some shielding for protection rather than having none and the noise at the output is low	- The third electrode goes to ground but it does not interact with the circuit.

Figure 2.8: Table comparing the amplifiers showing their advantages and disadvantages

Each amplifier has its advantages and disadvantages, and all were simulated to compare their performance.

2.4) Simulation of the amplifiers

The amplifiers were simulated using the unrestricted freeware simulation program LTSpice from Linear Technology. The noise level and small signal AC magnitude responses were of primary interest.

Because the instrumental amplifiers are intended for use in an ECG application, the Common Mode Rejection Ratio (CMRR) was also considered. Higher CMRR can help to cancel out the signals common to both inputs. Fig.2.9 shows the results obtained for the amplifiers during their simulation in LTSpice.

Amplifier	Gain	Noise	CMRR
AD620A	213	60uV/sqrt(Hz)	130 dB
AD624	400	400uV/sqrt(Hz)	120 dB
AD623	18dB	40uV/sqrt(Hz)	110 dB
INA118	-	3uV/sqrt(Hz)	125 dB
INA326	-	800pV/sqrt(Hz)	114 dB

Figure 2.9: Comparison of the simulation results

Fig 2.9 shows that the AD620A provides the best CMRR, and the AD623 the worst. Based on fig.2.9, AD624, AD620A and INA326 were selected for prototyping.

2.5) Prototyping the instrumental amplifiers

Use of a breadboard for prototyping was possible because the ECG frequencies did not exceed 150Hz [2.9]. Two breadboards were considered, the AD-12 [2.10] and the Matsuhama [2.11] (fig.2.10). The latter was selected because its size enabled prototyping all three circuits together, which made comparative measurements easier.

	Matsuhama	KandH AD-12
Size	243x 195x 20mm	184x 168x 24mm
Contacts	2420	1906
Bornes	4	5
Jump Wire Kit	Yes	Yes

Figure 2.10: Comparison of two breadboards

The breadboard was divided in such a way that made it easy to find any component and its parent circuit, in case any changes were necessary . Once the whole prototyping was completed, each connection was tested with a digital multimeter for short circuits and wrong connections before powering up the breadboard. The prototyped board is shown in fig 2.11.

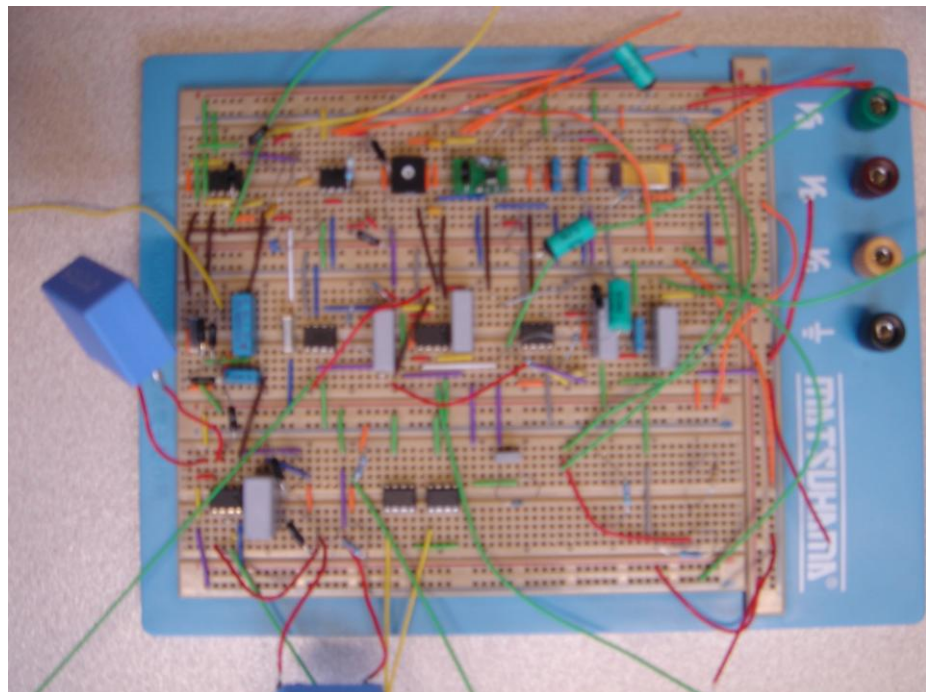


Figure 2.11: Prototyped breadboard that includes all of the instrumental amplifiers

2.6) Testing of the amplifiers on a breadboard

2.6.1) Potential divider for testing the amplifiers in sinusoidal mode

As discussed earlier, the human ECG signal can vary between 0.1 and 5mV. Therefore, the amplifiers needed to be tested using comparable voltage levels. A signal generator available in the UDSP Laboratory could produce a minimum output voltage of 250mV [2.12]. This voltage was attenuated by a potential divider (fig.2.12 presents a one stage divider that created too much interference; thus, the two stage divider shown in fig.2.13 was used for measurements).

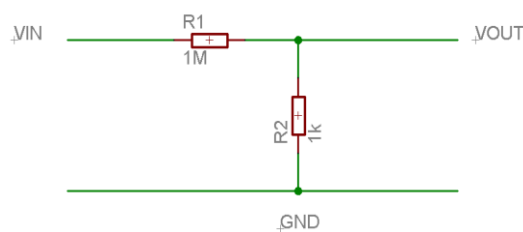


Fig 2.12: First version of potential divider

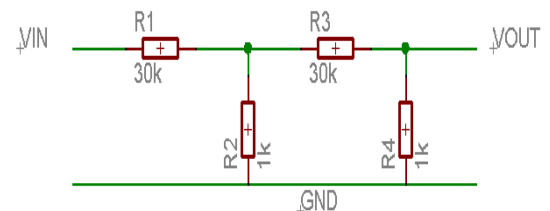


Fig 2.13: Final version of potential divider

2.6.2) Supply voltage source

When a sinusoidal input signal was applied to the assembled breadboard, the output noise level was 236.2 mV (fig 2.14). This noise was caused by the power supply used (fig.2.15, the noise level is stated at the bottom left of the diagram).

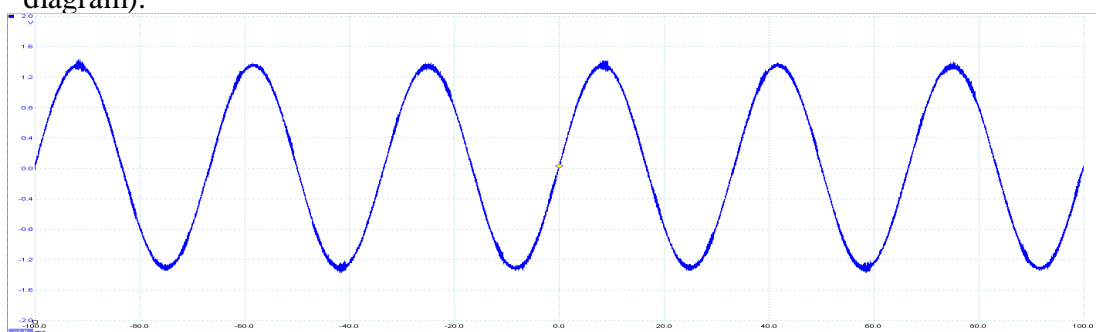


Figure 2.14: Output waveform showing high noise level

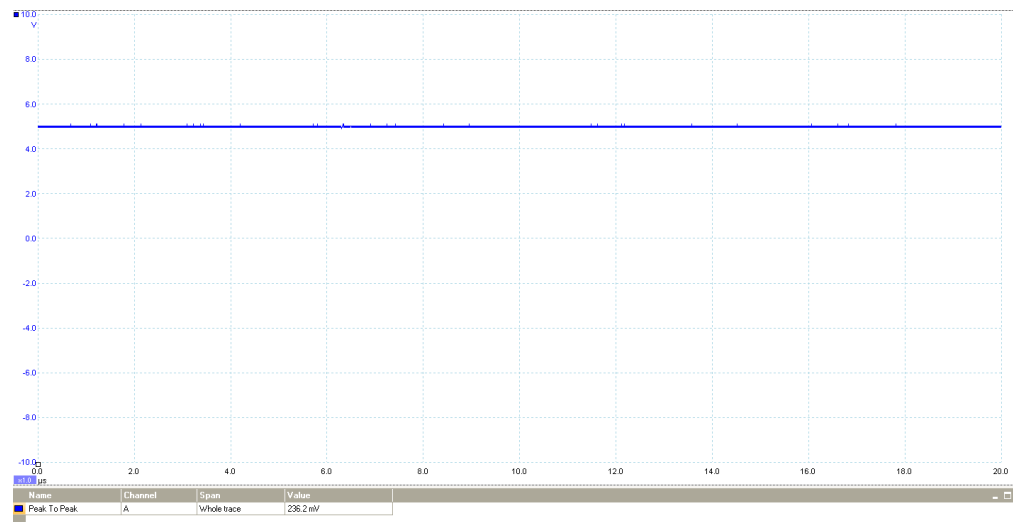


Figure 2.15: The output voltage of the laboratory power supply (the noise level is stated in the bottom left corner)

The power supply datasheet stated that it had a maximum noise level of 100mVpp [2.13]. This noise level was considered unsuitable for the application alone, because the operation of an ECG monitor is subject to interference from factors such as:

- Power-line interference (where harmonics and 50-60 Hz pickup could occur from the power mains)
- Electromagnetic interference, which could occur from other electronic devices, with the electrode wires serving as antennas, and noise coupled from other electronic devices, usually at high frequencies.

Therefore, the power supply unit was built on a veroboard and it included voltage regulators. Fig.2.16 and 2.17 present the schematic and a photograph of the assembled power supply.

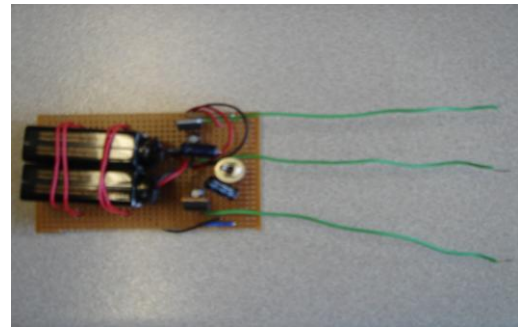
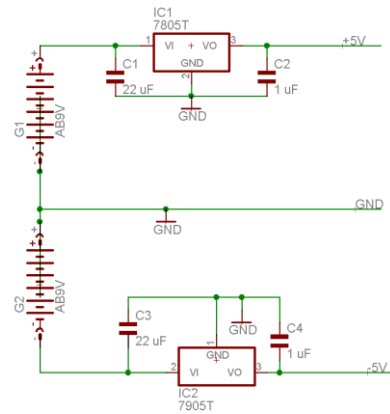


Figure 2.16: The schematic diagram of the developed power supply Figure 2.17: Photograph of the assembled power supply

The assembled power supply provided noise of 7.087mV pp only (fig 2.18), and ensured much clearer output waveform (fig 2.19).

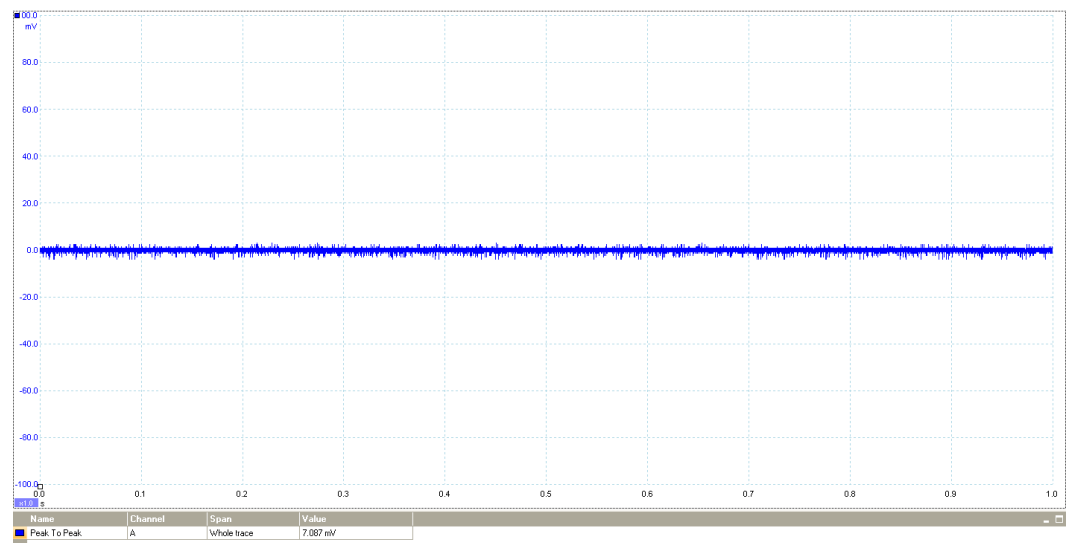


Figure 2.18: AC waveform of the voltage at the output of the developed power supply (the noise level is stated in the bottom left corner)



Figure 2.19: The improved output waveform of the ECG monitor

2.6.3) AD624 testing

The AD624 was tested first with a sinusoidal input. The gain was set to 1000 and the output signal is presented in fig 2.20.

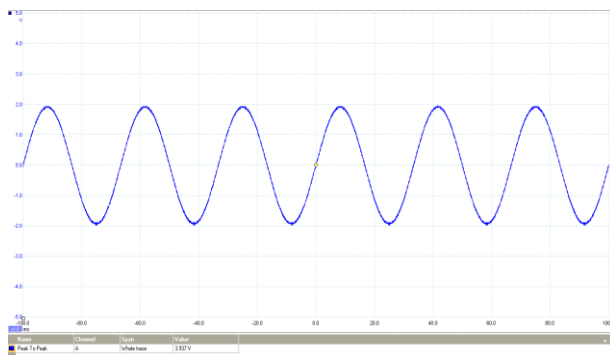


Figure 2.20: Waveform of the output signal

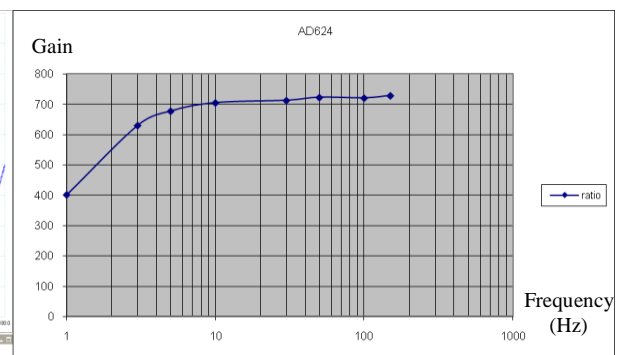


Figure 2.21: Frequency response of the AD624

The magnitude response of the AD624 was measured at the set of frequencies (1, 3, 5, 10, 30, 50, 100, 150 Hz), and is presented in fig.2.21. After preparation of suitable ECG cables (this is discussed later), an in vivo ECG waveform was acquired from a patient (fig.2.22).

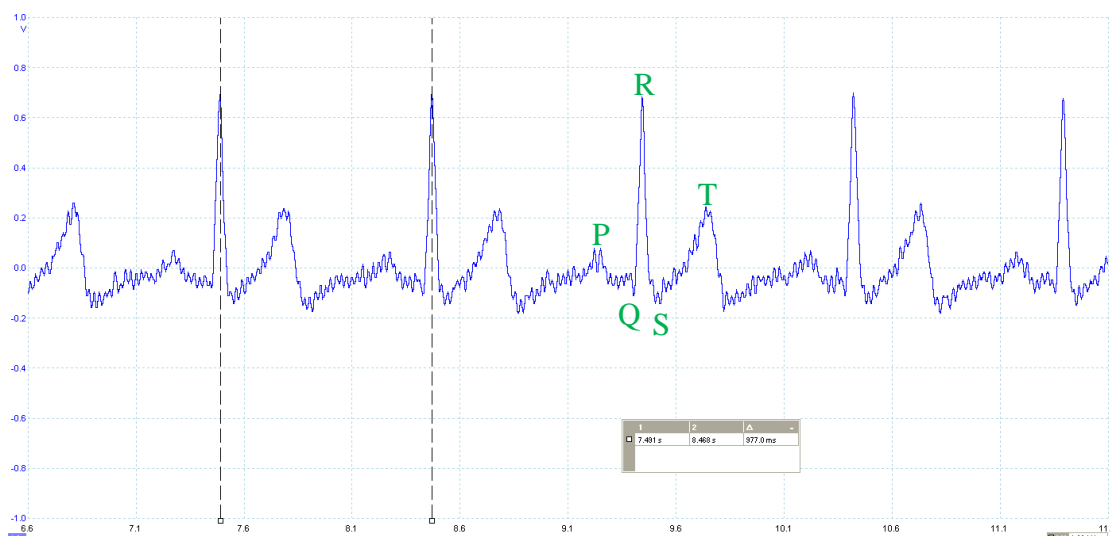


Figure 2.22: ECG signal recorded in vivo using the AD624

The P, R and T waves are clearly visible in fig.2.22 whilst Q and S waves are obscured with noise. Relevant amplitudes and intervals discussed in chapter 1.3 were found within the expected range. The amplitude of the R wave (that corresponds to the maximum amplitude of the complete signal) was 881.9mV.

The low pass filter that was used at the output of the instrumental amplifier to reject the unwanted noise interference performed well and it was decided that this filter (available on the breadboard) would be used for the other amplifiers if required.

2.6.4) AD620

Initially, the assembled circuit did not work, and it was decided to replace the leg driver with a resistor, and to use a single resistor to set the amplifier gain. According to the AD624, the resistor value was calculated as follows:

$$G = \frac{49.4k\Omega}{R_G} + 1$$

$$R_G = \frac{49.4k\Omega}{G - 1} = \frac{49.4k\Omega}{1000 - 1} = 49.45\Omega$$

Therefore, the circuit was modified as shown in fig 2.23.

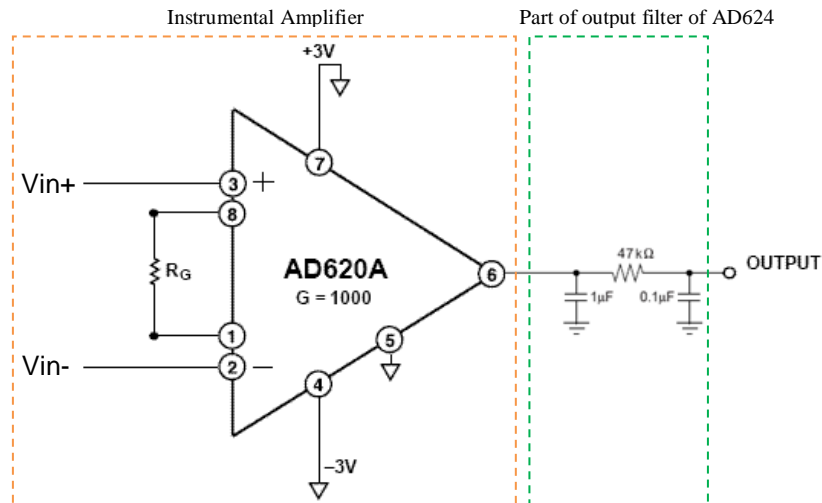


Figure 2.23: Modified schematic for the AD620A

First, the assembly was tested for sinusoidal input signals. The example output waveform is presented in fig.2.24, and the magnitude response in fig.2.25.

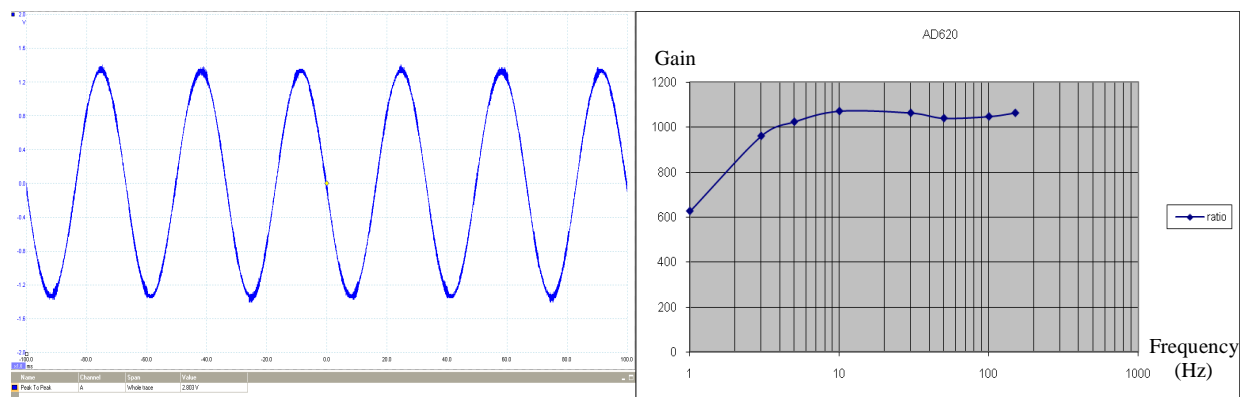


Figure 2.24: Waveform of the output signal Figure 2.25: Magnitude response of the AD620A

An example ECG waveform, recorded in vivo from the same subject as before, is presented in fig.2.26.

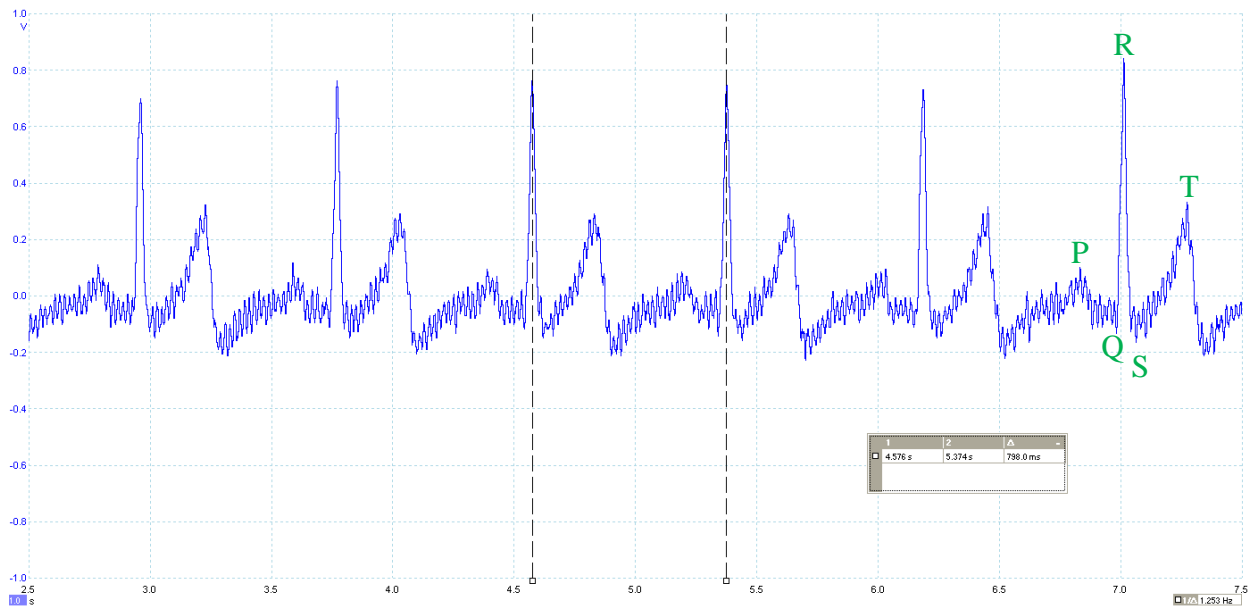


Figure 2.26: ECG signal recorded in vivo using the AD620A

Regarding the previous instrumental amplifier, the P, R and T waves could be easily identified. However, Q and S waves were obscured with noise, as before. The noise level was slightly greater than that obtained with the AD624.

2.6.5) INA326

The circuit assembled on a breadboard according to the schematic discussed above did not work initially, and it was replaced by a simpler circuit from the datasheet, with a low pass filter at the output (fig.2.27).

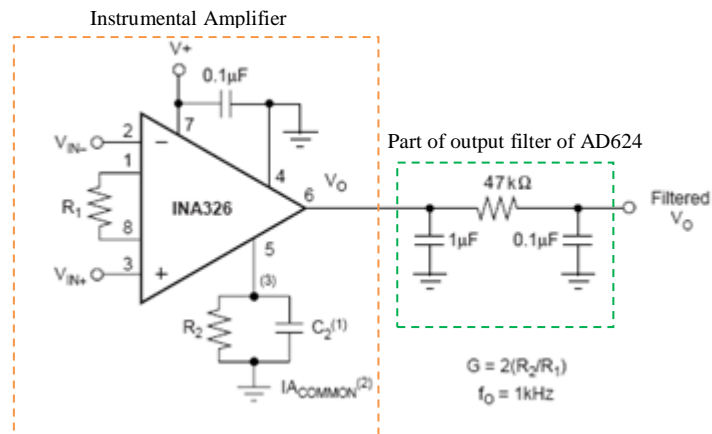


Figure 2.27: Schematic for single step amplification with INA326 that includes the output low pass filter

For the gain of 1000, the datasheet recommends the following values:

$R_1=2\text{k}\Omega$, $R_2=1\text{M}\Omega$ and $C_2=0.1\text{nF}$. After this modification, the IC was tested for sinusoidal input signals (fig 2.28 and 2.29).

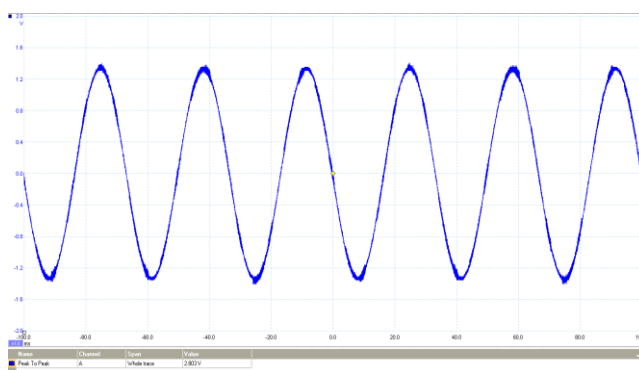


Figure 2.28: Waveform of the output signal

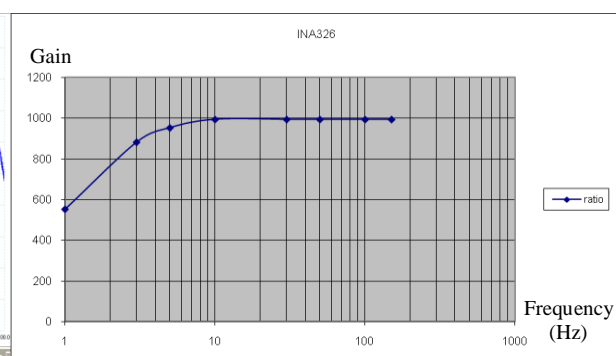


Figure 2.29: Magnitude response of the INA326

An example of an ECG, recorded in vivo from the same subject as before, is presented in fig.2.30.

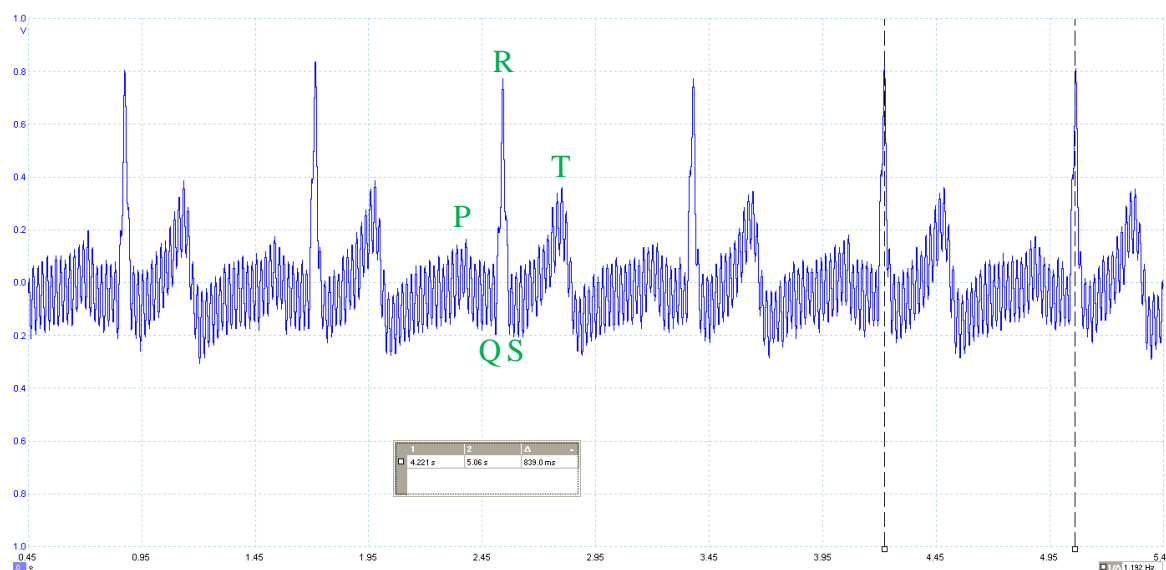


Figure 2.30: ECG signal recorded in vivo using the INA326 without output low pass filter

Regarding the previous instrumental amplifiers, the P, R and T waves could be easily identified. Q and S waves were obscured with noise as before. The noise level was slightly greater than that for the previously tested ICs. Nevertheless, it was decided to use this amplifier as it provided the convenience of using a unipolar power supply unlike its alternatives.

2.6.6) ECG pads

A wide choice of suitable ECG electrodes was available [2.14]. After analysis of the questionnaires filled out by medical practitioners (page 178 in the appendix A), wet gel flexible disposable electrodes were chosen for use [2.15, 2.16]. These electrodes provide the following advantages:

- their flexibility allows for better electrical contact as body contours are often irregular;
- regularly shaped rigid electrodes may not always work;

- disposable electrodes prevent the possibility of spreading infection;
- they have a convenient and secure connector for conventional banana plugs.

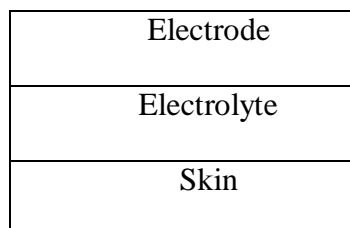


Figure 2.31: The layers between the electrode and the skin [2.17]

The selected electrodes are made out of Ag/AgCl, which has a potential difference of +1.2V compared to the Hydrogen electrode [2.17]. Good contact between the skin and the electrode is provided by a layer of electrolyte (fig.2.31), e.g. saline or an ECG gel. The potential difference between the electrodes for the saline and the ECG gel is 0.25mV and 0.47mV respectively [2.17]. If the electrodes are not in a good permanent electrical contact with the skin, they will pick up extra noise.

Other reasons for possible poor contact with the skin include motion of the patient (even breathing results in slight hand movements) and evaporation of the electrolyte after some time.

2.6.7) Connecting the ECG electrodes to the ECG monitor

The three wires connecting the electrodes to the ECG monitor should be of equal length in order to maintain the balance of the ECG monitor input stage. The selected ECG pads are connected to the cable with banana plugs, and 4mm banana connectors were considered for the input of the ECG monitor to maintain consistency of connectors. Use of unshielded wires

(fig.2.32) resulted in high level of noise, both for sinusoidal waves and for the ECGs. Therefore, shielded wires (fig.2.33) were used instead.



Figure 2.32: Unshielded unbendable wires for connections

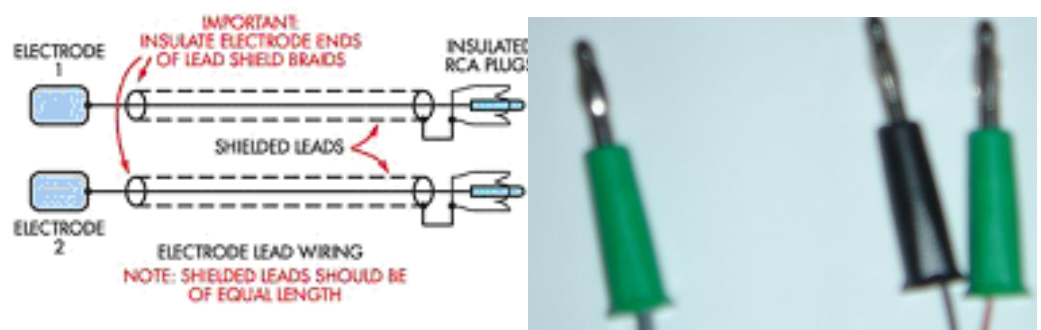


Figure 2.33: Shielded bendable wires

Three differently coded cables (green for leg, red for right hand, blue for left hand) were prepared and they performed in an acceptable manner.

2.6.8) Filters

Analogue filtering of the raw ECG signals is required to remove artefacts, and a combination of high pass (cut off frequency of 0.5 Hz) and low pass (cut off frequency of 40 Hz or above) is recommended for ECG monitoring [2.18]. A diagnostic mode would require a high pass filter with a cut off frequency of 0.05Hz and different selection of low pass filter with either 40, 100 or even 150Hz cut off frequencies to allow accurate measurements of the

ST segment duration for clinical information [2.18]. Even higher frequencies exist in ECG signals [2.19]. Use of a low pass filter with a cut off frequency of 40Hz or less results in some loss of important clinical information because such filtering decreases the amplitude of the ECG waves [2.20]. However, if the cut off frequency is set above 40 Hz, this results in the presence of power line interference and muscle artefacts [2.21]. In this development, which concerns triggering of an ultrasonic instrument at a specific point in the cardiac cycle, the cut off frequency can be lowered. We considered a 20 Hz cut off frequency in addition to 40 Hz.

A filter in signal processing is a circuit that removes specific unwanted features of a signal. In this development, different filters could be applied, as shown in fig.2.34.

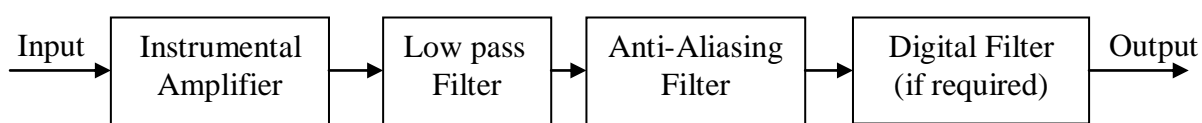


Figure 2.34: Diagram showing the interconnection of different filters for the ECG monitor

An anti-aliasing analogue filter is required before the analogue-to-digital conversion in order to remove spectral components above half of the sampling frequency, and the digital filter could reduce the noise further, if necessary. Of the types of analogue filters available (namely Bessel, Butterworth or Chebyshev), the Bessel filter was selected due to its better phase response (flatter group delay) compared to the others (fig. 2.35, [2.22]).

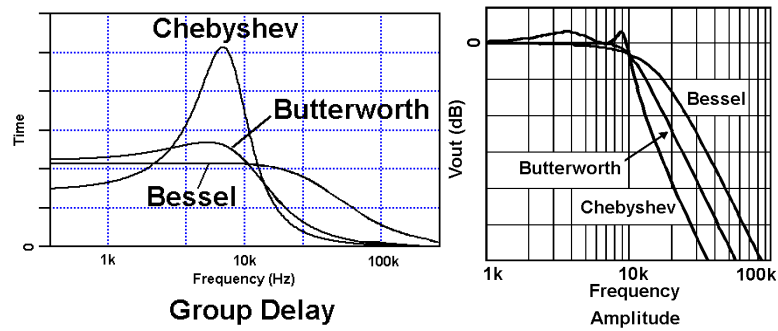


Figure 2.35: Group delays and magnitude responses
of the considered filters

This feature minimises linear signal distortions to the input signal that seemed important for the ECG, as it contains separately triggered pulse waves. The digital filtering could be provided by the PIC before the transmission.

A “FilterLab” program (developed by Microchip [2.23]) was used to design the anti-aliasing filter with the cut off frequencies of 20 and 40 Hz. The schematics of both of the filters can be found on pages 180-181 in the appendix B and C. The frequency response of both the filters created by the software is shown in fig 2.36 and fig 2.37.

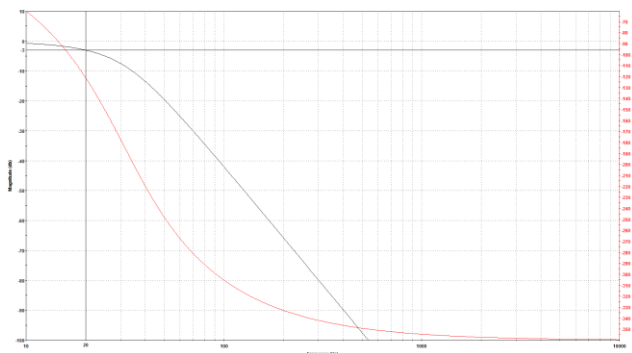


Figure 2.36: Calculated frequency response
of the 20Hz filter

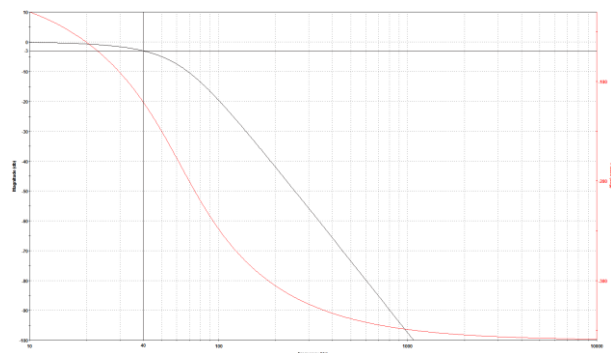


Figure 2.37: Calculated frequency
response of the 40Hz filter

These calculated values were compared with the measured values (fig 2.38 and 2.39) for the filters prototyped on the breadboard and were found compatible.

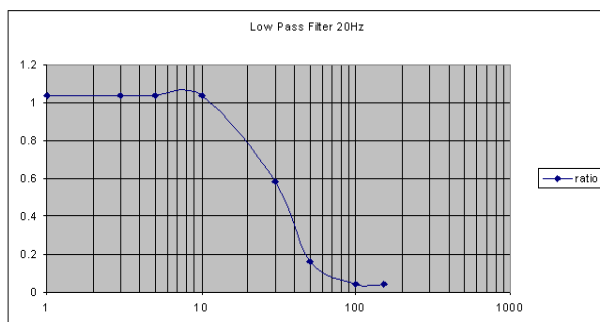


Figure 2.38: Measured magnitude response of the 20Hz filter

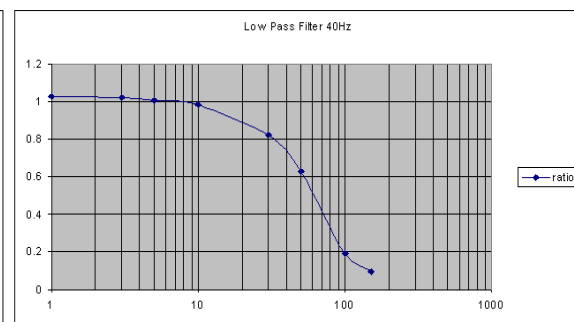


Figure 2.39: Measured magnitude response of the 40Hz filter

The filter with the 20 Hz cut off frequency allowed better rejection of the mains interference compared to the other one. Because the mains interference was observed as the major noise source during the experiments, the former filter was selected for later use.

2.7) Digital filter

All of the required ECG signals were acquired from the same person in order to have a controlled environment for fair comparison. Once all of the data were collected from the three instrumental amplifier circuits, they were saved in Matlab file format, which could then be used to examine the data that were acquired.

The processing algorithm is shown in fig 2.40. First, the data that has been recorded using the digital oscilloscope with a very high sampling

frequency (200 kHz) were decimated to the sampling frequency of 1 kHz. A linear-phase FIR filter was then created using the Parks-McClellan algorithm to digitally filter out the high frequency noise. The raw data of the recorded ECG and their frequency spectrum were plotted before and after processing, in order to find the correct order and cut off frequency for the clearest ECG.

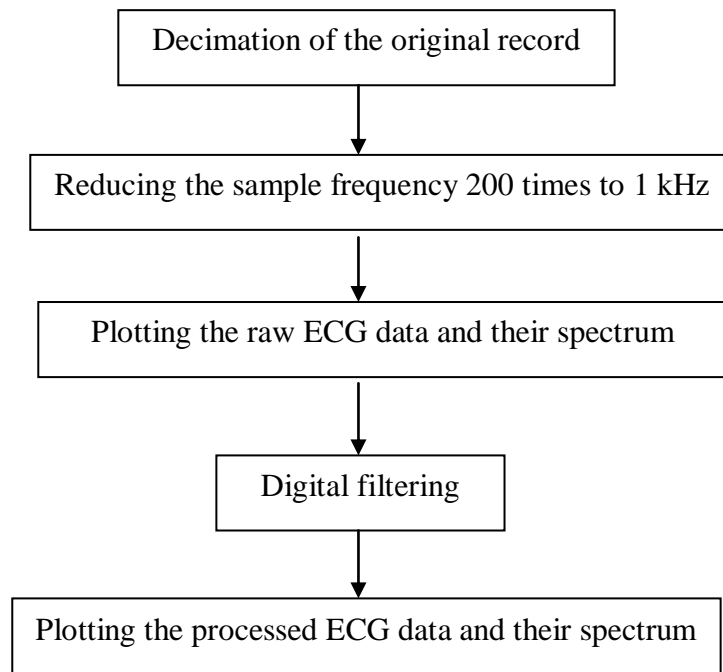


Figure 2.40: Flow diagram of the digital filtering done in Matlab

The data were collected for all three prototyped amplifiers and the results are shown in fig.2.41. It is necessary to mention that the red graph was accidentally acquired at the sampling frequency higher than 200 kHz but was not detected at the time of the data acquisition. For this reason, the frequency of the principal interference appears at a lower frequency than the 50 Hz mains frequency, and higher harmonics of the mains frequency are missing from the graph.

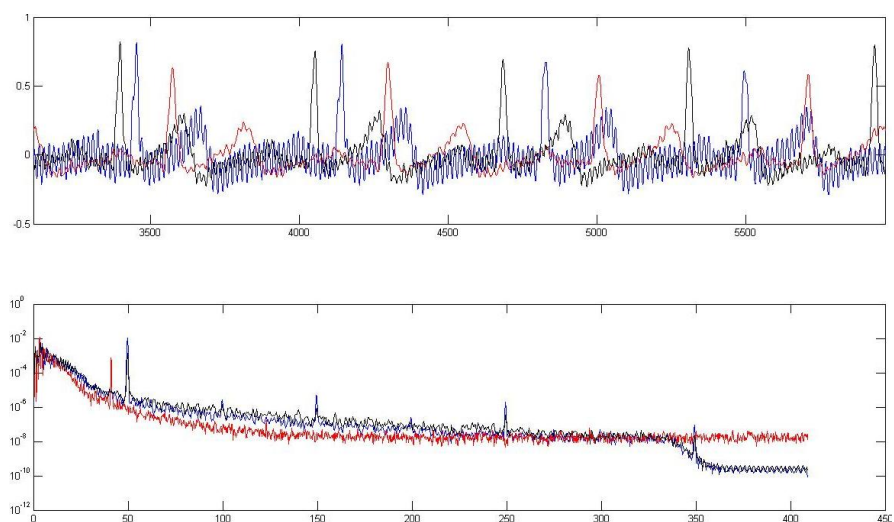


Figure 2.41: Waveforms and spectra of ECG signals acquired in vivo

Fig.2.41 shows that a substantial level of the mains interference was present in the signal, even after the analogue low pass filtering. A band stop digital linear phase filter with a notch frequency of 50Hz was designed in order to reduce this noise. After considering various values for the filter order, the desired magnitude response and the weight function, the filter eliminated much of the mains noise, as shown in fig.2.42.

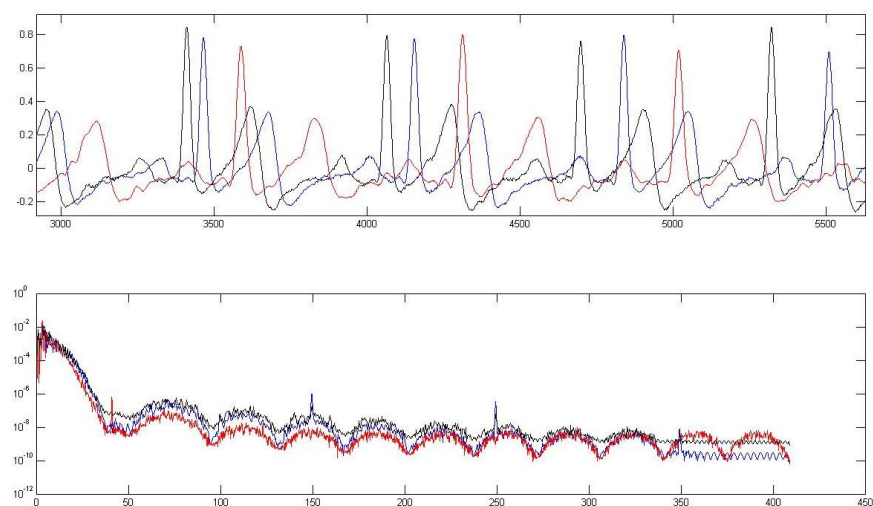


Figure 2.42: Waveform and frequency spectrum of the ECG signals processed by the designed digital filter

The spectra of the processed signals show that the third and fifth harmonics of the mains frequency were intact for two signals. Because of the improper sampling frequency, the mains interference was not completely eliminated for the third signal. However, the processed signals were considered to be sufficient to trigger the ultrasonic scans.

During subsequent experimentation, the generated trigger signal was found to be stable even without using the digital filter, because the triggering was related to the well recognisable R wave peak.

2.8) Power supply

The most important issue to be considered is the patient's safety. Running an ECG machine from the mains power supply adaptor would put the patient at a potential risk of an electric shock in the case of fatal equipment failure.

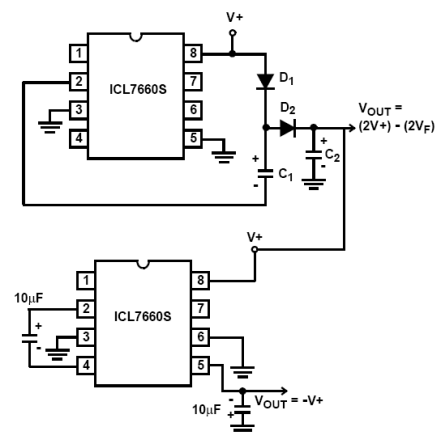


Figure 2.43: Schematic of the voltage doubler and inverter

To overcome this problem, battery powered medical instrumentation can be used. A battery (or rechargeable battery, or two or more batteries used in series) was estimated to provide at least 3V for the ECG monitor. This

voltage would not be sufficient for the operation of the rfPIC, and some of the amplifiers discussed above required a bipolar power supply.

Consequently, the use of a DC/DC converter was considered (fig 2.43). Fig.2.44 shows the experimentally measured voltages when the converters were prototyped on the breadboard.

	Voltage In	Voltage Out
Test 1	5 V	9.41 V
Test 2	3 V	5.15 V

Figure 2.44: Table showing the different voltage outputs

The output voltage is lower than two times the input voltage because of the voltage drop at the diodes, as described by the following equation:

$$V_{out} = 2V - 2V_f,$$

where V_{out} is the output voltage, V_f is the forward voltage drop of the diodes.

A photograph of the fully completed breadboard is shown in fig.2.45. Different parts of the ECG prototype are shown bounded by lines of different colours.

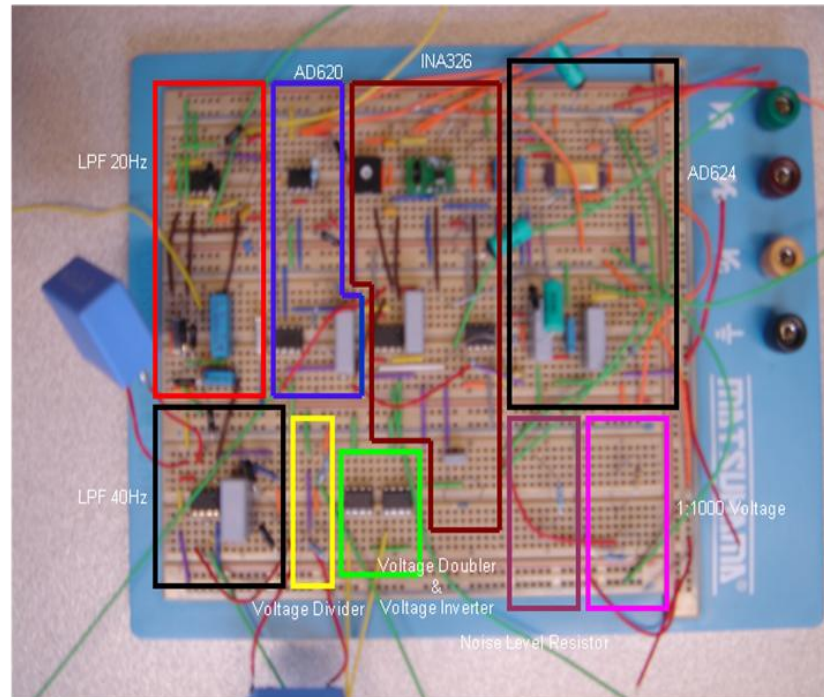


Figure 2.45: Photograph of the complete prototype breadboard

2.9) Selection of a microcontroller capable of RF communications

Several options were available for a design of a microcontroller capable of some RF communication [2.24]. After consideration of alternatives, the rfPIC was selected because some expertise and development tools for this microcontroller were available in the department. The rfPIC can be used as an interface between the ECG amplifier and the ultrasound machine to trigger ultrasonic scans at a specified time to obtain the IMT of the patient. Another advantage of this device is its re-programmability, which allows easy debugging. The rfPIC Development Kit was available from the department to familiarise with the rfPIC. Of the two operating frequencies available for rfPICs (315 MHz and 433.92 MHz that require no license to operate), the lower was selected for operation. The analysis of the schematic for the rfPIC

development kit [2.25] showed that it can be easily adapted for the ECG monitor with some changes to ADC inputs and digital input/output pins, shown by dashed rectangles in fig.2.46.

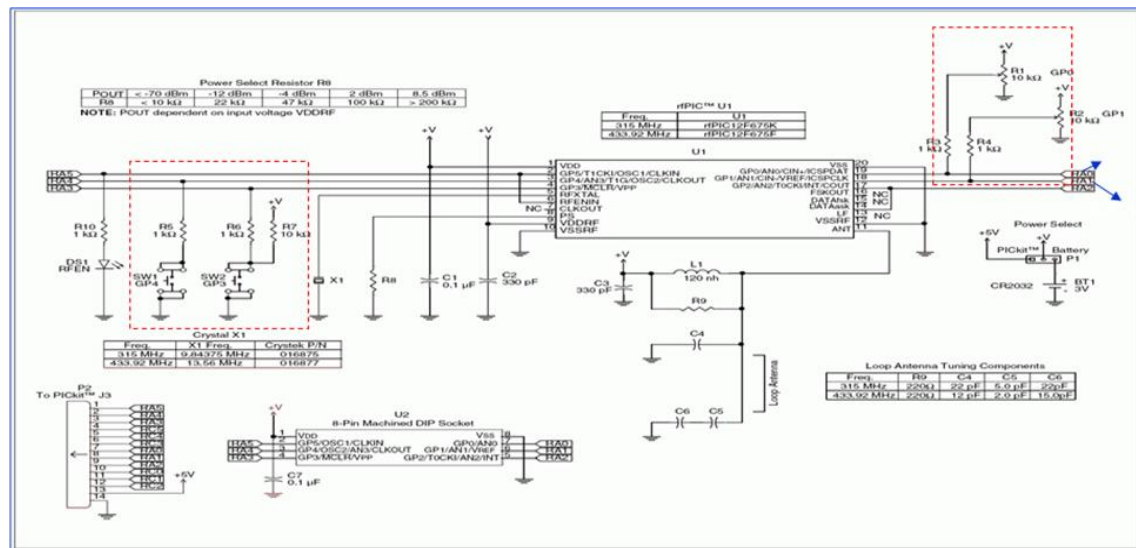


Figure 2.46: Schematic of the rfPIC development kit [2.25] showing the modifications for the ECG monitor

Because only minor changes for the schematic were anticipated, it was not necessary to prototype the rfPIC part of the ECG monitor on a breadboard.

2.10) Voltage reference

A voltage reference IC produces a fixed voltage independent of factors such as the load on the component, power supply voltage and temperature changes. Voltage references are used to obtain a specific and exact voltage value that is independent of the voltage from the power supply. These voltage references are used for variety of precision applications, but mainly for analogue-to-digital conversions [2.26].

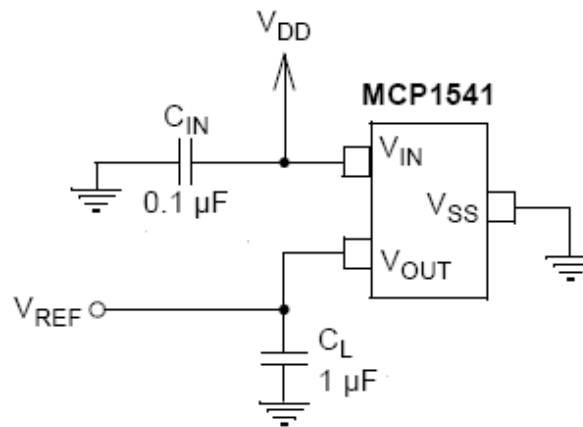


Figure 2.47: Schematic of the voltage reference

The voltage reference will be used with the rPIC in order to supply a reference voltage of 4.096V for the 10-bit Analogue to Digital Converter from the Vref output (fig 2.47). This circuit was prototyped and tested, and the results obtained were fully compliant with the datasheet specifications [2.27].

2.11) References:

- [2.1] <http://faculty.etsu.edu/currie/electrocardiography.htm>, Accessed October 2008
- [2.2] Waddington, Richard, Feasibility study of application of dsPICs to medical electronics, 2005, The University of Nottingham
- [2.3] Datasheet of AD620, http://www.analog.com/static/imported-files/data_sheets/AD620.pdf
- [2.4] <http://www.analog.com/library/analogDialogue/archives/37-11/ecg.pdf>
- [2.5] <http://focus.ti.com/lit/ml/slyb108b/slyb108b.pdf>
- [2.6] Datasheet of INA326, <http://focus.ti.com/lit/ds/symlink/ina326.pdf>
- [2.7] Datasheet of INA118, <http://focus.ti.com/lit/ds/symlink/ina118.pdf>

- [2.8] USB Electrocardiograph, Jim Rowe, Everyday Practical Electronics, Vol. 36 No. 1, November 2007, 02623617
- [2.9] Guler NF, Fidan U. Wireless Transmission of ECG signal. J Med Systems 2006; 30(3):231-235
- [2.10] Datasheet of kandh AD-12 breadboard,
http://www.kandh.com.tw/kh/e_product/yellow/AD%20Series.pdf
- [2.11] Specifications of matsuhama breadboard,
<http://cpc.farnell.com/jsp/level5/module.jsp?moduleId=cpc/263325.xml>
- [2.12] Datasheet of Picoscope 5200,
<http://www.picotech.com/document/pdf/ps5000-en.pdf>
- [2.13] Datasheet of power supply, <http://www.lascarelectronics.com/pdf-usb-datalogging/data-logger0848619001197300050.pdf>
- [2.14]
http://www3.3m.com/catalog/uk/en002/healthcare/hospital_community/node_S5VS2C7KQ3be/root_K3BHNB8005gv/vroot_KQ98DZHKZ4ge/gvel_C5B8TM34HSgl/theme_uk_hospitalcommunity_3_0/command_AbcPageHandler/output_html
- [2.15]
http://www3.3m.com/catalog/uk/en002/healthcare/hospital_community/node_Q56R1WZ52Wbe/root_K3BHNB8005gv/vroot_KQ98DZHKZ4ge/gvel_C5B8TM34HSgl/theme_uk_hospitalcommunity_3_0/command_AbcPageHandler/output_html
- [2.16]
<http://multimedia.3m.com/mws/mediawebserver?66666UuZjcFSLXTtlXMX5XTXEVuQEcuZgVs6EVs6E666666-->

- [2.17] Electronics in Medicine and Biomedical Instrumentation, Nandini K. Jog, 2006, 8120329260
- [2.18] <http://en.wikipedia.org/wiki/Ecg>
- [2.19] Trägårdh E, Schlegel TT. High-frequency QRS electrocardiogram, Clin Physiol Funct Imaging 2007; 27 (4):197 - 204
- [2.20] García-Niebla J, Serra-Autonell G. Effects of inadequate low-pass filter application, J Electrocardiol 2009; 42 (4): 303-304
- [2.21] Weay CT , Horng FC, Nadarajah S. PC based ECG monitoring system, http://www3.ntu.edu.sg/eee/urop/congress2003/Proceedings/abstract/NTU_SCE/Foh-SCE.pdf
- [2.22] <http://www-k.ext.ti.com/SRVS/Data/ti/KnowledgeBases/analog/document/faqs/bes.htm>
- [2.23] Filterlab from Microchip, http://www.microchip.com/stellent/idcplg?IdcService=SS_GET_PAGE&nodeId=1406&dDocName=en010007
- [2.24] Embedded wireless transceivers and applications in lightweight wearable platforms, Mathew Laibowitz and Joseph A. Paradiso, Responsive Environments Group, MIT Media Laboratory, http://www.media.mit.edu/resenv/pubs/papers/2003-12-circuit_cellar5.1.pdf
- [2.25] Datasheet of rfPIC12f675 transmitter, <http://ww1.microchip.com/downloads/en/AppNotes/tb069a.pdf>

[2.26] Precision voltage references, By Perry Miller and Doug Moore,

Analog Applications Journal, November 1999,

<http://focus.ti.com.cn/cn/lit/an/slyt183/slyt183.pdf>

[2.27] Datasheet of MCP1541,

<http://ww1.microchip.com/downloads/en/DeviceDoc/21653b.pdf>

Chapter 3 - Development of the PCB for the ECG monitor with RF communications

3.1) Introduction

A printed circuit board is a board with conductive paths that connect different electronic components and all of these are fixed on top of a non-conductive surface. PCBs are widely used today because they are much more reliable in operation and cheaper to assemble in quantities compared to breadboard or veroboard equivalents. They do require time for their design, but once the design is complete, they can be produced in large quantities at low cost.

The EAGLE Layout Editor was used for the PCB design, to document the schematic and route the components after placing them on the board. An important parameter of a PCB is the number of layers it contains, as 1, 2, 4 and more layers can be produced. More layers allows for greater flexibility but at higher cost of the PCB. For this development, a two layer PCB was found sufficient.

3.2) Schematic of the front end of the system

A PCB can be assembled using traditional holes or the more recently developed surface mount devices (SMD). The same component could be available in different packages, such as most resistors and capacitors. At the time of routing the board, all packages must be defined, and these were either taken from the EAGLE libraries or prepared based on the information

provided by the EAGLE developers [3.1]. Most of the components used for the design were SMDs because this option enabled reduction in the size and the weight of the board.

3.2.1) Instrumental amplifier

At the prototyping stage, the INA326 instrumental amplifier was selected for the ECG monitor and the adopted schematic followed the recommendations from the datasheet [3.2], with the addition of the low pass filter at the output (fig 3.1).

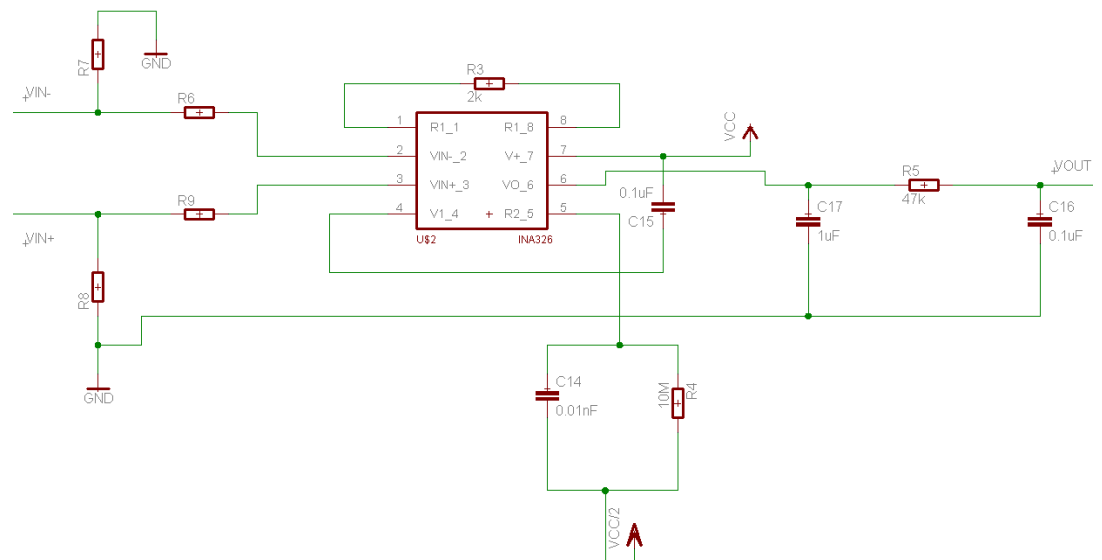


Figure 3.1: Schematic for the instrumental amplifier prepared in EAGLE

The four additional resistors at the input (two at each input) have their values unmarked in the schematic. This was done to allow for some experimentation on the assembled board with the cables and electrodes attached, as the value of these components can vary across a wide range. The values of the resistors R3, R4 and the capacitor C14 ensured the overall gain of 1000.

The filter used at the output of the AD624 was also used at the output of this instrumental amplifier to filter the unwanted noise present in the signal. The output after the filter circuit of the instrumental amplifier will be input to the active low pass filter.

3.2.2) Input connectors

A choice was available between case mounted connectors [3.3] and 4mm PCB sockets [3.4], and the latter component was selected. Each wire that carries an ECG voltage has two connection ports (fig 3.2) because the wires are shielded. A third connector was added to provide a better reference point from the leg. R14 was added between the ground of the device and the reference (leg) electrode for safety reasons. It would limit the current applied to the patient if the ground of the device became subjected to a high level of voltage due to some serious failure. These three connectors (fig 3.2) were colour coded so that it was easier to distinguish them.

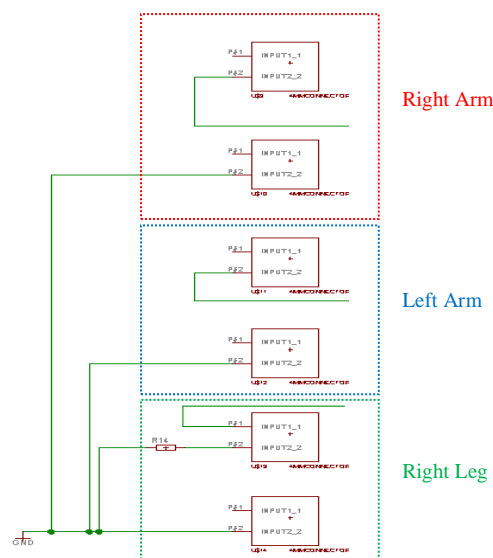


Figure 3.2: ECG wire connectors

3.2.3) Active Low Pass Filter

The signal that was acquired from the patient, amplified and filtered, is then input to the 4th order low pass Bessel filter with a cut off frequency of 20 Hz before the ADC conversion. As the recorded voltage at the output of the low pass filter had an amplitude of about 800 mV, the active filter needed to provide an amplification of about 5 times to better utilise the input range of the ADC built into the PIC microcontroller. This voltage should not exceed the reference voltage of 4.096V, to prevent the ADC saturation. The FilterLab software was used for the design of the active filter (fig 3.3).

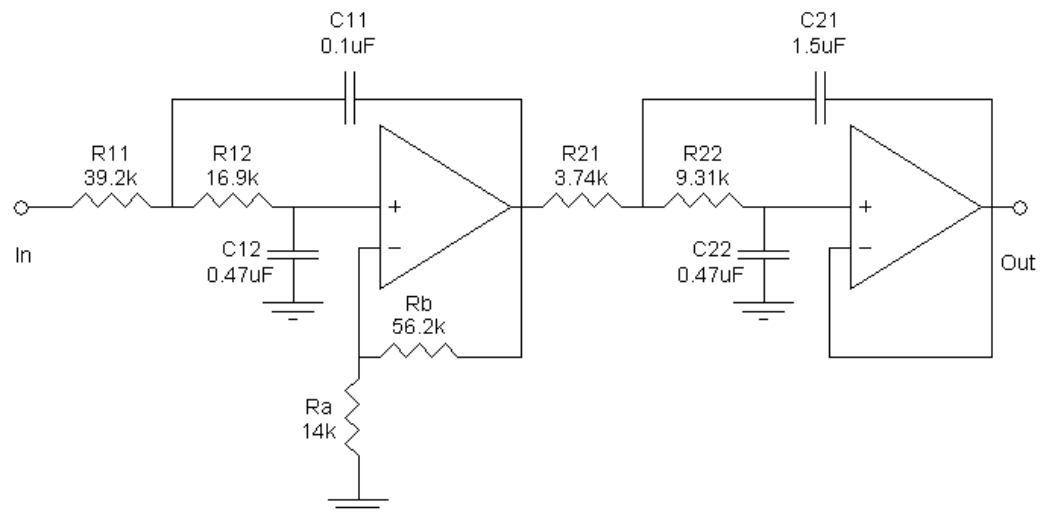


Figure 3.3: 4th order 20Hz low pass Bessel filter with the gain of 5

By comparing the schematic of the prototyped 4th order 20Hz low pass Bessel filter with a gain of 1 (Appendix B) to the schematic of the 4th order 20Hz low pass Bessel filter with a gain of 5 (fig 3.3), the first stage of the filter was changed in order to provide the required amplification.

OPA2604AUE4 operating amplifiers [3.5] were selected for the active filter, and the complete EAGLE schematic is presented in fig.3.4.

This doubler and inverter would supply +5V, -5V, +2.5V, +3V and the ground potential for the whole circuit. The schematic fig.3.5 shows the SMD diodes [3.8]. A jumper was added to the circuit to disconnect the battery when the device was not in use. Another jumper was added to enable powering the rfPIC with either 3V or 5V.

3.2.5 Reference voltage

The voltage reference component [3.9] was created from another library component with the same dimensions. The voltage reference was powered from the doubled voltage to give an output voltage of 4.096V as a reference for the rfPIC's ADC.

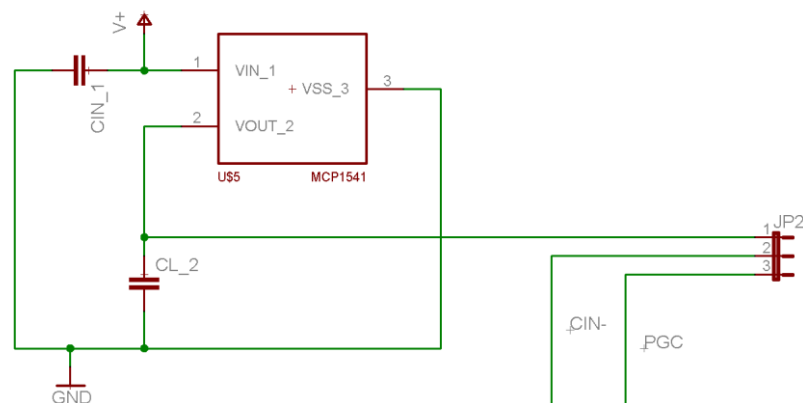


Figure 3.6: Schematic of the voltage reference (4.096V)

Fig 3.6 shows a jumper that allowed the Cin-/GP1 pin of the rfPIC to be used either as a voltage reference input pin (normal operation of the device) or as the PGC programming input pin (writing the program into the PIC).

3.2.6) rfPIC

The rfPIC12f675k component description for the PCB design was found on the EAGLE website [3.1]. The schematic of the rfPIC development kit was adopted, with minor modifications (fig 3.7).

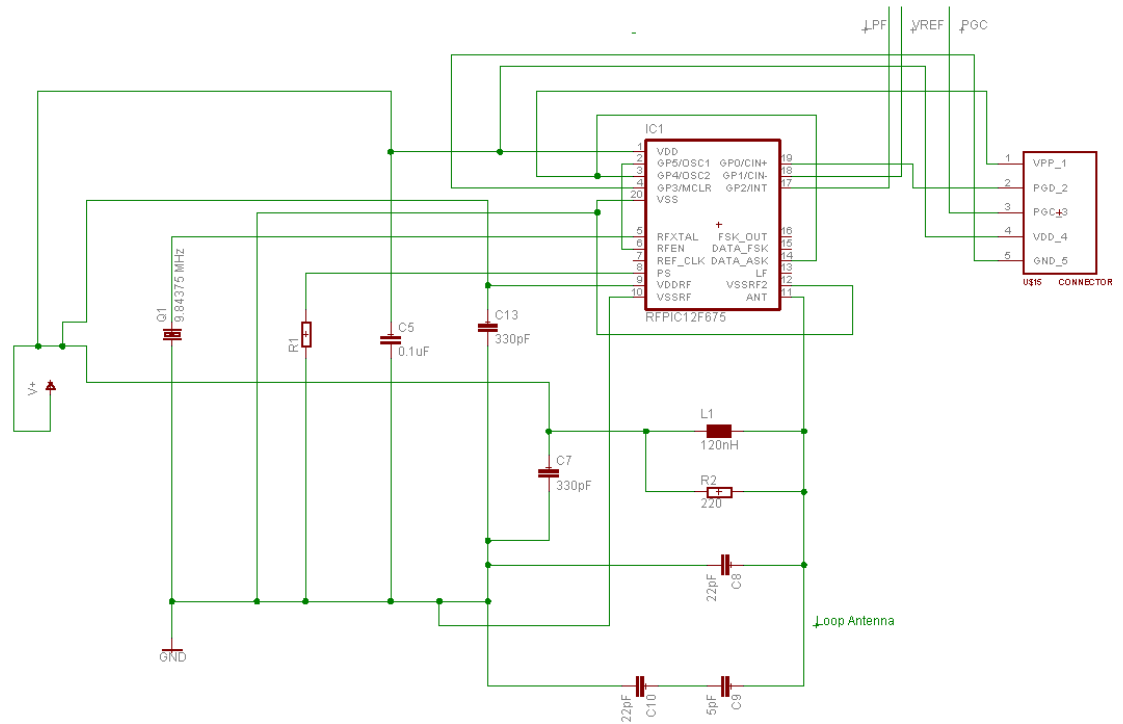


Figure 3.7: Schematic of the rfPIC part of the ECG monitor

An ICSP socket was added to the schematic (fig 3.7) in order to program the rfPIC using the PICkit2 debugger/programmer. Five specific pins are required for rfPIC programming (namely VPP, VDD, PGC, PGD and GND). The PCB design was completed with the PCB loop antenna that had its dimensions taken from the rfPIC datasheet.

3.2.7) Test points

Once the schematic was completed, some test points were added before and after each stage to allow easy exploration of the signals using an oscilloscope. The schematic for the test point is presented in fig 3.8.

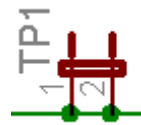


Figure 3.8: Schematic design of a test point

3.3) The final schematic

All the necessary component packages were created and linked to the schematic components. The final schematic of the front-end can be seen on page 182 in appendix D. The error rule check (ERC) function was performed and a copy of the error report produced by EAGLE is shown in appendix E on page 183. In total, 11 warnings and 1 error were reported but these warnings and error were not found to be important since they were all related to the rFPIC package created by another user. A similar issue was experienced with the 4mm PCB socket. The socket has 2 pins that could be connected and since only one was connected, the software thought that there was an error.

3.4) Printed circuit board of the front end

The components were manually placed on the PCB and the tracks were routed using the autorouter available in EAGLE. The design rule check (DRC) was then performed, which checks the design outcome against the specifications for a particular PCB manufacturing house (PCB Train [3.10] in

our case). Small errors like conductive lines being too close to each other were fixed manually after performing the DRC.

The final design of the PCB and its photographs from two sides are presented in fig 3.9 and fig 3.10 respectively.

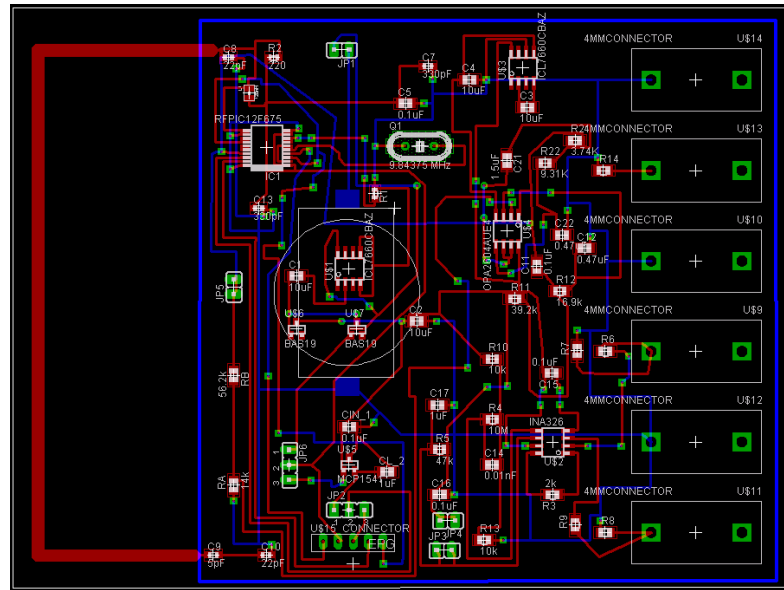


Figure 3.9: Final view of the PCB design of the front end

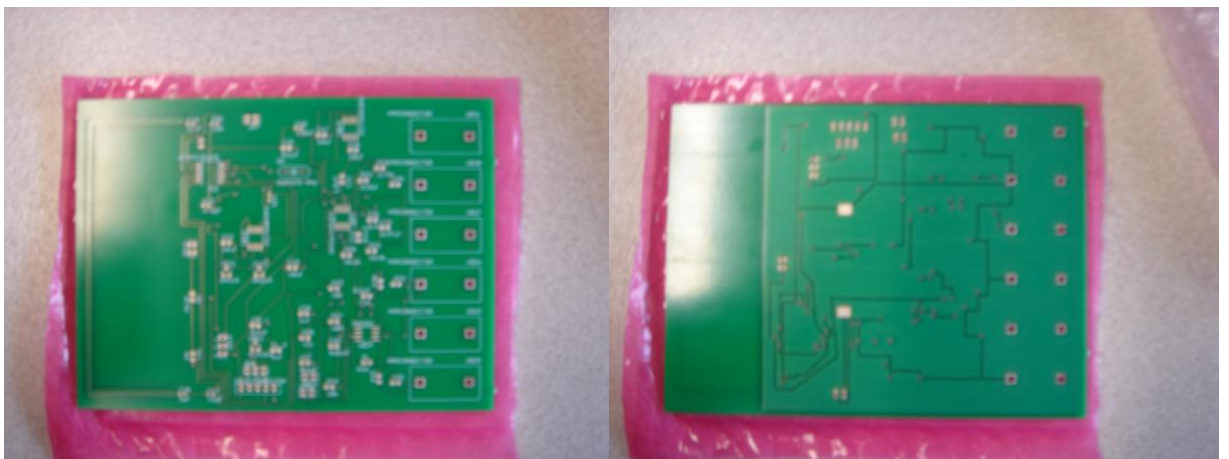


Figure 3.10: Picture of both layers of the manufactured PCB
of the front end

3.5) References:

- [3.1] Cadsoft's library page, http://www.cadsoft.de/cgi-bin/download.pl?page=/home/cadsoft/html_public/download.htm.en&dir=eagle/userfiles/libraries
- [3.2] Datasheet of INA326, <http://focus.ti.com/lit/ds/symlink/ina326.pdf>
- [3.3] Datasheet of banana connector,
<http://www.farnell.com/datasheets/43704.pdf>
- [3.4] Datasheet of 4mm connector,
<http://www.farnell.com/datasheets/92718.pdf>
- [3.5] Datasheet for OPA2604, <http://focus.ti.com/lit/ds/symlink/opa2604.pdf>
- [3.6] Datasheet for CR2032,
http://www.panasonic.com/industrial/battery/oem/images/pdf/Panasonic_Lithium_CR2032_CR2330.pdf
- [3.7] Datasheet for SMTU 2032-1-LF, <http://www.ryston.cz/windows-1250/renatabh.htm>
- [3.8] Datasheet for BAS-19,
<http://www.fairchildsemi.com/ds/BA%2FBAS19.pdf>
- [3.9] Datasheet for MCP1541,
<http://ww1.microchip.com/downloads/en/DeviceDoc/21653b.pdf>
- [3.10] Datasheet for PCBTrain Rule Specifications,
<http://pcbtrain.co.uk/specs.php>

Chapter 4 - Programming, prototyping and testing the ECG monitor on a veroboard

4.1) Changes to the development plan

Because of some personal circumstances, the original registration for the PhD degree program was changed to the MPhil degree program soon after the point when the PCB was designed and sent for manufacturing. This made it difficult to pursue the original work plan, and some changes to it were inevitable, in order to complete the design of the instrument in one year. Additionally, the RF communication between the ECG device and the ultrasonic scan triggering circuit could be undesirable in a hospital environment [4.1] and at the same time, it could limit the operating frequencies of the ECG device [4.2]. Therefore, the assembly and debugging of the PCB was abandoned and another speedier development of the ECG part of the instrument took place, which used a veroboard instead.

4.2) The veroboard featuring the rfPIC development module

The veroboard included the ECG connectors, the instrumental amplifier and the active low pass filter with a socket for the rfPIC development module (fig 4.1). This design allowed for the development of the rfPIC control program that would be compatible with the PCB board described in chapter 3.

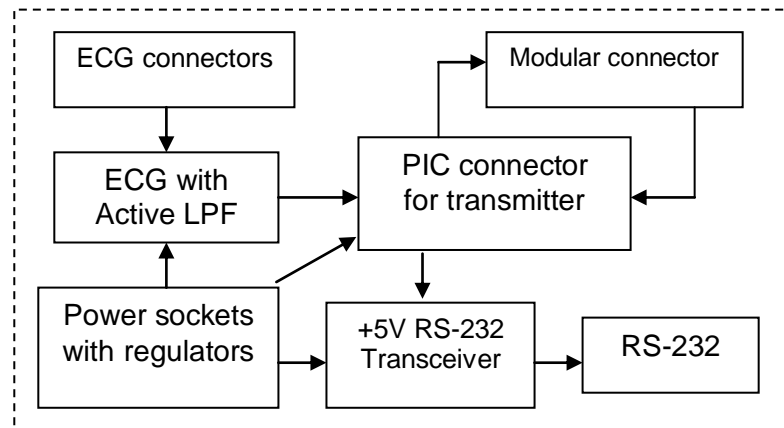


Figure 4.1: Block diagram for the veroboard that included the rfPIC development module

4.2.1) ICD header

The modular connector [4.3] provides the advantage of easy in circuit connection of the PIC to the MPLAB IDE development environment, without removing the PIC from the socket.

4.2.2) RS-232

A DB9 RS-232 socket [4.4] was used to interlink the development board and the serial port of the computer for debugging.

4.2.3) 5V powered RS-232 transceiver

Of the options available (e.g., [4.5]), the Maxim-202CPE transceiver [4.6] was selected. It generates $\pm 12\text{V}$ signals required by the RS-232 standard from a single +5V power supply. The typical operating circuit requires a few external capacitors only and is easy to implement [4.6].

4.2.4) Board connectors

Four different sockets were used in the circuit. The first one was a connector to link the rPIC development module to the veroboard. The module has a 14 pin connector so a 14 pin socket was made out of two (10+5) pin sockets [4.7]. The extra pin in the socket was marked to avoid plugging the transmitter in the wrong way. The second socket was the BNC socket [4.8]. This socket would send the trigger signal from the output of the microcontroller to the FPGA board to start the ultrasonic scan. The ECG sockets [4.9] (used for the PCB) were also used for this veroboard. Finally, two power sockets were used to connect the power supplies, one for the positive (+5V) and the other for the negative (-5V) voltage [4.10].

4.2.5) Regulators

The on board circuits require both a +5V and a -5V power supply and the power adapters used provided 9V each. Therefore, regulators were used to stabilize the voltages to +5V and -5V. The regulators for the negative [4.11] and positive [4.12] power supplies were different to each other and were connected according to the relevant datasheets.

After the selection of the components, the development board was designed (Appendix F on page 184) and prototyped (fig 4.2) so it could be used to test the ECG monitor in part and as a whole.

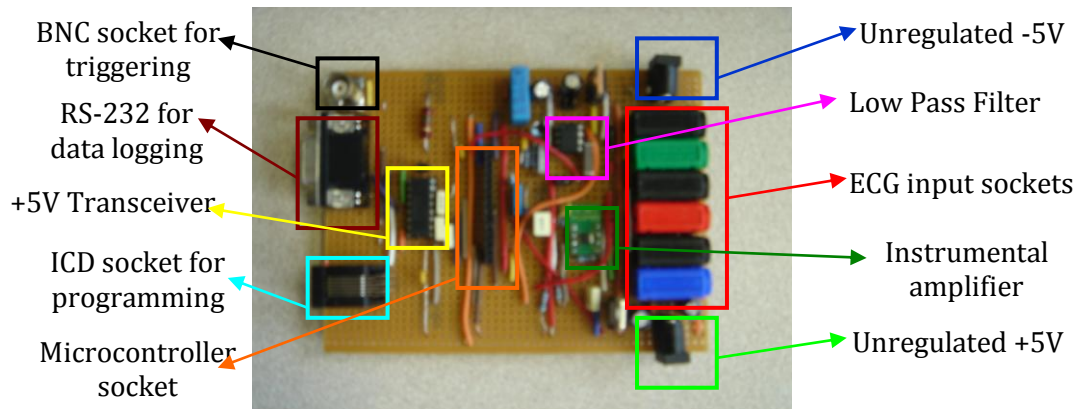


Figure 4.2: Picture of the completed veroboard

The advantage of having this board (compared to a PCB design) is that more than one microcontroller module can be tested. As well, more components can be simultaneously added, if necessary. In addition, this type of development board could be designed and assembled in the laboratory without the delays related to PCB manufacturing.

4.3) Testing of the developed veroboard

First of all, a digital multimeter was used with the schematic of the whole board to check for short circuits. Some short circuits were found in the board at first. By looking at the top layer, where the components were placed, no short circuits could be seen, but after looking in detail at the bottom layer with a magnifying glass, very small patches of solder were noted between tracks and these caused the short circuits. These short circuiting materials were removed with a sharp blade by scratching between the tracks.

After that, the whole board became operational, but the output voltage was found noisy. The capacitors at the input of the regulators were changed from a 22 μ F to a 100 μ F and the output capacitor was changed from 1 μ F to a 0.1 μ F. This change of capacitors vastly lowered the noise level at the output.

Finally, some jumpers were added at a few points in the circuit to ease debugging. One of these jumpers was put at the RS-232 output to enable/disable the data logging to the computer. The same thing was done to the ECG signal; the jumper was added in between the input of the microcontroller and the output of the filter. This made it possible to isolate functional parts of the design from each other to inspect relevant output waveforms without the influence of loading circuits.

4.4) Programming the microcontroller

4.4.1) Main Program (wrap.asm)

The first thing to be done is to link processor specific variable definitions to the microcontroller being used. The RF12F675K is used both on the development and on PCB boards. Together with the processor-specific header files, it starts the program. After this, the configuration bits are set. These bits include oscillator selection, code protection, reset, power-up and watchdog timer, as well as some pin functions and brown-out detection. Both the data and program memory code protections were disabled for the ease of debugging. Some peripherals, such as Brown-out detection, power-up and watchdog timers, were disabled because they were not required. The GP3/MCLR pin, which is connected to a push button, is configured for the

master clear (MCLR) function. The internal oscillator in the PIC is used for clocking.

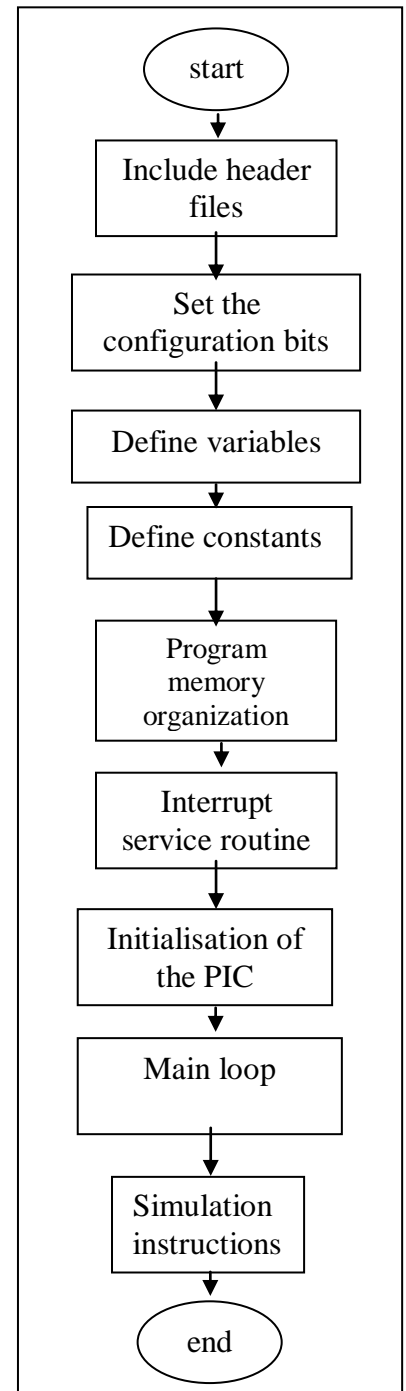
Next, the code defines the variables that are going to be used throughout all four programs. The variables were typed, line by line, after each other, after a special instruction (cblock 0x20) that told the microcontroller that the names mentioned here would be mapped to the general purpose registers. It is also important to end the cblock section by putting an end (endc) to it when finished declaring the variables.

While creating the variables to be used throughout the programs, some constants were also defined. These definitions enable use of particular constants by name, and these can be applied to configuration code, constants, pin definitions and register bits.

Six general-purpose input/output (GPIO) pins were available that could be used and they are bi-directional. Of these, three were used as inputs and the other three were used as outputs.

The inputs are used for:

- the analogue ECG signal acquired from the patient
- reading variable resistor (R1) to set the delay between the peak value of the ECG and the ultrasonic trigger
- an optional input from the RS-232 port.



The outputs were used for:

- generation of the rising edge for triggering the ultrasonic instrument;
- output that used the RF line as wired on the PIC module;
- an output to the RS-232 cable for communication of the ECG data.

The configurations were defined as constants so it would be easy to change them in one place, rather than having to change everything all around the program (soft coded configuration). These constants included configuration of A/D control register for reading two different channels using the ADC module (one channel for the ECG signal, and the other for reading the setting of the potentiometer), the configuration of analog select register for using different conversion frequencies and configuration of digital input/output pins for either output or input as required. A configuration constant was also stated for the option register (particularly to set the prescaler value). A configuration code had to be created for the comparator control register because the comparator is enabled as the default. Therefore, it had to be disabled since it was not used in this application.

Finally, there were two constants, one for marking the output data when the trigger occurred and one for a constant value to be used in defining the delay to trigger.

The program memory starts from a reset vector at the address 00h. A NOP instruction (no operation) is placed there to allow usage of the ICD (in-circuit debugger). After this instruction, the program jumps to the initializing program that will be discussed later. After initialisation of the hardware and

software variables, the interrupts will be enabled. The interrupt service routine is located at the address 04h.

When the main program is interrupted, the control is passed to the interrupt service routine (ISR). When this routine finishes, the processor returns to the main program again to continue execution of the interrupted program by executing the **IRET** instruction.

The main section of the program presents an empty superloop, because all the required actions are initiated by the Timer0 (T0) interrupt, and are performed by the ISR.

4.4.2) Initialisation Program (init.asm)

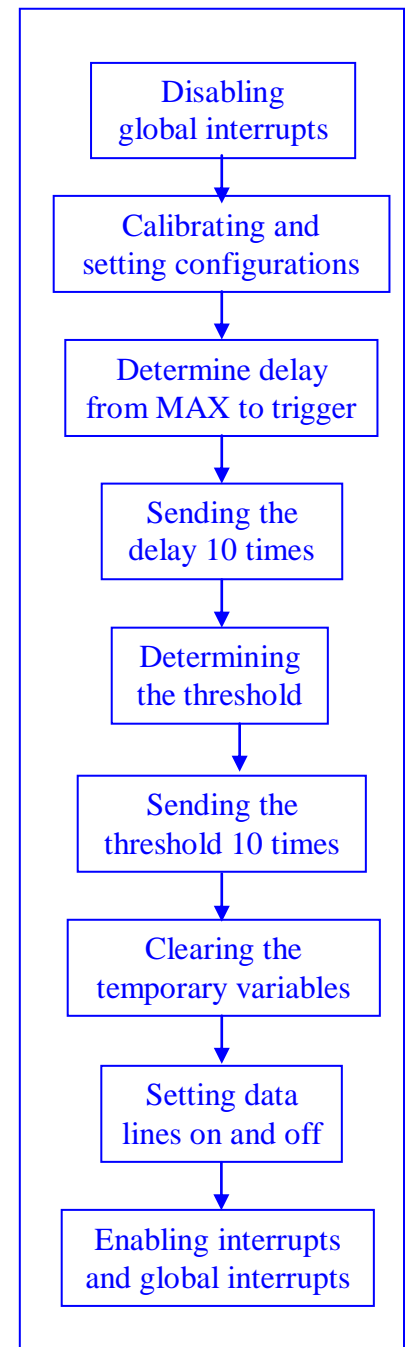
This program was written to set the PIC hardware and program variables as required before entering the superloop that is interrupted by the timer T0. First, the global interrupts were disabled and bank 1 was selected for writing the configuration codes. Before setting them in their correct places, the factory calibration value for the built-in oscillator was retrieved. After that, the general purpose pins were set to input and output, as required.

The next line sets the option register to the desired prescaler value and also links the built in oscillator output to the input of the timer T0. Finally, the analogue to digital conversion clock configuration code is set for the ADC. Then the code switches back to bank 0, and the comparator is set off. After the hardware initialisation, the variables were initialised.

Two main variables need initialisation: the first one to determine the delay from the peak value of the ECG (R wave) to trigger. The voltage at a variable resistor will be read to set the required delay for triggering the ultrasonic instrument after the peak of the R wave. Once the value is read from the potentiometer, it would be stored in the variable Delay. This value would be sent 10 times over RS-232 for debugging.

The second variable that needs initialisation is the threshold voltage. The Channel 3 analogue input is read by the ADC (this channel is the ECG signal that is acquired from the output of the low pass filter). After completing the digitising process, it will return the value for the ECG sample that will be moved into a temporary variable. If this value is larger than the previously detected maximum ECG voltage, the latter will be updated to this new value. This analysis is performed for about 3 seconds to

make sure that several R peaks are detected. After that, the value is halved and is then used as a threshold for the detection of the peak of the R wave. The use of this threshold allows cutting off the other waves from consideration – when this level is crossed, the R-wave is detected. It is still necessary for every detected R wave to find its peak, which is to be done in



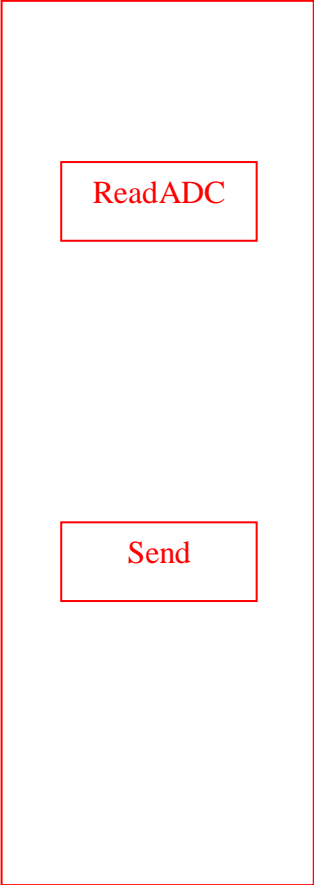
the ISR. Finally, the global interrupts and Timer0 (T0) interrupts are enabled in the initialisation section.

4.4.3) Subroutines (subr.asm)

Two subroutines were written: the first one the ReadADC subroutine and the second one the SEND subroutine. The ADC conversion can be done by calling the ReadADC subroutine, and the analogue input channel that needs conversion must be selected before this call. When a new channel was selected, enough time has to be given for circuit switching and this value depends on the charging time of the internal capacitor.

The safe delay was stated as 22 μ s in the datasheet, and a loop that counts down from 7 to 0 wastes 22 instruction cycles. This gives a required delay at 4 MHz PIC clock frequency because one instruction cycle (T_{cy}) consists of 4 clock cycles (T_{clk}) for the PIC16 microcontrollers. After the delay, the A/D conversion starts.

The DONE flag of the ADC is monitored, and the conversion is finished in about 22 μ s according to the datasheet and the settings used. Therefore getting one sample requires less than 50 μ s, and the maximum sampling frequency could be up to about 20 kHz. However, this frequency is excessive for the ECG monitor, and after the conversion, the ADC module is switched off to conserve power. Finally, the subroutine returns control to the calling code.



ReadADC

Send

The second subroutine (SEND subroutine) allows a byte to be sent using the RS-232 at a baud rate of 38400. This baud rate was selected because it was the maximum rate possible for the wireless RF transmission by the rfPIC. Sending one bit of data at this baud rate takes 26 μ s, and a complete transmission of 8 data bits with 1 stop bit, no parity and no flow control will take 234 μ s. Finally, the subroutine will return control back to the position from where it was called.

Therefore, sampling and transmitting a single sample will take less than 300 μ s, and the maximum sampling rate of the ECG signal could be up to about 3 kHz. The Timer0 was programmed for the interrupt frequency of 1 MHz/1024 < 1 kHz; thus, sufficient time was allowed for both the conversion and communication to take place in real time for every sample.

4.4.4) Interrupt Service Routine (isr.asm)

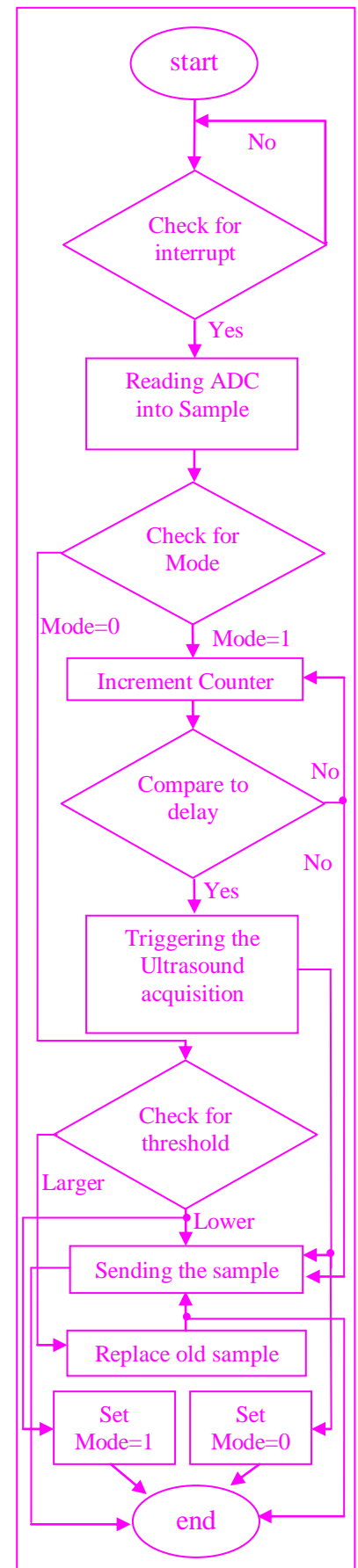
Every time the ISR is invoked, it will acquire an ECG signal sample, trigger the ultrasonic instrument if necessary, and send the sample over the RF communication. Once it takes control, it clears the T0 interrupt flag so it can process the following interrupt request. Channel 3 is used to convert the ECG signal that is acquired from the output of the low pass filter. The variable Mode will then be used.

The value mode=0 implies that the ECG signal peak needs to be determined, whereas the value mode=1 implies that the maximum does not need detection. If Mode=1, then no detection is needed, so the program will increment the temporary counter. This value holds the number of samples taken after the detection of the peak of the R-wave, and is compared to the

desired delay determined in the initialisation code by the user (by turning the potentiometer connected to the channel 0 of the ADC). If the counter does not reach the required value, then the code will send the acquired sample. However, if it does reach the required delay value, then triggering occurs (this is done by enabling the trigger output for the ultrasound acquisition) and the marker value (instead of the actual value of the sample) will be sent using the SEND subroutine. After this, the value of the variable Mode is reset to 0.

If the value of Mode is 0, a peak of the R-wave is to be detected. First, the acquired sample is compared with the threshold, and if it is lower than the threshold, the sample is sent and processing terminates. Otherwise, the monitor processes the R-wave, and it will additionally compare the newly acquired sample with that previously acquired. If the new sample is larger, it will replace the old sample and it will be sent wirelessly, terminating the processing. If it is lower, the previous sample was the peak of the R wave, the sample is sent, the mode is changed to 1 and processing is terminated.

The complete program flow diagram is presented in fig.4.3.



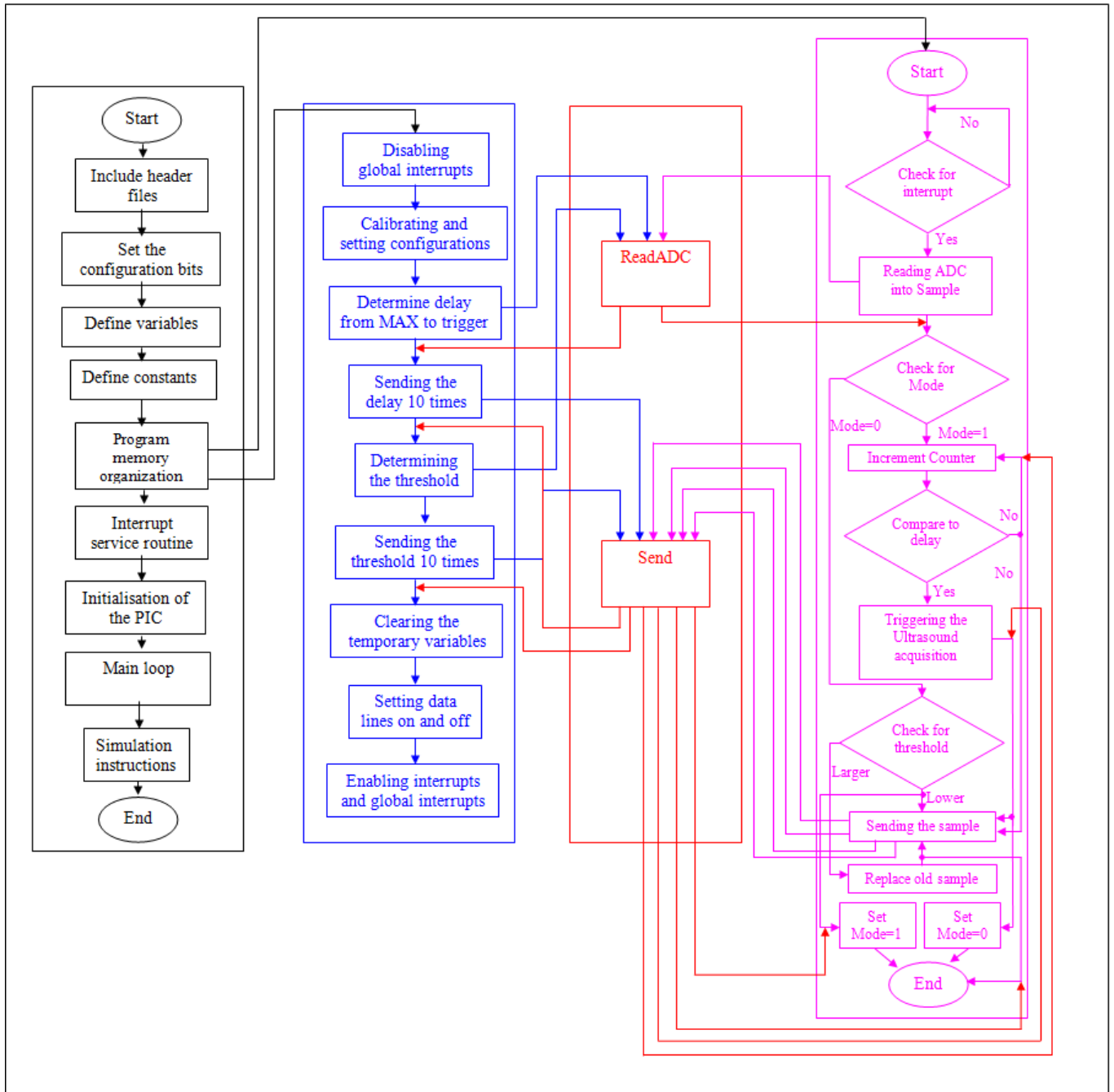


Figure 4.3: Flow diagram of the overall program showing the interlink between them

4.5) Testing the program with the rfPIC microcontroller module

A program written in Matlab takes the input from the RS-232 PC port, connected to the veroboard by a standard cable, and records the output of the microcontroller. First of all, the rfPIC microcontroller module (fig 4.4) was tested without the ECG input connected (the jumper was removed).

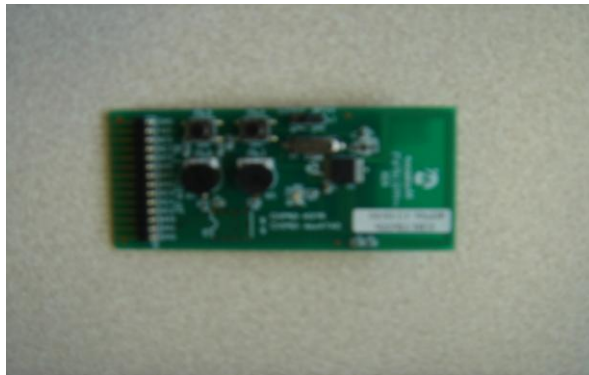


Figure 4.4: The rfpic12f675 development module

Therefore, the noise in the circuit was the input to the rfPIC's ADC. When the whole circuit is switched on, the Matlab program will start recording data. The rfPIC program could be restarted at will by pressing the RESET button. The Matlab program is started by typing the name of the file and, once the script starts, the reset button is released. Once the script starts, it will go through a number of steps (fig 4.5).

First, it will clear all of the Matlab workspace variables and it will close the open Matlab figures and the serial port. The serial port will then be set to receive 8 data bits at a baud rate of 38400 through the COM1 port.

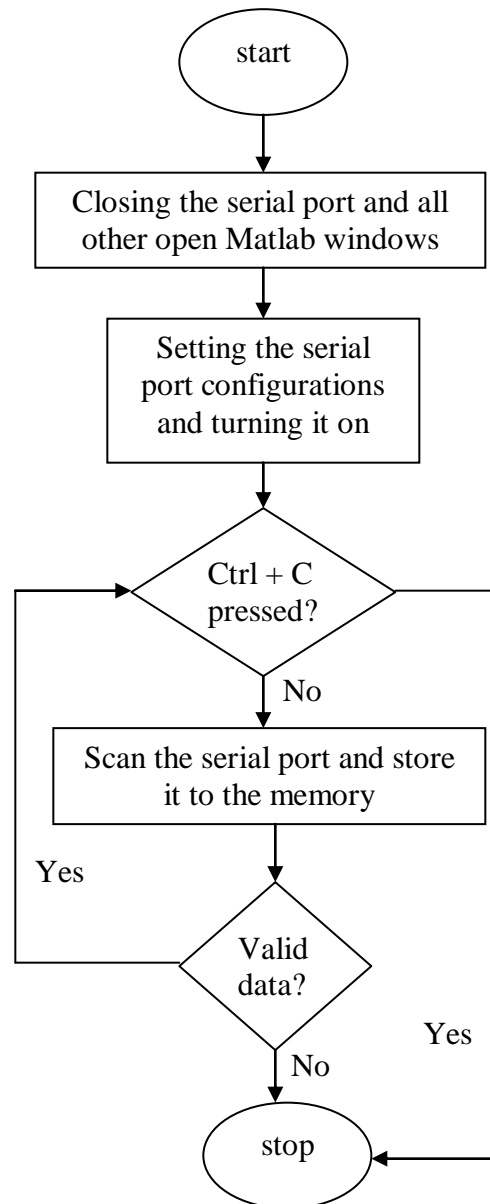


Figure 4.5: Flow diagram of the RS_Comm script

The script then checks the validity of the received data. If they are valid, the acquisition will continue; otherwise, the program will stop. After some time, when enough data are collected, the “Ctrl” and “C” buttons would be pressed to halt the program. When the program is terminated, the data that were recorded by then in the PC’s memory will be plotted.

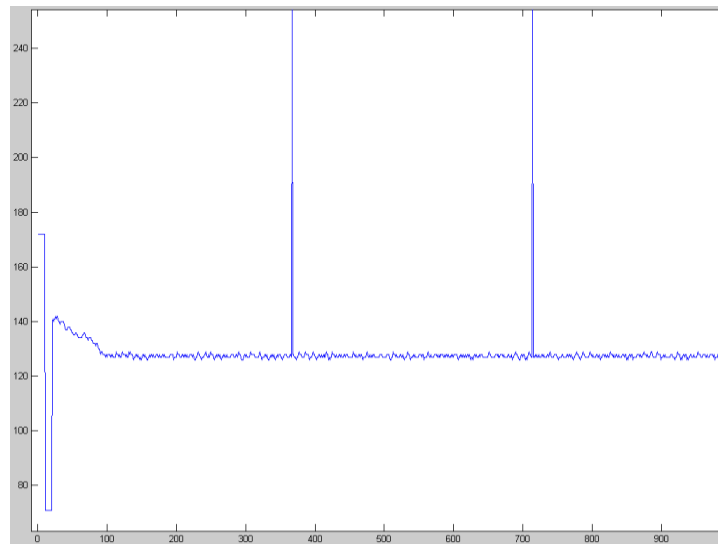


Figure 4.6: Graph showing the recorded data with no ECG signal

Fig.4.6 shows a typical record obtained without the ECG signal connected to the rfPIC. At the start of the recording, the delay and the threshold values are sent after each other (displayed in fig.4.6 by two steps at the beginning of the waveform). From the graph, the delay and the threshold values are 172 and 71 respectively for this record. The delay is used to determine the time between the R peak and the instant when the ultrasonic scan is triggered. As PIC microcontroller uses 8 bits for data, a delay multiplier was used to extend the permissible range of delay values beyond the 8-bit range of 0...255. In the program that was used to obtain fig.4.6 this multiplier was set to 2; therefore delay setting of 172 resulted in the trigger after $172 \times 2 = 344$ samples after the first local maximum was detected. The threshold value to detect the R wave is determined by looking for the maximum amplitude of the ECG signal for a set time, and halving this maximum amplitude. (This means that during the initial observation, the maximum amplitude observed by the ADC was $142 = 71 \times 2$.) The

high peaks in fig.4.7 show instances when the trigger signal will be sent to the ultrasonic scanner. The whole process was repeated again after connecting the ECG signal (fig 4.7).

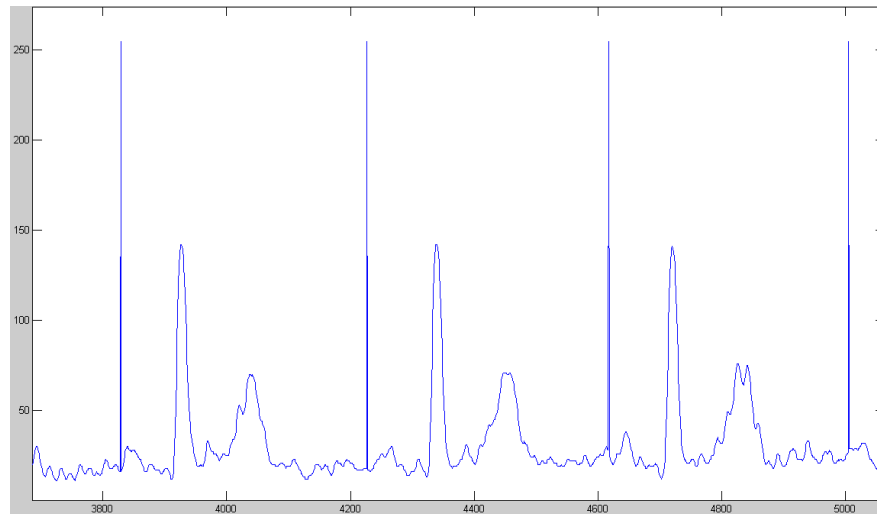


Figure 4.7: ECG signal received through the serial port that shows peaks for the trigger event (the delay for the trigger was set to about 300 samples, the first trigger relates to the R peak that occurred outside of the scope of the graph on the left)

Fig.4.7 shows noticeable differences between R-peaks and following triggers that could be estimated at approximately $\pm 2.5\%$. These differences were attributed to the remaining noise that resulted in appearances of local maxima in the waveform before the actual R-peak.

4.6) Development of a PIC16F688 veroboard module

Although the rfPIC development module was successfully used for the waveform acquisition, it did not allow in-circuit debugging of the program. Another PIC module was developed to provide the in-circuit debugging

capability useful for program development. This module included a 15 pin connector [4.13], push button [4.14], an LED and a PIC16F688 microcontroller [4.15] (fig.4.8). This microcontroller was selected because it could be replaced in the DIP socket with the pin compatible PIC16F688-ICD part that allows for direct connection of the in-circuit programmer/debugger. The photographs of the developed module with a conventional PIC and the ICD part are presented in fig.4.9 and 4.10, respectively.

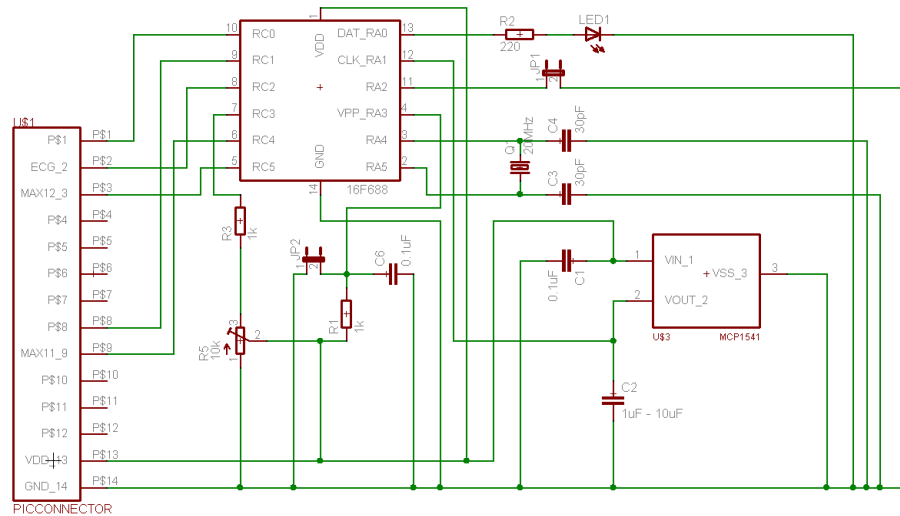


Figure 4.8: Schematic of the new veroboard with the PIC16F688 microcontroller

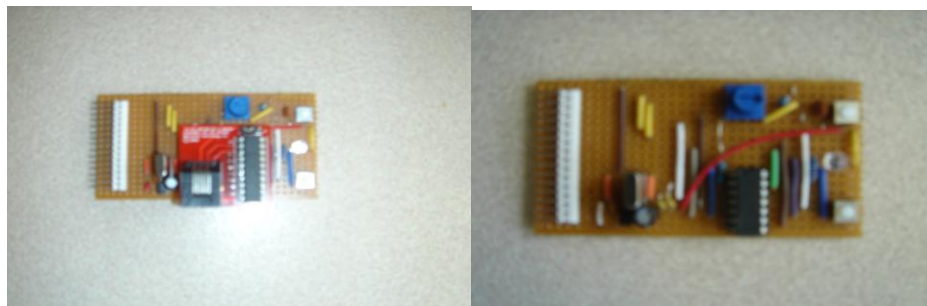


Figure 4.9: PIC16F688 module with with an ICD part

Figure 4.10: PIC16F688 module with a conventional part

4.7) Testing the PIC16F688 module

This module allowed communication at 115200 baud, three times faster than for the rfPIC module. The previously used MATLAB program had to be manually halted and a plotting command then had to be entered, again manually. The previously used script was modified to accept 5000 samples, plot them and then stop (fig 4.11).

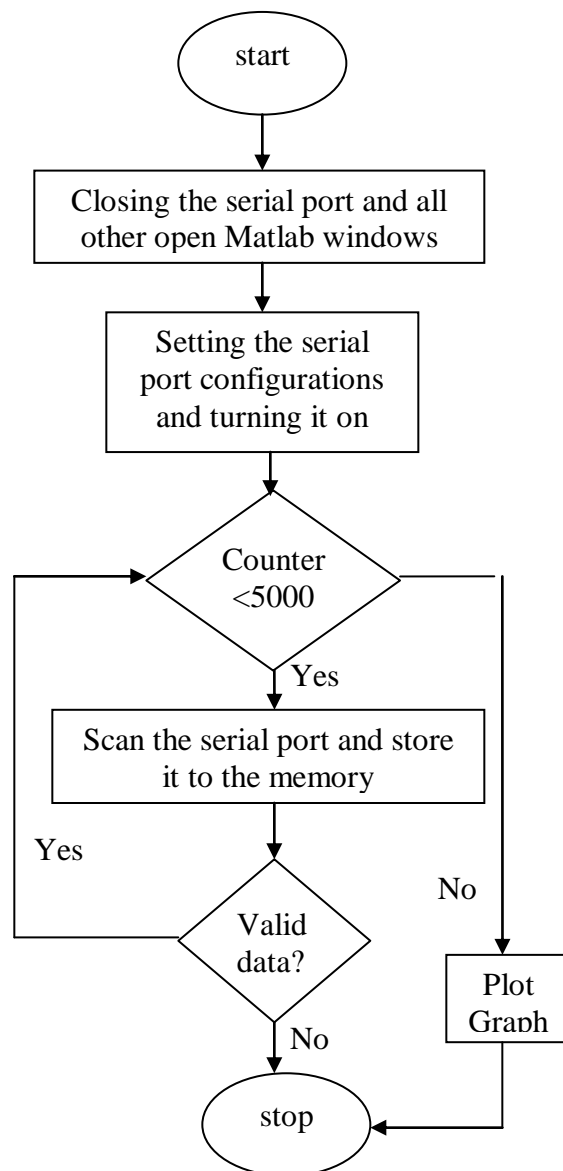


Figure 4.11: Flow diagram of the new RS_Comm script

At first, the delay was set to a maximum, with no input from the ECG, and the reset button was pressed, which was depressed when the script was run. The result for the maximum delay is shown in fig 4.12.

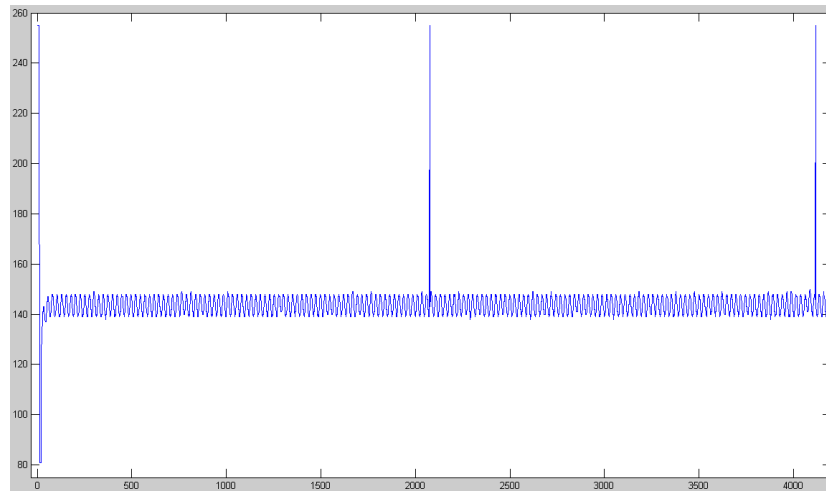


Figure 4.12: Recorded data with no ECG signal and maximum delay of about 2000 samples (horizontal axis – Sample number, vertical – Amplitude)

At the start of the recording, the delay and the threshold values were sent after each other, as before. The delay and the threshold values were 255 and 81 respectively (fig.4.12). The delay is set by the potentiometer as stated before. In order to increase the possible delay time up to 2 s the multiplier for the delay setting was increased to 8 for the veroboard module with PIC16F688. Therefore the maximum set delay of 255 resulted in the trigger after $8 * 255 = 2040$ samples.

The delay was left the same and the whole experiment was repeated with the ECG (associated jumper closed the circuit) and the recorded ECG is shown in fig

4.13. Here, the peak of the R wave is below a code of 100; thus, the threshold was below the code 50. Therefore, false triggers were produced by noise, about 2000 samples after the previous trigger, as the noise exceeded the threshold for the most of the waveform. Because of the increased level of noise, compared to the rfPIC module, the rfPIC was used for triggering the ultrasonic instrument. The debugging option was not used, as the previously described program covered all of the needs of the ECG monitor.

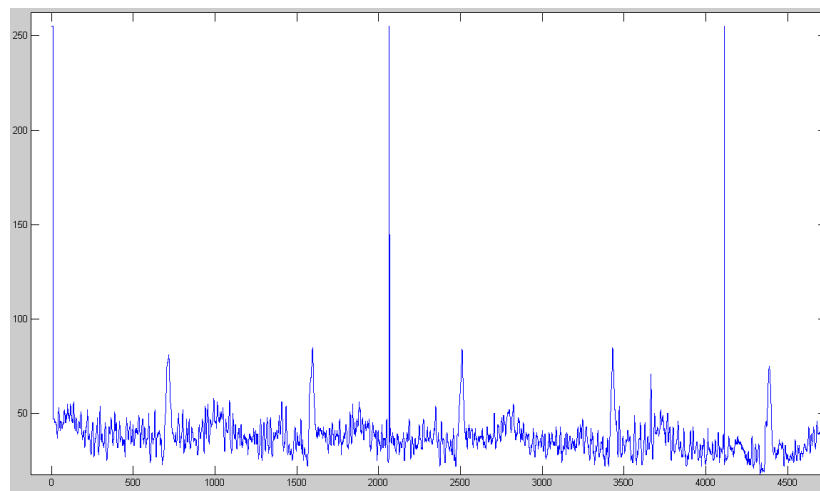


Figure 4.13: The recorded ECG signal with the false trigger events
(horizontal axis – Sample number, vertical – Amplitude)

This output trigger signal from the rfPIC module was delayed after the peak of the R wave by the time set by the potentiometer (fig.4.7). The results presented in this section demonstrated that the developed ECG monitor produced both digital output for the ECG signal samples and trigger signal as required. However there was a slight disparity in the detection of the R-wave, likely due to remaining

noise. The development of the instrument progressed to the FPGA modification stage.

4.8) References:

[4.1] RFID Systems May Disrupt the Function of Medical Devices, By Sandra

Upson, First Published June 2008, IEEE Spectrum,

<http://www.spectrum.ieee.org/jun08/6405>

[4.2] Embedded wireless transceivers and applications in lightweight wearable

platforms, Mathew Laibowitz and Joseph A. Paradiso, Responsive

Environments Group, MIT Media Laboratory,

[http://www.media.mit.edu/resenv/pubs/papers/2003-12-](http://www.media.mit.edu/resenv/pubs/papers/2003-12-circuit_cellar5.1.pdf)

[circuit_cellar5.1.pdf](http://www.media.mit.edu/resenv/pubs/papers/2003-12-circuit_cellar5.1.pdf)

[4.3] MPLAB ICD 2 In-Circuit Debugger User's Guide,

<http://ww1.microchip.com/downloads/en/DeviceDoc/51331c.pdf>

[4.4] Datasheet of 8LCM009S-304B-XX — MULTICOMP,

<http://www.farnell.com/datasheets/32792.pdf>

[4.5] Choosing the Right RS-232 Transceiver, [http://pdfserv.maxim-](http://pdfserv.maxim-ic.com/en/an/AN2020.pdf)

[ic.com/en/an/AN2020.pdf](http://pdfserv.maxim-ic.com/en/an/AN2020.pdf)

[4.6] Datasheet of Max202CPE, [http://pdfserv.maxim-ic.com/en/ds/MAX200-](http://pdfserv.maxim-ic.com/en/ds/MAX200-MAX214.pdf)

[MAX214.pdf](http://pdfserv.maxim-ic.com/en/ds/MAX200-MAX214.pdf)

[4.7] Datasheet for 10 way socket,

<http://www.harwin.com/include/downloads/drawings/M20-786.PDF>

Datasheet for 5 way socket,

<http://www.harwin.com/include/downloads/drawings/M22-714.PDF>

[4.8] Datasheet for the BNC connector,

<http://www.farnell.com/datasheets/102677.pdf>

[4.9] Datasheet for ECG socket, <http://www.farnell.com/datasheets/92718.pdf>

[4.10] Datasheet for power socket, <http://www.farnell.com/datasheets/79787.pdf>

[4.11] Datasheet for the -5V regulator,

<http://www.st.com/stonline/products/literature/ds/2149.pdf>

[4.12] Datasheet for the +5V regulator,

<http://www.st.com/stonline/books/pdf/docs/2143.pdf>

[4.13] Datasheet for 15 way right angle connector,

<http://www.farnell.com/datasheets/30217.pdf>

[4.14] Datasheet for push button, <http://www.farnell.com/datasheets/304.pdf>

[4.15] Datasheet of pic16f688,

<http://ww1.microchip.com/downloads/en/DeviceDoc/41203D.pdf>

Chapter 5 – Operation of the ultrasonic instrument and its modification for external triggering

5.1) Operating the ultrasonic instrument

The ultrasonic scanner developed in the applied ultrasonic device is triggered manually and it required modifications in order to be used with the trigger from the ECG monitor. The graphic user interface (GUI) for the existing system is shown below (fig.5.1), and was used without changes. The operation of the ultrasonic instrument is initiated by pressing the “Measure” GUI button (fig.5.1). After that, the instrument produces the excitation signal and receives the echo, according to the parameters selected by the user (fig.5.1).

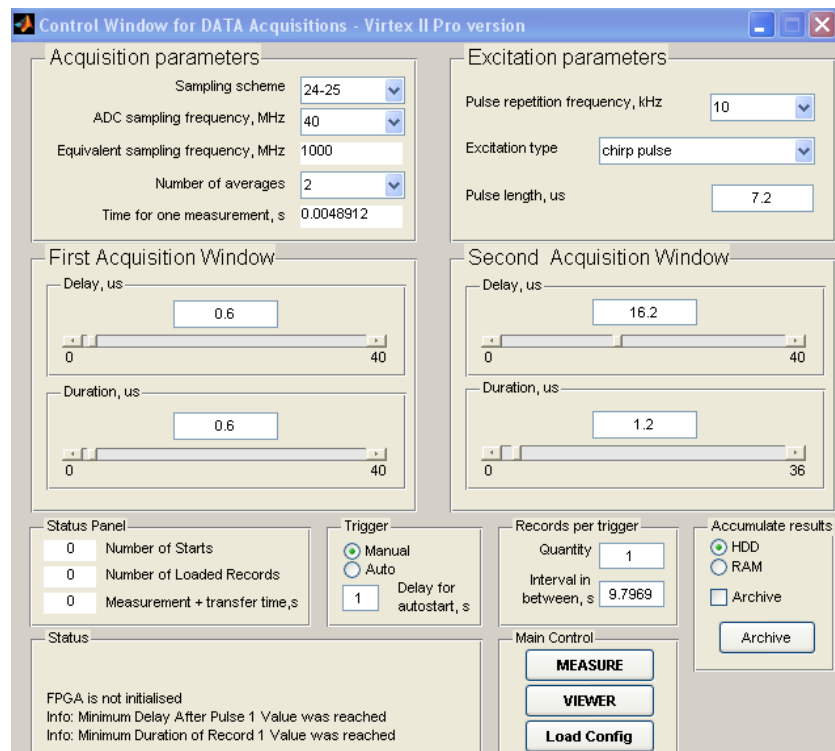


Figure 5.1: Screenshot of the GUI for the existing ultrasound system

Two sets of parameters are used for excitation of an ultrasonic pulse and acquisition of the echo. Excitation refers to the generation of the ultrasonic pulse, using the output FPGA signal that triggers the external ultrasonic pulser receiver (UPR). For the developed application, it was desirable to set the pulse repetition frequency (how many excitation pulses are produced within 1 second) as high as possible. The higher the pulse repetition frequency, the smaller the measurement time; thus, an accurate scan can be obtained. The reason for this is that the artery and blood can be considered static for a short time only. On the other hand, setting this frequency too high can result in artefacts if there are echoes with substantial amplitudes from the previous excitation that arrive after the following excitation. These echoes will be superimposed with the proper echo signal related to the following excitation, and it will be not possible to eliminate them. The higher the pulse repetition frequency, the lower the depth will be that the signal can travel and vice versa. This can be shown using the following formula:

$$f = \frac{1}{T} \Rightarrow T = \frac{1}{f},$$

where f is the pulse repetition frequency, T is the interval between excitation pulses. All the echoes with substantial amplitudes must have delay less than T .

The total measurement time can be seen in the acquisition parameters panel, where it is calculated automatically based on the requested interleaving factor and number of averages. For our application, “Excitation type” is “single pulse” (there are some other types available, namely chirp pulse, Golay code, Barker code and M sequence). The pulse length value shown in the GUI panel

“Excitation parameters” is used to trigger the UPR, while the duration of the excitation pulse is controlled separately using WinUPR software. This is set to a half-period of the transducer’s central frequency, to maximise the amount of electrical energy converted into ultrasonic wave energy. In turn, the excitation pulse length determines the axial resolution (the minimal distance between two separate objects that produce non-overlapped echoes), as follows:

$$\text{Axial Resolution} = \text{Pulse Length} \times \text{Wave Velocity}$$

Therefore using as high frequency transducer as possible is advantageous for increasing the resolution. We used a 20 MHz transducer instead of the 5-8 MHz transducers commonly used in ultrasonic scanners.

The echo that is acquired is the signal received back from the body of the subject, after the propagation of the excitation pulse. The acquisition parameters are set depending on the desired accuracy of the acquired signal. These parameters include the sampling scheme, ADC sampling frequency, its effective sampling frequency, the number of averages and the automatically calculated time for one measurement.

Increases in the ADC sampling frequency and/or in the number of averages increase the accuracy of the acquired signal at the expense of the measurement time. The time from one peak of the R wave to the following peak can be calculated as:

$$\text{Maximum pulse rate} = 180 \text{ beats/min} \Rightarrow 3 \text{ Hz}$$

$$f = 1/T \Rightarrow T = 1/f = 1/3 = 0.3 \text{ seconds}$$

Therefore, the acquisition time must be well below 0.3 seconds in order to statically interrogate the CCA. The sampling scheme consists of two numbers, where the first number is the multiplier of the base clock frequency for the excitation part, while the second number is that for the acquisition part. These numbers define the interleaving factor – or how many times the excitation must be repeated in order to complete a single signal record. For example, the 26-27 sampling scheme means that the effective sampling speed is 27 times faster than the operating frequency of the ADC. This relationship allows maintenance of a precise time shift from one excitation to another, and reconstruction of the complete waveform by interleaving the samples, obtained from all of the 27 subsequent acquisitions. The interleaving factor (27 as discussed above) is multiplied by the ADC sampling frequency (20-100MHz, defined by the ADC installed on the Xtreme DSP board) to get the equivalent sampling frequency.

The equivalent sampling frequency is shown directly in fig.5.1. Finally, the number of averages has a range of 2 to 32768, in steps of two. By looking at the calculated result for the total time for one measurement, one can find a compromise between the sampling scheme, ADC sampling frequency and the number of averages needed to achieve the required measurement time. This is shown in fig 5.2 using examples for the pulse repetition frequency of 10 kHz.

Sampling scheme	ADC Sampling frequency(MHz)	Equivalent sampling(MHz)	Number of averages	Total time for measurement (s)
26-27	100	2700	2	0.0054
4-5	100	500	128	0.0639

Figure 5.2: Measurement time versus different combinations of parameters

The number of averages (rather than the sampling scheme) determines the reduction in the amplitude of the additive noise. This noise can obscure echoes of interest if the amplitude of the latter is comparable with the amplitude of noise. However, any increase in the number of averages results in a proportional increase in the measurement time. In order to balance the noise reduction with the measurement time, the sampling scheme of 4-5 with the ADC sampling frequency of 100 MHz and 128 averages will be preferred but other setting will also be tried.

The number of excitations to complete a single interleaved and averaged record can be calculated using the following equation:

$$\text{Number of Excitations} = \text{Number of Averages} \times \text{Interleaving factor}$$

From the number of excitations, the total acquisition time can be calculated by using the pulse repetition rate:

$$\text{Total Acquisition Time} = \text{Number of Excitations} / \text{Pulse Repetition Rate}$$

Finally the Total Acquisition Time can be related to the time from one peak of the R-wave to the following peak:

$$\text{Ratio} = \text{Total Acquisition Time} / \text{R-R time interval}$$

If this ratio is a low number, fewer changes in the blood flow occur during the measurements, and the ultrasonic scan becomes more accurate. For a blood pulse rate of 180 beats/min, ultrasonic pulse repetition frequency of 10 kHz, interleaving factor of 5 and 128 averages, the Ratio becomes:

$$\text{Ratio} = (5 * 128 / 10,000\text{Hz}) / 3\text{s}^{-1} \approx 1/50.$$

Consequently, in these conditions, it is possible to take 50 non-overlapped measurements for a single cardiac cycle as sufficient. After setting the acquisition parameters, the first and the second acquisition windows are set. The purpose of the two acquisition windows is to see the whole A-mode scan in two parts, rather than one whole scan, because the amount of memory available is limited and may not hold the complete echo record. For the first acquisition window, the delay and its duration will be set to see the excitation pulse itself; whereas, for the second acquisition window, the delay and duration will be set to record the echoes from the CCA boundaries. The delay for the second window is the time that is required after the excitation pulse for the ultrasonic wave to propagate to the CCA and back, while the duration is the time for the wave to propagate from inside the CCA and back.

The delay and duration variables for the second acquisition window can be found by calculations based on fig.5.3.

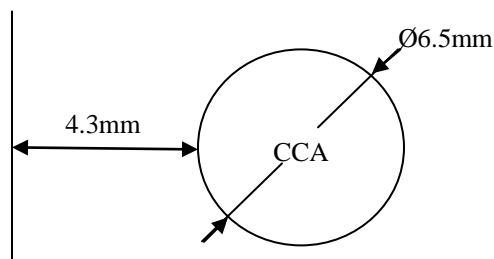


Figure 5.3: Diagram showing the approximate depths in the subject

The expected approximate CCA diameter is around 6.5mm, and the CCA is expected to be located at a depth of 4.3 mm. The above mentioned acquisition parameters for the second window then equate to:

$$\text{Delay} = \frac{l \times 2}{c} = \frac{4.3\text{mm} \times 2}{1500\text{m/s}} = 5.7\mu\text{s};$$

$$\text{Duration} = \frac{l \times 2}{c} = \frac{6.5\text{mm} \times 2}{1500\text{m/s}} = 8.7\mu\text{s}$$

At the time of measurement, the expected delay was lowered in order not to miss the beginning of the echo, while the expected duration was increased in order not to miss the end of the echo from the CCA. The GUI checks the entered values for validity and automatically transforms these to the binary values used by the Xtreme DSP board.

The results can be accumulated to either the HDD (hard disk drive) or the RAM (Random Access Memory). The HDD option will be selected in the “accumulate results” panel; thus, the data can be easily archived for later use.

A waveform viewer can be invoked to inspect archived data from previous scans from the main control panel (fig.5.1). The “load config” button can be used to load the configuration settings from a specific previously saved scan. After checking that all the parameters are set correctly, the “measure” button (fig.5.1) can be pressed to start the ultrasonic scan. The message box (fig.5.4) then prompts the user either to continue measurements or to exit (this option allows addition of more records to the present set of scans).



Figure 5.4: Message prompting the user either to acquire one more record or to archive the present set of records

When the user acquires the desired scans, the “Stop” button is pressed to return to the main windows (fig 5.1).

5.2) Changes to the design of the ultrasonic instrument

The ultrasonic instrument itself, developed in the applied ultrasonics laboratory, is a complex device that was designed using combination of various CAD tools (System generator, Xilinx ISE etc) and consists of various electronic integrated circuits (FPGA, ADC and DAC all assembled on the Xilinx Xtreme DSP development board). Therefore, some preliminary familiarisation was found

essential, and references [5.1-5.4] were used extensively throughout the development.

The whole project was analysed in order to find the procedure for the “Run” button, because the external trigger would interact with it. Looking at the diagram for this procedure (fig 5.5), the “Run” button can be seen to be defined as a port (4). Whenever the “Run” button is pressed, the click will be read by the input port (in_start), transferred into the register (Register2) and casted into the required format (Convert5) to initiate the waveform acquisition.

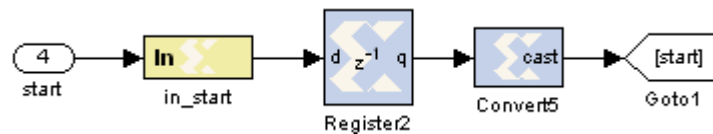


Figure 5.5: Diagram of the Start procedure

The FPGA board has 2 DACs, 2 ADCs and 1 CLK port. The DAC1 and ADC1 are used for the excitation and acquisition, respectively. The ADC2 port is unused; thus, it can be used to input the external trigger signal to the FPGA board. A flow diagram (fig 5.6) shows the operation of the system with external triggering.

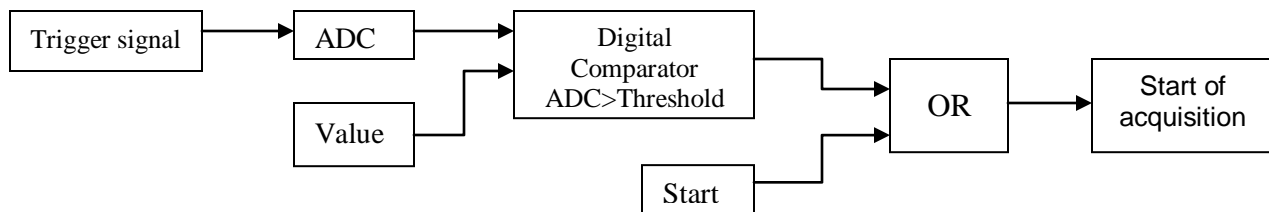


Figure 5.6: Flow diagram of the modified version of the Start procedure

The above flow diagram was implemented using System Generator as shown in fig 5.7, but this did not work.

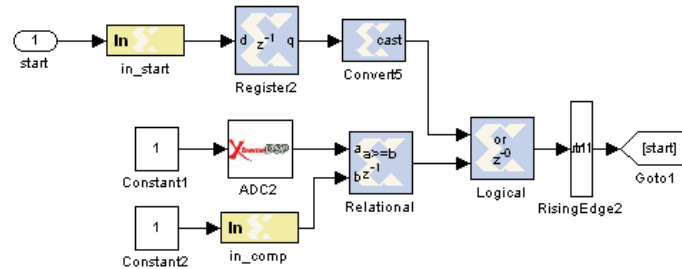


Figure 5.7: Implementation of the modified version of the Start procedure

An additional design that had output displays was used to check the correctness of operation of the ADC2 (fig.5.8), and the ADC2 operated satisfactorily.

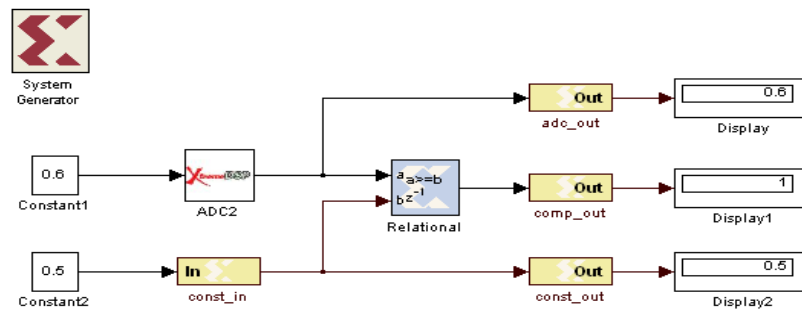


Figure 5.8: System Generator diagram for testing the ADC2

The next modification included addition of new ports to the VHDL code, and connecting the necessary port to the principal design, shown as a black box in fig.5.10. The updated design is shown in fig 5.9.

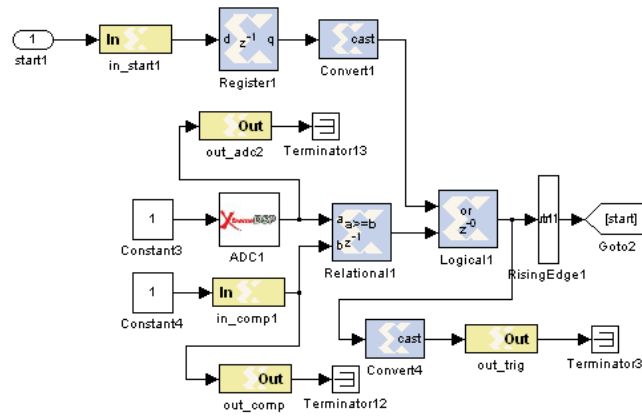


Figure 5.9: System Generator diagram with additional ports

However, this design also failed to work. Further analysis showed that simply bypassing the manual triggering was not possible. Therefore the next design used some parts of the design responsible for manual triggering (fig.5.11).

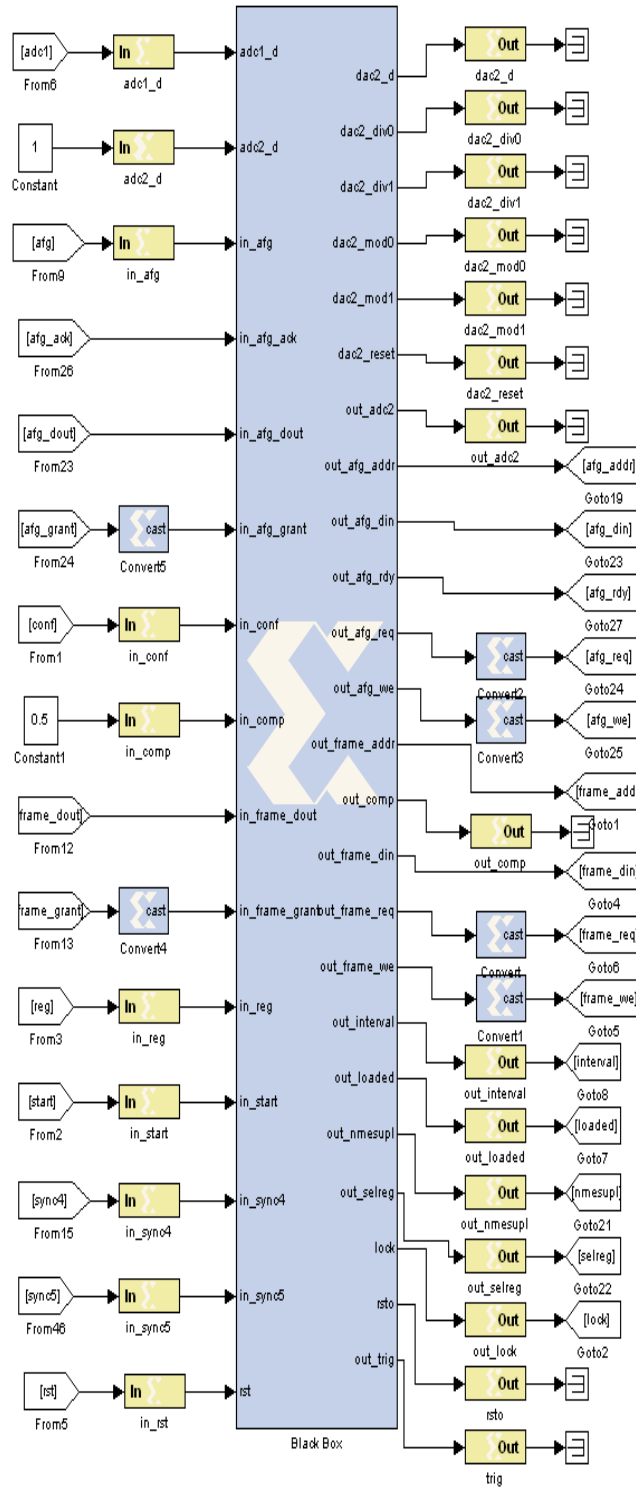


Figure 5.10: Diagram of the connections of the instrument's design (the Black box in the centre) to the input and output ports

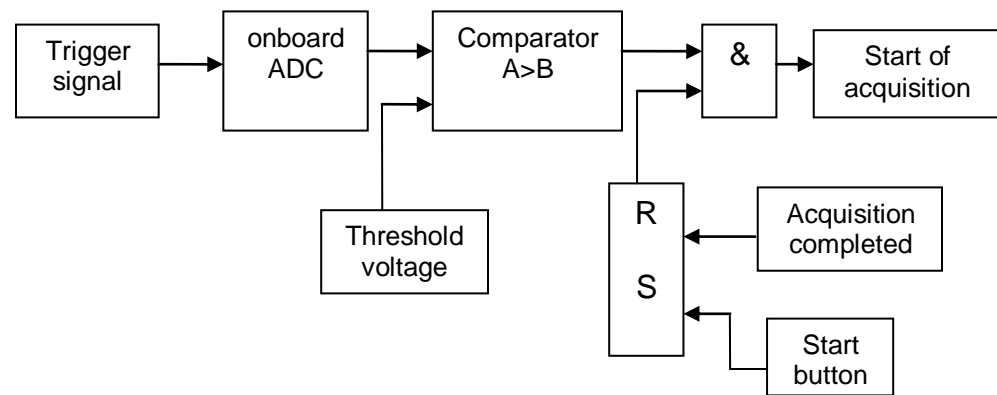


Figure 5.11: Block diagram of triggering that includes the procedure for the start button

As the trigger signal is activated from the ECG front end and is digitized using the ADC2, it will be compared with the threshold by the comparator. When the threshold is exceeded, the trigger will start the ultrasonic instrument. Whenever the start button is pressed from the acquisition window, it will set the RS trigger to the high level (1), which will allow triggering to occur. If the acquisition is completed, then the RS trigger will be reset to the low level (0), blocking triggering completely. The AND gate will trigger the ultrasound machine when the RS trigger is set (i.e., the start button was pressed in the GUI) and the trigger signal arrives. This block diagram was implemented in System Generator, as shown in fig 5.12.

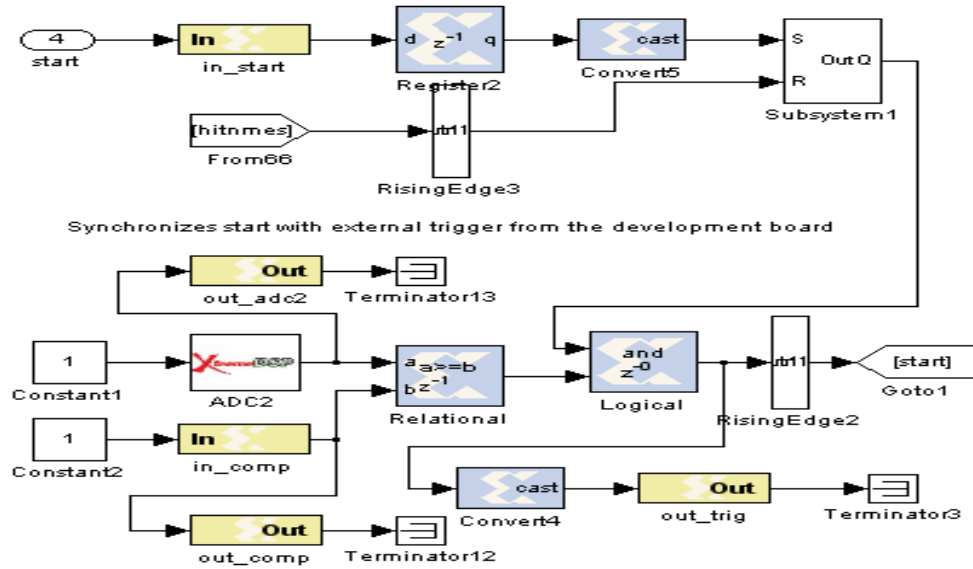


Figure 5.12: Final System generator diagram

This design was first simulated using the diagram in fig.5.13, and it worked as expected.

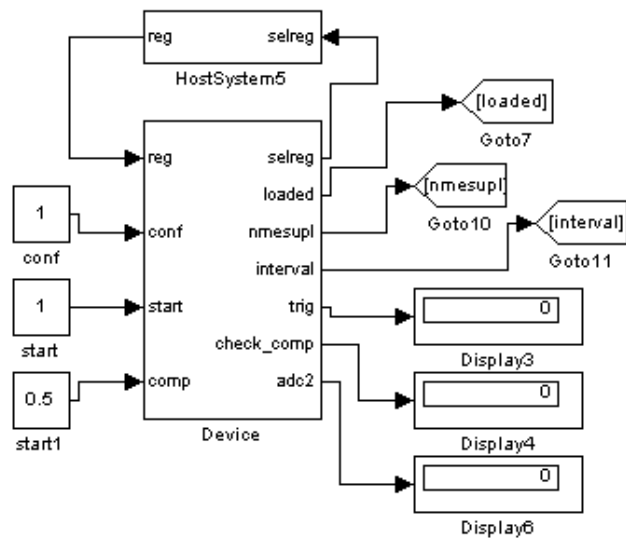


Figure 5.13: Design showing the required displays

5.3) Testing the ultrasonic instrument with the external trigger mode

A trigger source (fig 5.14) was built on a veroboard to test the design. It produced voltage, acceptable for the FPGA board (from -1V to +1V), and matched its 50 Ohm input impedance (fig.5.14-5.15).

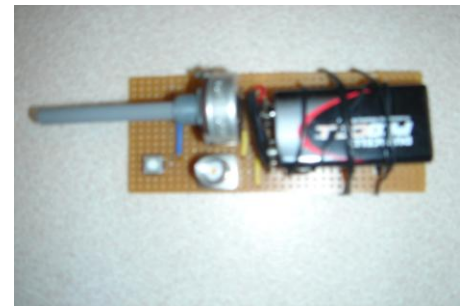
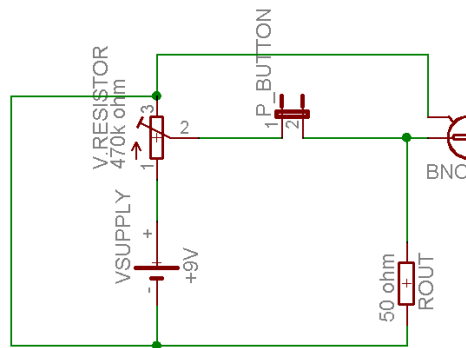


Figure 5.14: Schematic of the trigger source Figure 5.15: Prototyped trigger source

Various pulses can be generated by pressing the push button on the veroboard (fig 5.16), and their amplitude can be changed by adjusting the potentiometer.

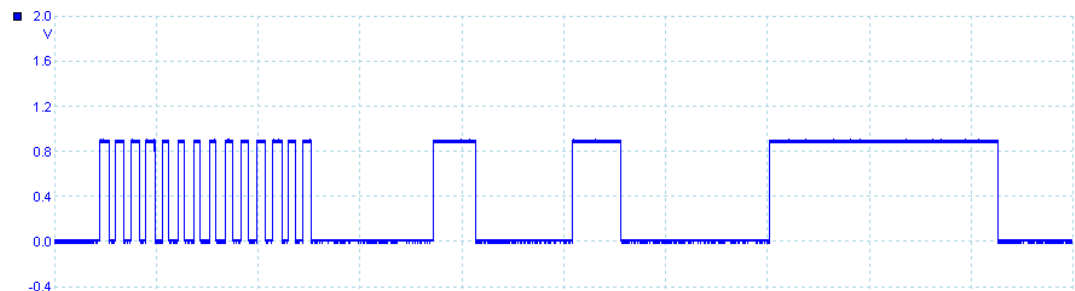


Figure 5.16: Example output waveform of the trigger source

The trigger source described above was sufficient for testing the design, because the RisingEdge component of System Generator reduces incoming

pulses of arbitrary duration to short pulses. (The ECG monitor itself outputs a short trigger pulse at the required part of the ECG signal.)

When the trigger source was connected to the FPGA board, the modified system was tested and showed that it operated as required. It waited until the “start” button was pressed by the user, and started the acquisition when the pulse arrived from the trigger source.

Finally, the trigger output of the ECG monitor was connected to the ADC2, and the operation of the ultrasonic instrument was tested with an ECG signal taken in vivo. After the “start” button was pressed by the user, the following trigger signal from the ECG monitor triggered the ultrasonic instrument. When the acquisition was finished, the user could produce more records at the same point of the cardiac cycle if necessary.

5.4) References:

[5.1] H63HDL lecture notes

[5.2]

http://www.xilinx.com/support/documentation/sw_manuals/sysgen_gs.pdf

[5.3]

http://www.xilinx.com/support/documentation/sw_manuals/sysgen_user.pdf

[5.4]

http://www.xilinx.com/support/documentation/sw_manuals/sysgen_ref.pdf

Chapter 6 – In vivo experiments

6.1) Locating the Common Carotid Artery (CCA)

Having read different articles and books on how to examine the CCA using ultrasonic transducers, the most appropriate way appeared to be to take longitudinal images from 3 imaging planes (fig 6.1). This helps in better analysis of the IMT, since it gives a rough 3D analysis. In addition, the left and the right CCA are measured to check for any inconsistencies between the left and right CCAs.

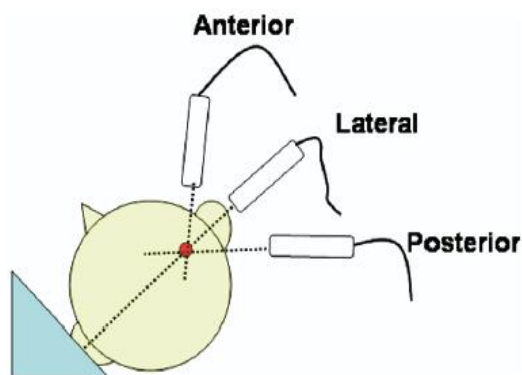


Figure 6.1: Planes of viewing the Common Carotid Artery (CCA) [6.1]

Additional aids, such as the Meijer arc (fig 6.2), can be used to help standardise transducer angles for different patients. All of the transducers referenced in the literature are B-mode transducers, which scan wide areas rather than the one point as the A-mode transducer does.



Figure 6.2: Using the Meijer arc to standardize the transducer angle [6.2]

This project intends to use a single A-mode transducer to prove that it is feasible to assess the IMT of the CCA at the same point in the cardiac cycle. Instead of using the Meijer arc, the CCA was located by going 1.5 inches above the joint between the breastbone and the collarbone [6.3].

6.2) Setting the analogue front end

As was discussed above, the GUI of the existing ultrasonic instrument was used. It is also necessary to control the analogue front end (ultrasonic pulser receiver – UPR- developed by NDT Solutions) to set the width of the excitation pulse and the gain for the received echo, using a separate application WinUPR (fig.6.3).

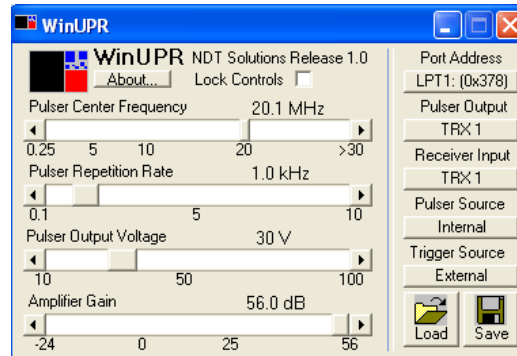


Figure 6.3: The GUI of WinUPR

The signal parameters are shown on the left of the GUI window (fig 6.3). These parameters depend on the transducers used as well as on the object under test. If a 20MHz transducer is used, then the pulser centre frequency would be set to $20\text{MHz} \pm 0.1 \text{ MHz}$.

The pulse repetition rate has the same meaning discussed above, if the internal trigger is used. However, in our experiments the UPR was triggered externally and this value can be set arbitrarily. The pulser output voltage can vary from 10V to 100V (lower voltage is used for lower noise environments).

The last parameter on the left side is the amplifier gain. This can be increased up to 56dB and is set to the value that does not saturate the ADC (-1...+1V input range).

On the right side of the GUI window are found buttons that define how the UPR operates and how it accepts the control parameters. The pulser-receiver system is connected to a computer via the parallel port and its port address is defined by the appropriate button.

As only one A-mode transducer will be used, the pulser input and output are connected to the same TRX1 socket. Finally, the trigger source will be external (produced by the ultrasonic instrument), whereas the pulser source will be internal (the pulse is generated by the UPR). The WinUPR GUI offers an option to save or load the settings from a previous scan, which was helpful when different transducers were used.

6.3) Taking ultrasonic scans

A 20 MHz transducer with a plastic buffer (or, informally, a ‘shoe’) was used for the scans. The buffer has two purposes in ultrasonic NDT. First, it provides a layer with an intermediate value of acoustic impedance between the high impedance of the transducer with the metal face and low impedance of the human tissue that is close to the acoustic impedance of water. Second, it eliminates the dead zone – the part of the object of interest closest to the transducer. This part cannot be seen without a buffer because, immediately after the excitation, the transducer discharges for some time and this process obscures the echo.

When the transducer with the buffer was operating in air, the delay and duration for the first acquisition window were determined from the received waveform. This was set to show the reflection from the buffer – air interface; that is, the moment when the ultrasonic wave enters the patient’s body. The expected delay for the second window (see chapter 5.1) was extended by this time.

Fig.6.4 presents a complete set of parameters set for the ultrasonic instrument used in experiments.

Sampling scheme	ADC sampling frequency (MHz)	Number of averages	First window delay (μs)	First window duration (μs)	Second window delay (μs)	Second window duration (μs)
4-5	100	128	5.88	2.24	10.92	14.4

Figure 6.4: Settings for the ultrasonic instrument using 20 MHz transducer

At first, the interleaving factor was kept low (value of 5), while the number of averages was set to 128 (fig.6.4). The total time taken for one measurement was 0.064 seconds. It was decided to take three records, with each subsequent record starting at the end of the previous one, per one trigger, to see changes among these records.

The settings for the UPR are shown in fig.6.5. The amplifier gain was set to the maximum value because the echo signal was very weak.

Pulser Centre Frequency (MHz)	Pulser Repetition Rate (kHz)	Pulser Output Voltage (V)	Output Gain (dB)
20.1	1.0	30	56

Figure 6.5: Settings for the UPR using 20 MHz transducer

The measurements were archived for detailed off line analysis, and were viewed on a computer using Matlab scripts (e.g., fig.6.6).

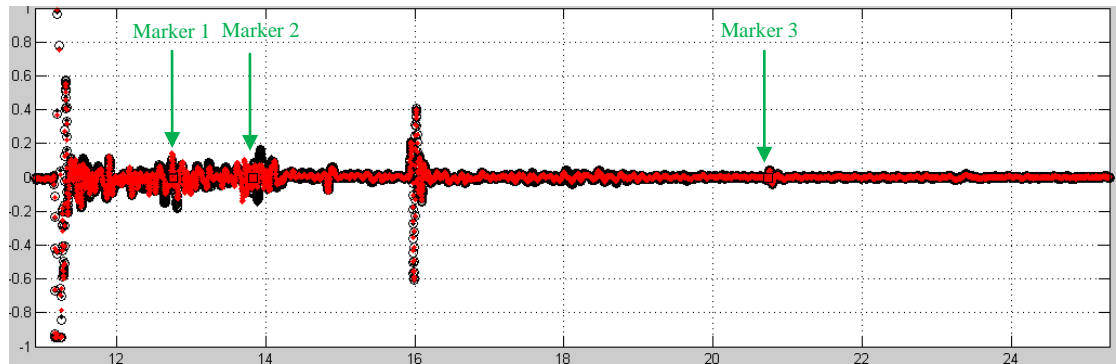


Figure 6.6: Three superimposed A-mode scans of the CCA with a 20MHz transducer with a buffer (horizontal axis – time in μs , vertical axis – recorded voltage in V)

Additional Matlab script was used to find the time when the waveform crossed the zero level, close to two points on the zoomed in graph specified by the user, and to calculate the time difference between the two. For example, for the markers shown in fig.6.6, the following delays were calculated:

- between marker 1 and 2 - $1.03\mu\text{s}$ (0.77mm);
- between markers 2 and 3 - $6.91\mu\text{s}$ (5.25mm).

These markers were put at the expected positions for the front wall intima-media (between markers 1 and 2) and the lumen (between markers 2 and 3). The distances in brackets were estimated assuming that the velocity in human tissues is close to that in water (1480 m/s), and accounting for the forward propagation of the excitation wave and back propagation of the echo:

$$\text{Distance} = \text{Delay} \times \frac{\text{Velocity}}{2}$$

The waveforms for three consecutive scans are presented in fig.6.7, 6.8 and 6.9.

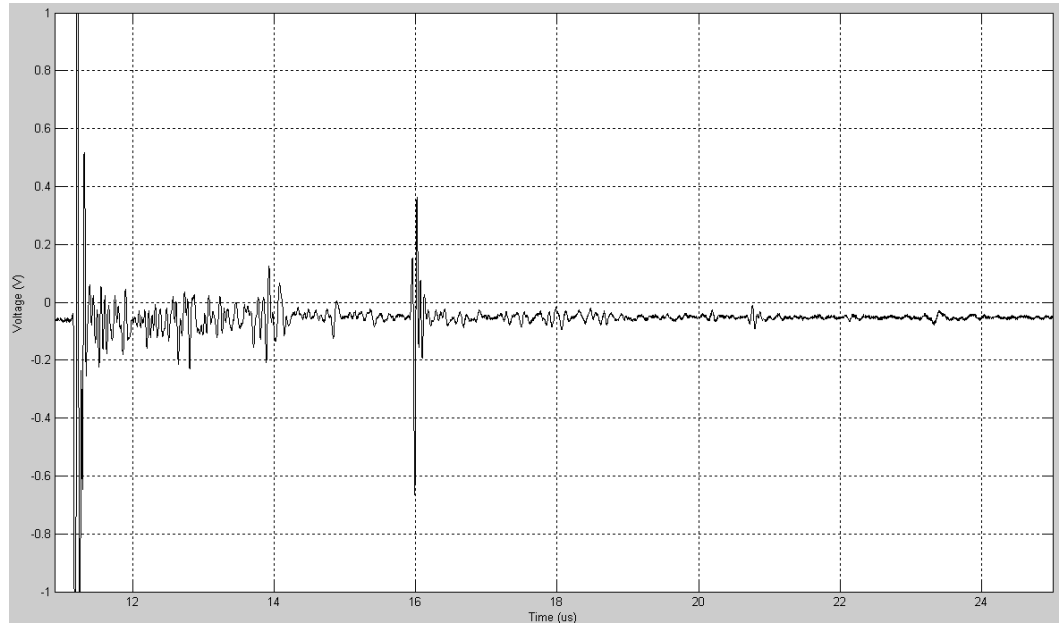


Fig 6.7: The first scan of the three measurements for fig 6.6 (horizontal axis – time in μs , vertical – recorded voltage in V)

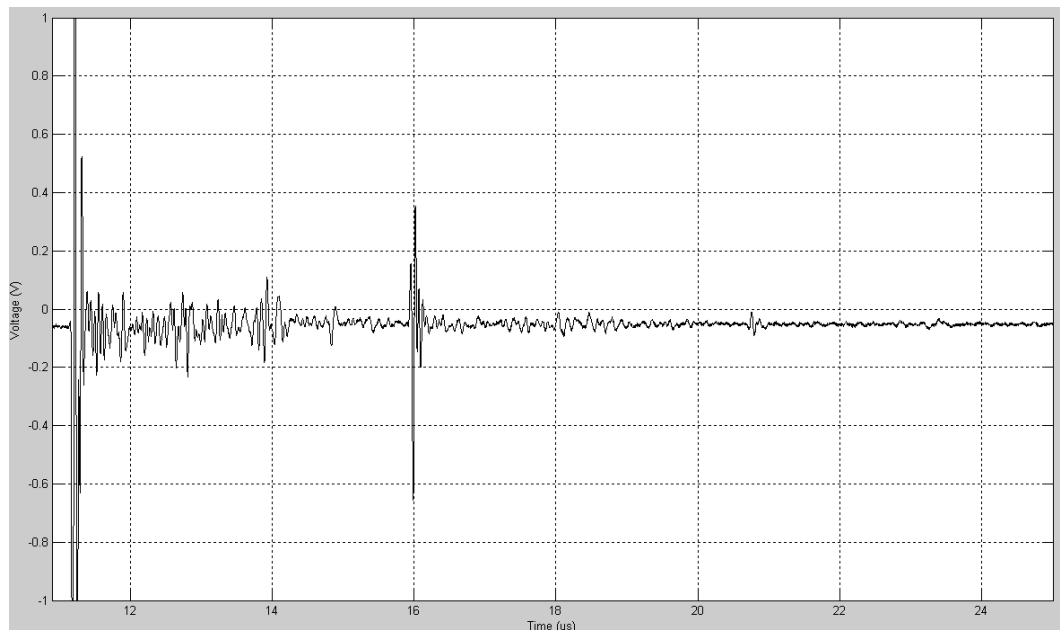


Fig 6.8: The second scan of the three measurements for fig 6.6 (horizontal axis – time in μs , vertical – recorded voltage in V)

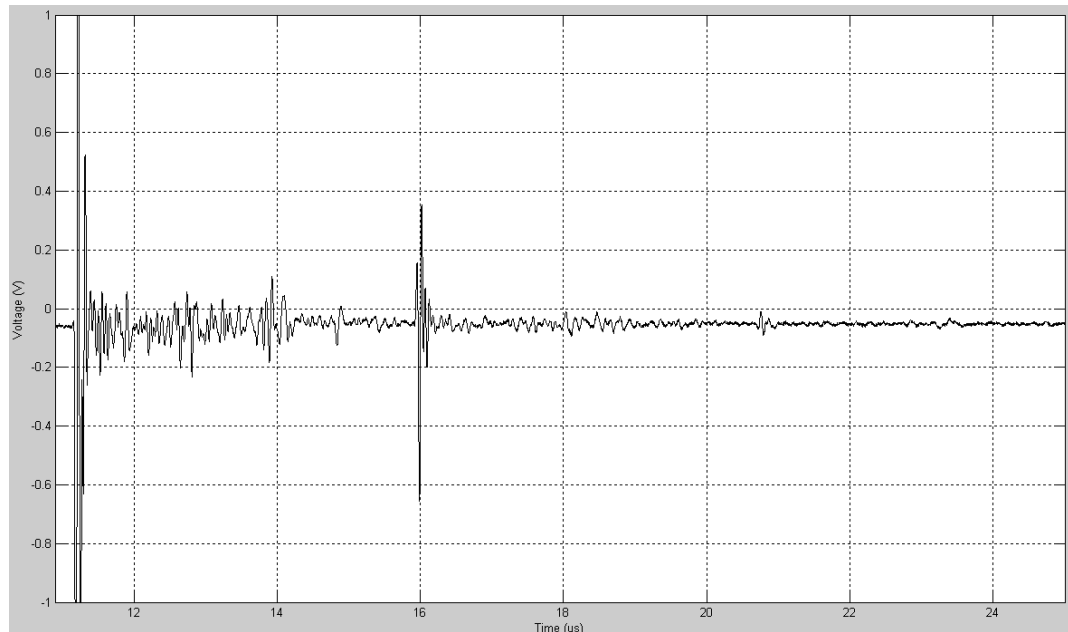


Fig 6.9: The third scan of the three measurements for fig 6.6 (horizontal axis – time in μs , vertical – recorded voltage in V)

These three waveforms were found compatible and consistent, although subtle differences were observed. The differences were attributed to noise influence and differences in blood flow at different times. Waveforms (fig 6.6 and fig.6.7-6.9) show that the echoes were weak and that the buffer returned a strong back echo at about $16\mu\text{s}$. This echo was related to reverberation of the ultrasonic wave inside the buffer, and it was not related to the echo coming from the patient. The presence of the strong echo from a buffer obscured echo returning from the patient at these time instants. However using the buffer was essential in order not to obscure the echo from the patient with the excitation pulse. Using a buffer for this purpose is a common practice for ultrasonic NDE measurements. According to fig.6.10 [6.4], taken in B-mode, the following layers should be identified from an A-mode scan: adventitia layer, the front wall, the lumen where the blood travels, the back wall and then the adventitia again.

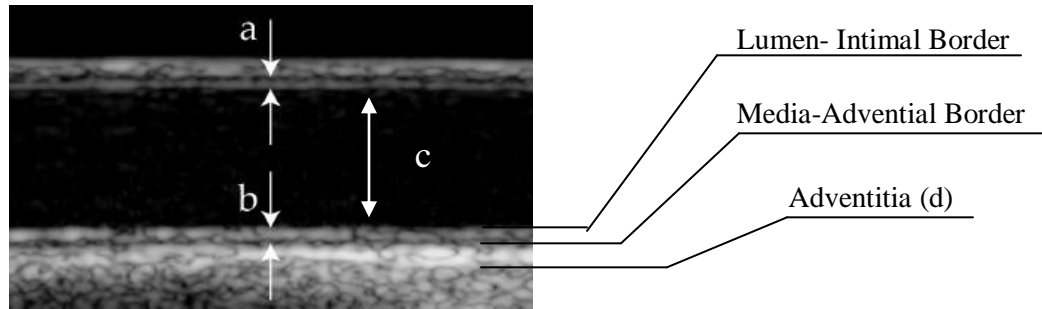


Figure 6.10: B-mode scan of the CCA [6.4]

The thicknesses for these layers, taken from different sources, are presented in fig.6.11. All were found compatible with the A-scan waveform given above, assuming the ultrasound velocity in human body to be roughly equal to the ultrasound velocity in water (around 1480 m/s).

Thickness (mm)	[6.5]	[6.6]	[6.4]
Adventitia (d)	1-3	1-4	1-5
Front wall IMT (a)	0.65	0.49-0.83	0.518-0.717
CCA Lumen (c)	7.72	6.82-8.7	5.310-7.460
Far wall IMT (b)	0.65	0.49-0.83	0.518-0.717

Figure 6.11: Different CCA-related thicknesses reported in literature

In addition to the 20MHz transducer, the 4.3MHz transducer was also employed to assess the advantages provided by using a higher frequency. The parameters for the GUI were amended, as shown in fig 6.12. The delay for the first acquisition window was derived from the received waveform, as was described above for the 20 MHz transducer.

Sampling scheme	ADC sampling frequency	Number of averages	First window delay(μ s)	First window duration(μ s)	Second window delay(μ s)	Second window duration(μ s)
4-5	100	128	5.88	2.24	10.92	14.4

Figure 6.12: Settings for the ultrasonic instrument using 4.3 MHz transducer

The required WinUPR are presented in fig 6.13.

Pulser Centre Frequency(MHz)	Pulser Repetition Rate (kHz)	Pulser Output Voltage (V)	Output Gain (dB)
4.3	1.0	30	56

Figure 6.13: Settings for the UPR using 4.3 MHz transducer

The waveform that was acquired with the 4.3MHz transducer is presented in fig.6.14.

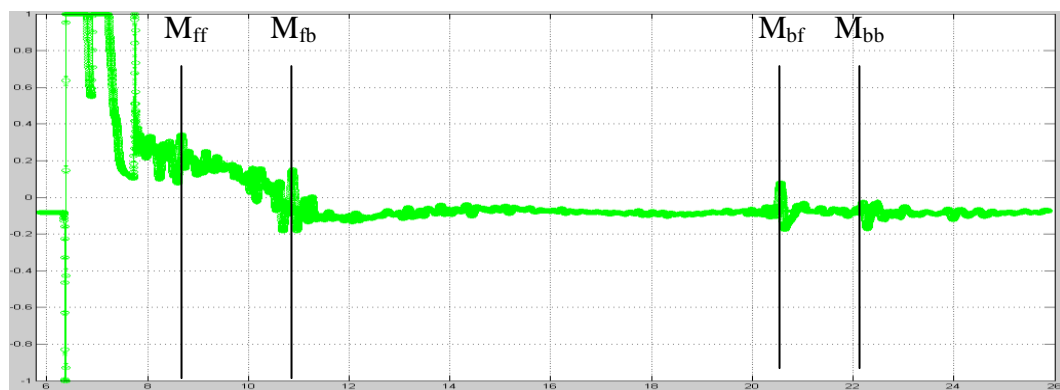


Figure 6.14. Three superimposed A-mode scans of the CCA with a 4.3MHz transducer with a buffer (horizontal axis – time in μ s, vertical – recorded voltage in V)

Markers were put at the expected positions for the intima media. The front wall thickness can be calculated from the delay between the M_{ff} and M_{fb} markers,

whereas the M_{bf} and M_{bb} markers determine thickness of the back wall. The delay between M_{bf} and M_{fb} determines the diameter of the lumen. The delays in the front wall, in the lumen and in the back wall were found to be 2.2 μ s, 9.68 μ s and 1.64 μ s, respectively. In the pulse-echo mode, the $\tau = \frac{l \times 2}{c}$ formula can be used to find the thicknesses of different layers. These thicknesses were estimated at 1.65mm, 7.26mm and 1.23mm for the front wall IMT, the lumen and the back wall IMT, respectively.

The waveforms for the 4.3MHz transducer were less clear compared to those obtained with the 20MHz transducer. The reason for this is the different duration of the excitation wave, which takes several cycles of the central frequency of the transducer. The number of these cycles increases with the decrease in the transducer bandwidth. For the same relative bandwidth, the 20 MHz transducer would produce about a 5 times (20/4.3) shorter pulse, and the reflections from close objects would be less likely to superimpose. The distance between two close objects that can be distinguished on an A-scan is referred to as axial resolution (e.g., [www.medcyclopaedia.com/library/topics/volume_i/a/axial_resolution.aspx])

Many reasons could exist for differences between the waveforms obtained using the above mentioned (4.3MHz and 20MHz) transducers, but one of the main sources for these differences was the diameter of the transducer. The diameter of the 20MHz transducer was 3mm, but was 5mm for the 4.3MHz transducer. The larger diameter of the transducer does not mean that it is better;

in fact, it is worse for the IMT measurements, as the transducer illuminates and received echoes from the tissues outside the region of interest (fig.6.15). A conventional B-mode ultrasonic transducer has 128 elements per 5cm. This means that the element size is around 0.4mm, or much smaller than the transducers used in this research. Because of this small element size, the B-scans can show better contrast between curved layers of different tissues, whereas larger transducers pick up backscatter signals and the curved interfaces reflect the excitation signal at different times (fig.6.15)

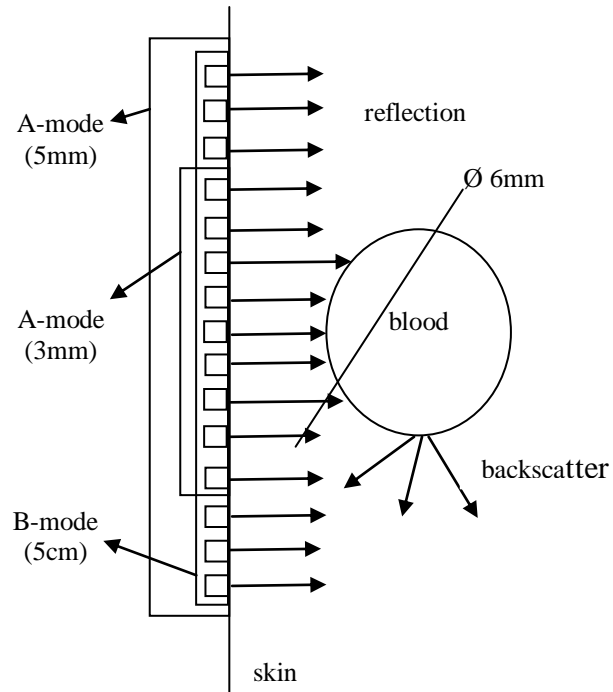


Figure 6.15: Operation of ultrasonic transducers with different sizes
(not to scale; small size transducer operates a single signal from a curved tissue interface, bigger size transducer picks up signals with different delays from the same interface, and backscatter signals)

Fig.6.16 shows what happens when a transducer is placed against lumens of different shapes. For a rectangular lumen, the transducer position is irrelevant, but this shape is not found in the human body. In addition, the ultrasonic scans will be different if the tissue layers surrounding the artery are not perfectly concentrated around the centre of the lumen (fig.6.16, bottom). This is another reason why a B-mode transducer could be preferable, since many differently angled transducers could sense curved and uneven surfaces better.

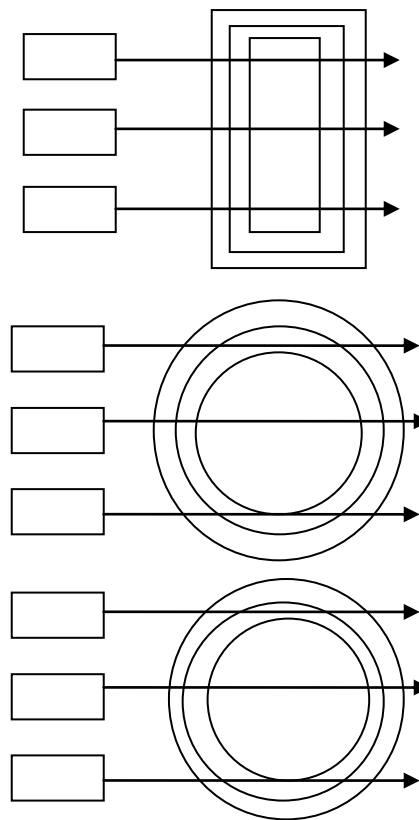


Figure 6.16: Ultrasound beam passing through flat (top), cylinder (middle) and uneven cylinder (bottom) surface

After analysing the first set of results obtained from the 4.3 and 20 MHz transducers, it was concluded that it was better to use the 20MHz transducer with

the buffer. The settings for the UPR were changed from Setting 1 to Setting 2, as shown in fig 6.17, to increase the signal-to-noise ratio, by employing the excitation pulse of higher voltage (excitation voltages of over 70 V were not used in vivo).

	Voltage (V)	Gain (dB)
Setting 1	30	56
Setting 2	70	48

Figure 6.17: Different settings for the UPR.

Setting 2 was used for the following experiments. The recorded waveform is shown in fig.6.18.

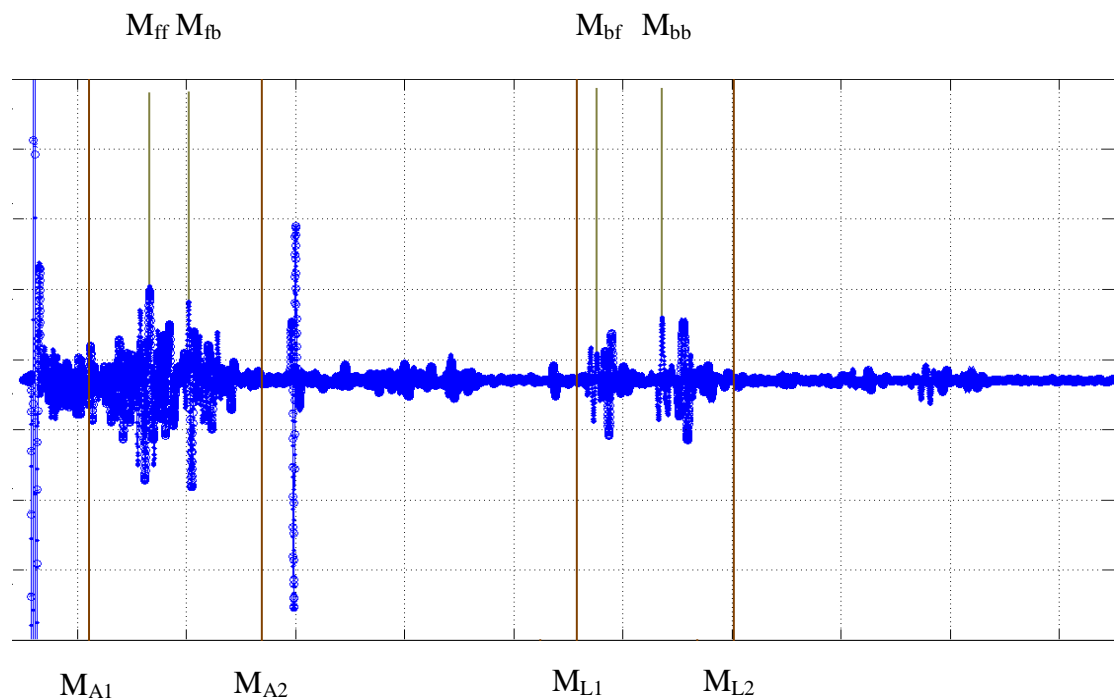


Figure 6.18: Three superimposed A-mode scans with the buffered 20MHz transducer, UPR Settings 2 (horizontal axis – time in μs , vertical – recorded voltage in V)

In fig 6.18, the first two markers (M_{A1} and M_{A2} below the graph) were used to locate the possible position of the front wall (M_{ff} and M_{fb} above the graph), taking it from the range presented in fig 6.11. Once the front wall was found, the position of the lumen (M_{L1} and M_{L2} below the graph) was assessed and marked from the range in fig.6.11. Finally, the back wall (M_{bf} and M_{bb} above the graph) was located. When the layers were isolated, their thicknesses were estimated at 0.54mm, 5.725mm and 0.7875mm for the front wall IMT, the lumen and back wall IMT, respectively. A single record from fig.6.18 is presented in fig.6.19.

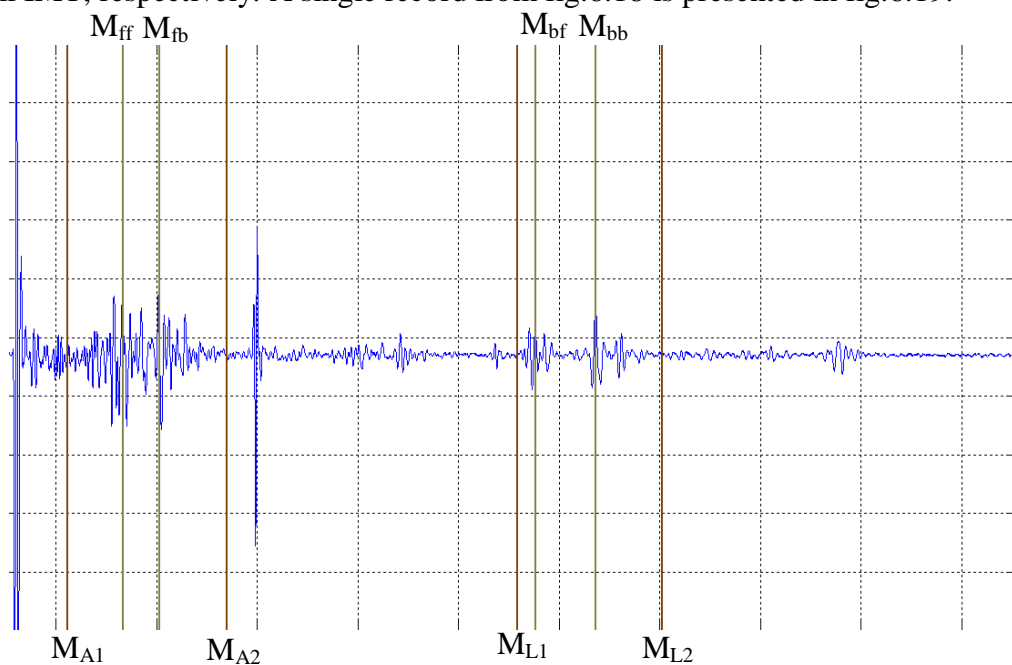


Figure 6.19: A single A-mode scan for the 20MHz transducer with buffer and the UPR Setting 2 (horizontal axis – time in μs , vertical – recorded voltage in V)

Another source of variability in recorded waveforms related to the pressure applied to the CCA during measurements. The diameter of a lumen decreases when the pressure applied to the CCA increases [6.7]. This will cause the lumen diameter to appear smaller than it really is. The first two markers (M_{A1} and M_{A2} ,

fig 6.19) were used to locate the possible position of the front wall (M_{ff} and M_{fb}) from the range presented in fig 6.11. Once the front wall was found by this procedure, the position of the lumen was assessed and marked (M_{L1} and M_{L2}) from the range presented in fig.6.11. Finally, the back wall (M_{bf} and M_{bb}) was marked. This change in the lumen diameter was observed experimentally when another A-scan was taken, with more pressure applied by hand through the transducer to the CCA (fig 6.20).

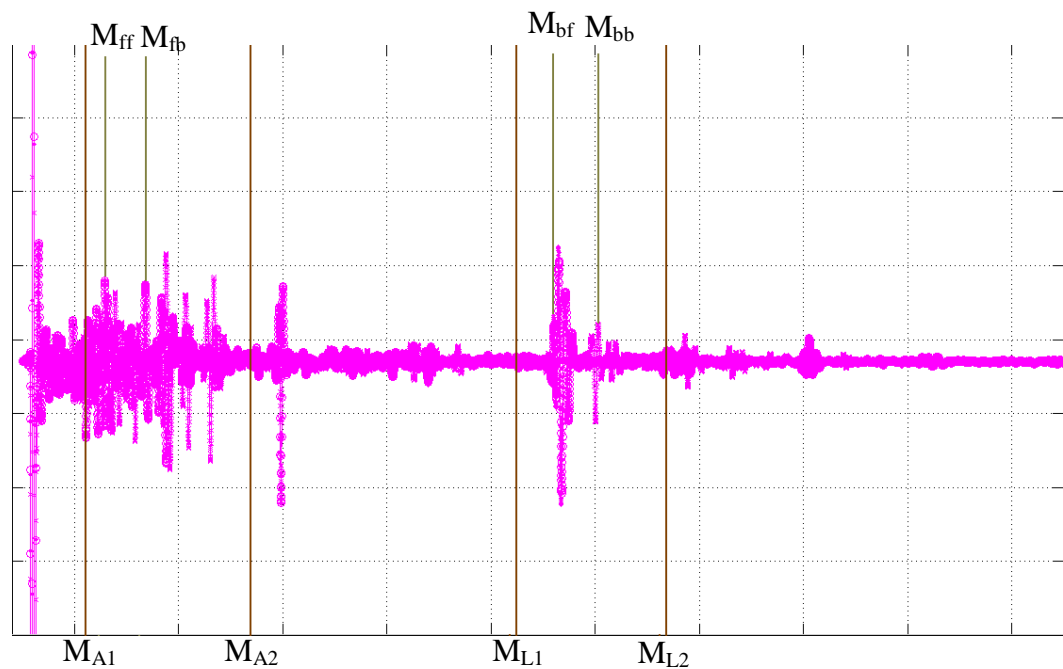


Figure 6.20: A-mode scan for the buffered 20MHz transducer, the UPR Setting 2

when a pressure was applied by hand to the CCA through the transducer

(horizontal axis – time in μs , vertical – recorded voltage in V)

Comparison of fig 6.20 with fig.6.19 shows the differences to the recorded A-scans caused by the extra hand pressure applied to the transducer.

6.4) Designing a new buffer for the 20 MHz transducer

The main reason for using a buffer with an ultrasonic transducer is to avoid the dead zone in pulse-echo mode. The dead zone is a part of the object close to the transducer whose echoes cannot be seen on the received waveform due to interference of any unfinished transitions caused by excitation. The buffer provides a delay that ensures that echoes from the close parts of the body arrive after the end of any excitation transitions, and these echoes become visible on the received waveform. The drawback is that the echoes from the buffer-object interface reverberate in the buffer, masking echoes from more distant parts of the object.

Fig.6.21 shows that these reverberating echoes masked the areas of interest on the waveform, and another buffer was designed to prevent this masking.

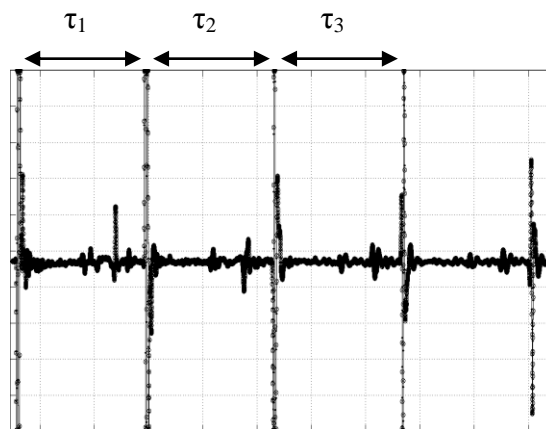


Figure 6.21: An A-mode scan with a 20MHz transducer and shoe

The new buffer was to provide a delay bigger than

$$\tau = \tau_1 + \tau_2 + \tau_3$$

$$\tau = (15.85-11.17) + (20.63-15.85) + (25.43-20.63)$$

$$\tau = 4.68 + 4.78 + 4.8$$

$$\tau = 14.26\mu\text{s}$$

The additional length for the new buffer can be calculated as :

$$\tau = \frac{l \times 2}{c} \Rightarrow l = \frac{\tau \times c}{2} \Rightarrow l = \frac{14.26 \times 1500}{2} \Rightarrow l = 10.7\text{mm}$$

The total length of the new buffer is:

$$L_t = L_o + L$$

(where L_t , L_o and L are the total length, original buffer length and additional buffer length respectively)

$$L_t = 5.5 + 10.7 = 16.2 \text{ mm}$$

In the formula $\tau = \frac{l \times 2}{c}$, the factor 2 refers to the pulse-echo mode as the wave travels in the shoe, forwards and backwards.

The dimensions for the new buffer are presented in the fig.6.22, and the drawings are shown in fig.6.23.

	L1 (mm)	L2 (mm)	LT (mm)	R1 (mm)	R2 (mm)
Present Buffer	1.3	4.2	5.5	4.7	6.3
New Buffer	1.3	15	16.3	4.7	6.3

Table 6.22: Table stating the specifications of the existing and new buffers

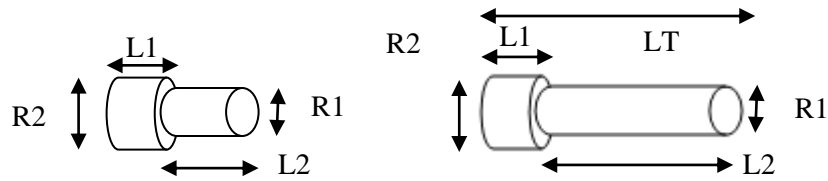


Figure 6.23: The existing and the new shoe

The buffer was manufactured from polycarbon, since rexalite or another suitable material [6.8] was not available from the school's workshop. The acoustic properties, such as attenuation and acoustic impedance of the polycarbon and rexalite, are compared in fig. 6.24.

	Acoustic Impedance, MRayl	Attenuation Coefficient (dB/cm) at 5MHz
Polycarbon	2.7	24.9
Rexalite	2.5	1.8

Figure 6.24: Table showing acoustic properties of two buffer materials

When ultrasound propagates through a boundary between two layers, the amount of ultrasound that can pass through and reflect from the boundary will depend on the acoustic impedances of both layers. The higher the mismatch between the acoustic impedances, the more energy is reflected back in the first layer and less energy propagates into the second layer. The recommended ratio of the acoustic impedances for the layers is below 5, but if the second layer is

liquid, then the ratio should be below 3 [6.9]. From this point of view, the lower impedance of polycarbonate (fig.6.24) is preferable for the buffer.

Attenuation describes the reduction of the amplitude of a wave while it travels through a medium. The attenuation coefficient takes the frequency of the wave and the distance travelled into account. Increases in any of these factors (frequency and distance) will lead to additional reduction in the wave amplitude. In this respect, polycarbonate is inferior to rexalite (fig.6.24).

6.5) Scanning the CCA with the new buffer

The parameters for the operation of the ultrasonic instrument with the new buffer were determined experimentally, as shown in fig 6.25. The parameters for WinUPR were set as presented in fig.6.17.

Sampling scheme	ADC sampling frequency	Number of averages	First window delay(μ s)	First window duration(μ s)	Second window delay(μ s)	Second window duration(μ s)
4-5	100	128	6.2	2	18	20

Figure 6.25: Parameters for 20MHz transducer and new buffer

The experimental waveform taken using the new buffer in vivo (fig 6.26) did not meet expectations, due to high losses in the buffer material. These losses masked reflections from distant tissues with noise. Therefore, the original buffer was used for subsequent scans.

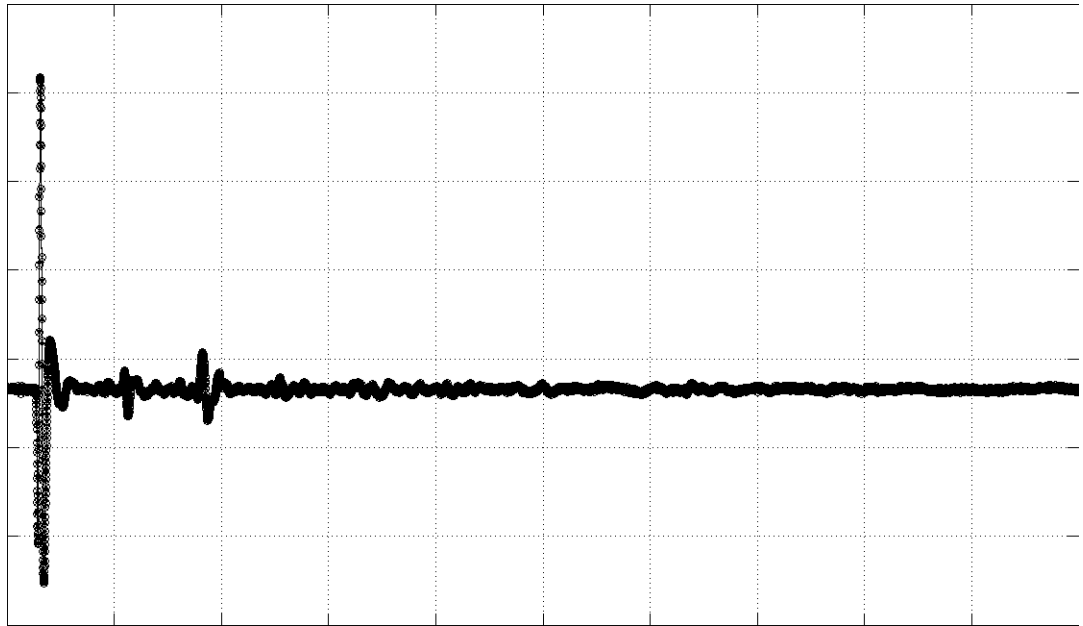


Figure 6.26: A-mode scans with a 20MHz transducer and
a new polycarbon shoe

6.6) Considerations on use of automated gain control (AGC) to improve clarity of ultrasonic scans

The analysis of ultrasonic scans is complicated because of a significant difference between amplitudes of echoes produced by close and distant objects. The amplitudes of echoes from distant objects could be several orders of magnitude lower and thus unrecognisable on the same waveform. The received signal can be attenuated by as much as 60dB compared to the ultrasonic signal being sent [6.10]. This can be addressed by using a method called AGC (Automated Gain Control) [6.11]. AGC usually increases the gain of the receiver amplifier with time (or, with distance travelled, which is the same) to compensate for extra attenuation experienced by ultrasonic waves to reach distant objects and

travel back. The gain is controlled by an automated system that sends different codes for different amplifications (fig 6.27). The amplifier provides non-linear increases in gain with time (fig 6.28). This results in an extra amplification for the signal from the back wall.

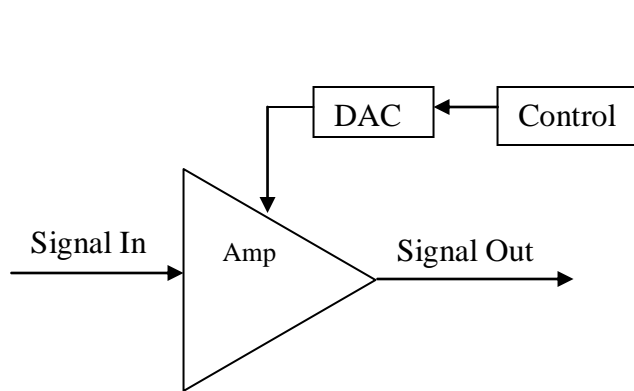


Figure 6.27: Hardware for AGC

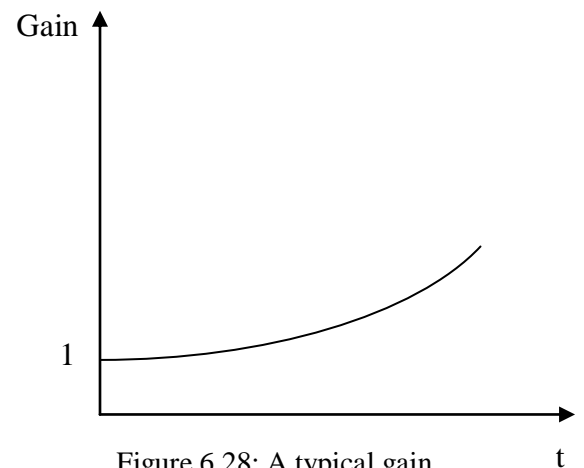


Figure 6.28: A typical gain

versus time AGC curve

For the AGC to be efficient and accurate, rather than just dependent on a quadratic function, a process called adaptive Time Gain Curves could be used [6.12]. The automatic gain control systems are usually implemented on the hardware side.

The drawbacks of AGC include the need for re-design of the receiver amplifier as it needs to be controllable. There is also a need for the echo signal to exceed the noise level, otherwise the distant echoes still will be invisible because of noise masking and there will be possible distortions to shapes of echo signals because of continuous gain changes. Because of these shortcomings, the AGC was not implemented in this project.

6.7) Taking ECG triggered ultrasonic scans in vivo

The complete setup is shown in fig.6.29 and included a personal computer with the Xtreme DSP FPGA board inside, the ECG monitor with a laptop to observe and record the ECG waveforms, and an oscilloscope to monitor the ultrasonic signals.

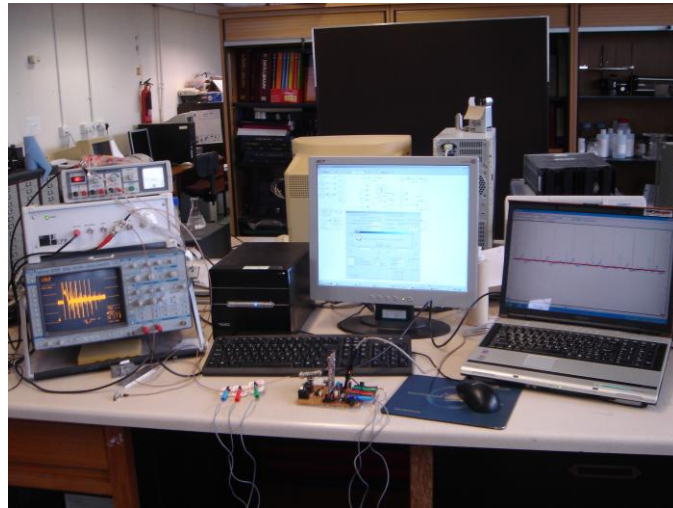


Figure 6.29: Laboratory setup for taking in vivo ultrasonic scans

The values of parameters of the ultrasonic instrument that were used for the experiments are presented in fig. 6.30.

Sampling scheme	ADC sampling frequency (MHz)	Number of averages	First window delay (μs)	First window duration (μs)	Second window delay (μs)	Second window duration (μs)
4-5	100	128	6.2	2	10	32

Figure 6.30: Parameters of the ultrasonic instruments used for in vivo scans

(20 MHz transducer with buffer)

The parameters set via WinUPR are presented in fig 6.31.

Pulser Centre Frequency(MHz)	Pulser Repetition Rate (kHz)	Pulser Output Voltage (V)	Output Gain (dB)
20.1	1.0	100	49.5

Figure 6.31: Parameters set for the UPR (20MHz transducer with buffer)

The whole system was connected and tested, using the same subject as before. Six scans were taken; the first three scans triggered at one specific instant in the ECG, whereas the next three scans were triggered at another instant in the ECG signal.

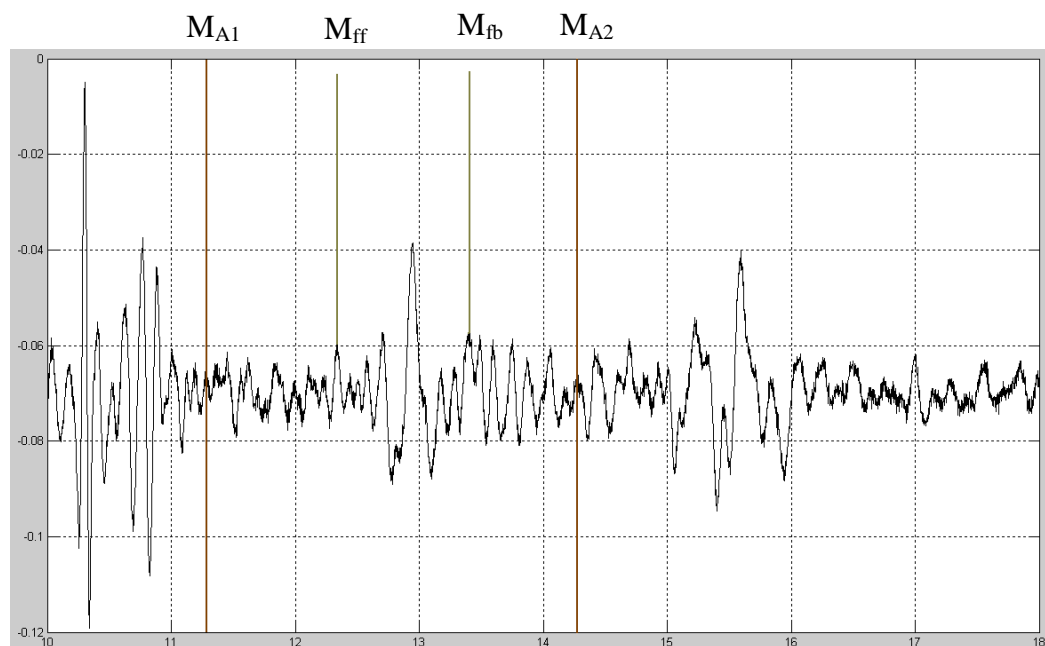


Figure 6.32: A-mode scan triggered at the S wave (20MHz transducer with

The first two markers are used to locate the possible position of the front wall, taking it from the range presented in fig 6.11 (fig 6.32). Once the front wall was found, the next step was to calculate the front wall IMT. For the first scan, the ECG was conditioned to trigger the ultrasonic scan at the S wave (fig 6.33).

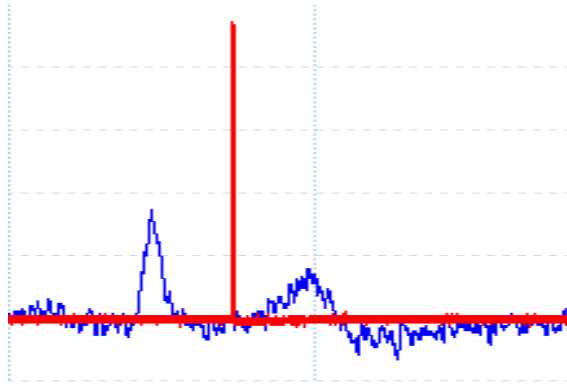


Figure 6.33: ECG waveform showing the trigger at the S-wave

The distance between the two markers, M_{ff} and M_{fb} , was estimated at about $1.0 \mu s$. As the ultrasonic instrument operated in the pulse echo mode, the ultrasonic wave first travelled to the reflector and then returned, covering the same distance. Therefore, the distance between the transducer and the reflector L is calculated using the following formula:

$$\begin{aligned} L &= (\text{wave velocity}) * (\text{time delay}) / 2 \\ &= (1500\text{m/s} * 1.0 \mu\text{s}) / 2 = 0.75 \text{ mm} \end{aligned}$$

This value belongs to the range of the expected IMT values.

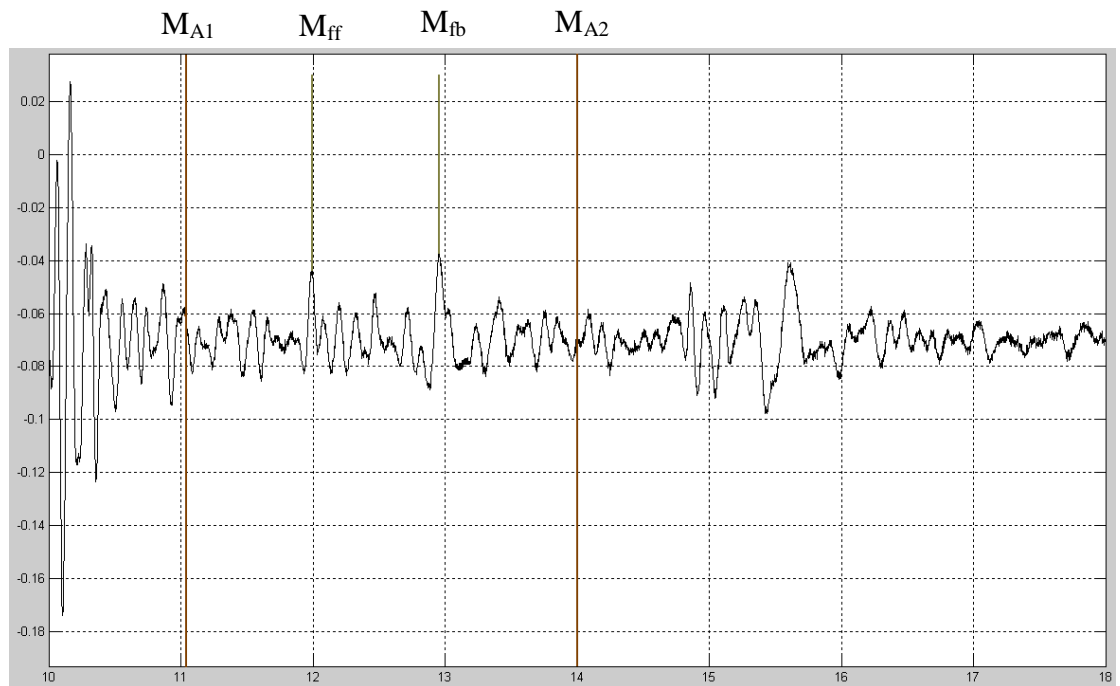


Figure 6.34: A-mode scan triggered at the U-wave (20MHz transducer with buffer) (horizontal axis – time in μs , vertical – recorded voltage in V)

The other scan (fig.6.34) was taken at a different point of the cardiac cycle; namely, at the U wave (fig.6.35).

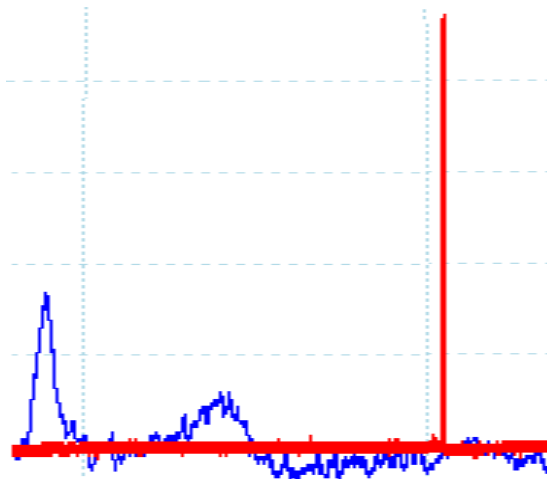


Figure 6.35: Ultrasonic scan triggered at U-wave

The delay value between first two markers was estimated at 0.97 μ s. Consequently the calculated IMT value in this case was different from the previous scan:

$$x = (1500\text{m/s} * 0.97 \mu\text{s}) / 2 = 0.73 \text{ mm.}$$

Therefore, the IMT estimates obtained for two ultrasonic scans triggered at different points of the cardiac cycle showed a difference of about 20 μ m. The front wall IMT is known to vary up to 80 μ m within a single cardiac cycle, depending on the patient [6.13]. Therefore, the obtained difference agrees with the published data; the designed instrument did not produce evidently erroneous experimental results.

6.8) Cardiovascular Disease Risk Assessment Protocol

By looking at the results that are presented in this chapter, the conclusion can be drawn that the hardware worked and it could accurately record the ultrasonic scans triggered in vivo by the ECG monitor in the subject.

A further study was required to comply with medical standards that would involve many patients. The results obtained with the developed instruments were to be checked against the results obtained with conventional instrumentation.

As discussed in chapter 1, while guidelines for detection of silent myocardial and lower limb ischemia are established, data on screening asymptomatic carotid lesions in diabetic patients remain scarce. In diabetic patients, Carotid IMT was recognized as a reliable prognostic indicator of heart attack and stroke. It worsens

with duration of diabetes and association with other risks. Diabetic patients carry an increased risk of ischemic cerebral attack and this risk is two to five times higher than that for the general population.

There are many ways to evaluate cardiovascular disease risk to the patient. Before doing an ultrasound scan to measure the IMT, it is always useful to do a cardiovascular disease risk assessment report, since there are many factors that affect the progression of the disease. This report can be used as a reference, together with the scan, to diagnose correct symptoms. The protocol (fig 6.36) should be efficient in identifying CVDs and not overly time consuming.

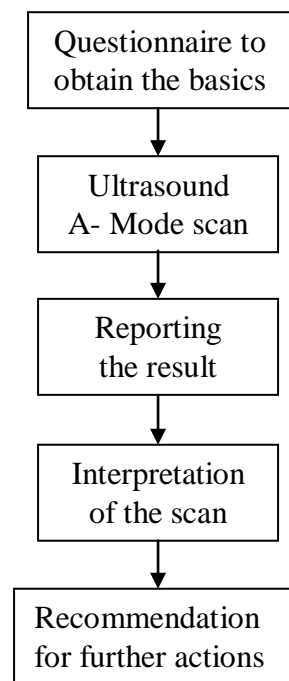


Figure 6.36: Diagram showing the steps that would be taken for the CVD protocol

6.8.1) Questionnaire

A questionnaire form will be given to the patients if it is their first time to have an ultrasonic scan for evaluation of the CVD risk. The questionnaire form will include hospital details of the patient and some personal information affecting the IMT such as age, sex, ethnicity and some others factors too. The final section of the questionnaire will include an agreement that the medical data are to be used for analysis only. It is important that the patient answers the questions accurately, since the data will be used in reporting and interpretation.

6.8.2) Ultrasonic scan

After filling in the questionnaire form, the patient will be sent to have an ultrasound scan. In order to perform the scans, the proposed machine will be used to measure the IMT of the CCA. This differs from conventional B-scans in that a single element transducer will be used rather than a linear array transducer. The developed instrument will use a single element transducer with a higher frequency and a removable buffer (commonly called a “shoe” in the field of ultrasonic NDE) to produce at least the same or even better images compared to those acquired using the linear array transducers.

The sonographer performing the scan will give the patient some information on what will be done. The patient has to be in the supine position with the neck rotated away from the probe so that longitudinal images of the three different positions (anterior, lateral and posterior) can be taken for the IMT measurement. These three positions are angled at around 45 degrees to each other, and can be

determined by using a Meijer arc. It is first necessary to find the point where the CCA splits into the internal and external carotid arteries. Scanning is preferable of the right CCA (RCCA) but it is better to take scans of both the RCCA and the LCCA (left CCA) in order to have extra data. The point of taking the ultrasonic scan related to the patient's cardiac cycle can be modified by the sonographer by changing the delay after the R wave, if necessary.

6.8.3) Data reporting

Once the ultrasonic instrument is triggered to take the scan, it will save these scans into the computer, where the scans will be analysed. To assure that the measurement is obtained accurately, both the near and the far wall will be considered using computer assisted tracing if applicable.

When the boundaries of the blood-intima and the media-adventitia are not very clear, a less accurate value of the IMT is measured. Allowing the user to change the boundaries detected by the computer-assisted tracing will be useful in areas where it is not possible to find the correct boundary exactly. The results of each view should be reported, taking into account that they should be within 0.05 mm of each other. Additionally, the mean value should be reported. The maximum value of each side will be useful for identifying the CVD risk at that point. Once all of the necessary measurements have been taken, they will be forwarded to a doctor for further analysis and recommendation.

6.8.4) Interpretation

After the IMT scan, the patient will have another appointment with the specialist doctor to interpret the results. The questionnaire form that was filled in before doing the scan is vital at this point, since it will be used to relate any past patient or family history to the values obtained. The results can be compared with the results obtained in the conventional way, but it is more accurate to state the IMT results in percentiles rather than just numerical values. This will make assessment of the progression of the artery easier.

The principal percentiles will be 25th and 75th percentiles and the percentiles in between. The reason for using two percentiles and values between them is that any value below 25th percentile would show that there is some increase, but this increase is not of a high risk. The values between the 25th and 75th percentiles will show that there is not much CVD risk. However, actions could be taken to prevent further increase if necessary. Finally, the IMT values above 75th percentile would be taken as a very high risk of CVD, since it has increased to a level where the CCA is nearly completely blocked out.

6.8.5) Recommendations

Depending on the results obtained from the ultrasound scan, recommendation for further actions will be given based on the values mentioned above. At the same time, further actions can be recommended, such as diet changes and exercising, and the patient could be introduced to some therapeutic and chemical treatments, such as prescribing aspirin or vitamin E tablets, if necessary. All of

the patients that have an IMT value greater than 75th percentile will be at high risk and should be treated urgently to reduce this value as much as possible, in order to prevent surgery and intense treatment required otherwise. At this stage, stenting and chemical treatment are usually preferred. A later ultrasonic scan, as a check-up to observe further IMT changes, may be recommended for all of the screened patients.

6.9) References:

- [6.1] Stein JH, Korcarz CE, Hurst RT, Lonn E, Kendall CB, Mohler ER, Najjar SS, Rembold CM, Post WS. Use of Carotid Ultrasound to Identify Subclinical Vascular Disease and Evaluate Cardiovascular Disease Risk: A Consensus Statement from the American Society of Echocardiography Carotid Intima-Media Thickness Task Force *Endorsed by the Society for Vascular Medicine*. *J Am Soc Echocardiogr* 2008; 21(2): 93-111.
- [6.2] Vos LE, Oren A, Uiterwaal C, Gorissen WHM, Grobbee DE, Bots ML. Adolescent blood pressure and blood pressure tracking into young adulthood are related to subclinical atherosclerosis: the Atherosclerosis Risk in Young Adults (ARYA) study. *Am J Hypertens* 2006; 16: 549-555; doi:10.1016/S0895-7061(03)00857-4
- [6.3] <http://www.soilandhealth.org/02/0201hyglibcat/020146.lindlahr.nat.thera.p/Nat.Thera.Pt5.htm> Accessed 2/9/2008

- [6.4] Cinthio, M.; Jansson, T.; Persson, H.W.; Lindstrom, K.; Ahlgren, A.R.,
"New non-invasive method for intima-media thickness and intima-media
compression measurements," *Ultrasonics Symposium, 2005 IEEE* , vol.1,
no., pp. 385-388, 18-21 Sept. 2005
- [6.5] Eigenbrodt ML, Bursac Z, Tracy RE, Mehta JL, Rose KM, Couper DJ. B-
mode ultrasound common carotid artery intima-media thickness and
external diameter: cross-sectional and longitudinal associations with
carotid atherosclerosis in a large population sample. *Cardiovasc
Ultrasound* 2008; 6:10doi:10.1186/1476-7120-6-10
- [6.6] Eigenbrodt ML, Sukhija R, Rose KM, Tracy RE, Couper DJ, Evans GW,
Bursac Z, Mehta JL. Common carotid artery wall thickness and external
diameter as predictors of prevalent and incident cardiac events in a large
population study. *Cardiovasc Ultrasound* 2007; 5:11doi:10.1186/1476-
7120-5-11
- [6.7] Miele FR., Mucci R, Gallant SL. Method and apparatus for assessing
hemodynamic parameters within the circulatory system of a living
subject, United States Tensys Medical, Inc. (San Diego, CA, US), 2006;
7048691, <http://www.freepatentsonline.com/7048691.html>
- [6.8] Eichert ES, Storey WT 1971 Delay line having non planar ground plane,
each loop bracketing two runs of meandering signal line, United States
Technitrol, Inc. (Philadelphia, PA) 3581250
<http://www.freepatentsonline.com/3581250.html>

- [6.9] Greenwood MS, Lail JC - Ultrasonic fluid densitometry and densitometer, US Patent 5708191, PatentStorm, 13 Jan 1998
- [6.10] Bryant AW, Herrick TJ. Adaptive gain control and contrast improvement for medical diagnostic ultrasound B-mode imaging system using charge-coupled devices. Circuits and Systems, 1991, Proceedings of the 34th Midwest Symposium on, Volume , Issue , 14-17 May 1991 Page(s):685 - 687 vol.2
- [6.11] Bryant AW, Herrick TJ. Automated gain control for medical diagnostic ultrasound imaging. Circuits and Systems, 1990, Proceedings of the 33rd Midwest Symposium on, Volume , Issue , 12-14 Aug 1990 Page(s):208 - 210 vol.1
- [6.12] Richard B, Charliac O. A New Digital Adaptive Time Gain Correction For B-mode Ultrasonic Imaging. Engineering in Medicine and Biology Society, 1992. Vol.14. Conf Proc IEEE Eng Med Biol Soc 1992; 5(29):2131 - 2132
- [6.13] Realtime velocimetry for evaluation of change in thickness of myocardium and arterial wall, Kanai, H.Chubachi, N., Koiwa, Y., Tanaka, M., Dept. of Electr. Eng., Tohoku Univ., Sendai; Ultrasonics Symposium, 1998. Proceedings 1998; 2:1365-1368

http://www.sciencedirect.com/science?_ob=MImg&_imagekey=B6TW2-3YWX3V2-2N-1&_cdi=5550&_user=5939061&_orig=search&_coverDate=03%2F31%2F

[2F2000&_sk=999619998&view=c&wchp=dGLzVzz-](#)

[zSkWb&md5=f12b1481b3682c74dab181e7da8db625&ie=/sdarticle.pdf](#)

Chapter 7 - Discussion and Conclusions

The main aim of the project was to build a system where the vascular ultrasonic scans are synchronised with the heart activity using the ECG signal. The project involved diverse areas of medicine and engineering. The medicine side included cardiovascular, cardiology and radiology, whereas the engineering side was more related to hardware and software developments. The following activities were undertaken:

- researching and visiting a hospital to get more knowledge about the medical side, to aid the decision making throughout the project;
- simulating circuits with LTSpice and comparing the results to real measurements;
- designing PCBs and circuit components using EAGLE;
- designing support hardware and firmware for PIC microcontrollers;
- understanding how the existing FPGA design worked and designing a modified version that could be triggered from the ECG monitor;
- using Matlab in many areas of the project either to capture or analyse the data ;
- prototyping electronic circuits using various means;
- understanding operation, control and use of ultrasonic instruments and transducers.

The above list shows the key points of the whole project. The findings that were discovered throughout the project are summarized and brief conclusions on each are given in this chapter.

First of all, the different topologies of ECG circuits were reviewed at the beginning of the second chapter. Each topology had some advantages and disadvantages in terms of circuitry, safety, filtering and amplification. The simulation program, LTSpice, was used for each of the candidate amplifiers, but the simulated noise level, gain and ac analysis were not found with the desired precision. Therefore, the circuits in question were prototyped. The instrumental amplifier from Texas Instrument (INA326) performed much better over the other candidate amplifiers, and its single voltage power supply gave additional advantages. It was therefore selected for the ECG monitor.

Detailed design of the ECG monitor was described in chapter 3. Significant work went into the design of the PCB. The required components, which did not exist in the software library, were created. The error rule checks were done on the whole device to verify that the design was compatible with the manufacturing house technology. The change of the degree program, due to personal circumstances, forced the necessity of a design of a different front end. The proposed front end consisted of an instrumental amplifier, an active low pass filter, and regulators. It included various connections for programming or detecting or triggering such as RS-232, BNC and ICD, and microcontroller sockets. A +5V transceiver was used between the front end and the RS-232

socket to provide the required communication voltages. The completed front end was tested and performed as expected.

Wireless ECG signal transmission was the preferred choice in this project, due to safety considerations and because the mobility of the patient would not be restricted. After the occurrence of personal problems, another possibility was considered. However, the microcontroller program for the wireless transfer was written and discussed in chapter 4. Its testing showed that the rfPIC microcontroller had its debug limitations and an additional module was developed to ease debugging. The experimental results of both microcontrollers were compared. This completed the design of the front end of the system.

The next task was to understand the operation of the existing ultrasonic system and to modify it to suit the developed application. The existing system is described in chapter 5, and the design that was initially considered was applied, but was not successful. Once the problem was identified, an alternative design was applied to the existing system. The validity of the change in the GUI for the front end to start the triggering was verified with an additional trigger veroboard, which sent out triggering signals to the ADC on the FPGA board.

The different ways of locating the CCA were reviewed at the beginning of chapter 6. The simplest way of finding it was chosen, out of several options available. For the ultrasound scans, the main challenge comes from the optimization and tradeoffs between noise, gain and visibility. For example, the pulser output voltage and the amplifier gain have different effects on these factors. The number of averages, the sampling scheme and the pulse repetition

rate affected the noise level and signal visibility level. A significant number of ultrasonic scans taken using various parameters was analysed to aid in understanding and processing. Use of a buffer with the ultrasonic transducer resulted in much more consistent echoes from the CCA. In order to aid further signal enhancement, a new buffer for the existing 20 MHz transducer was created. This buffer was found unsatisfactory though because of high signal losses.

From all of the ultrasonic scans examined, the back wall of the artery was not easy to distinguish because of the small amplitude of its echo signal. Regardless of the presence or absence of a transducer buffer, the visibility of the back wall was not sufficient in any of the cases. Therefore, the old buffer with the transducer was used to look for the front wall of the CCA. The ultrasonic scans were triggered at different phases of the cardiac cycle by setting different delays to the trigger after the R wave peak. The estimated IMT values were found to be different, and the difference was within the range expected from the literature. Therefore, in vivo experiments did not give evidently erroneous results.

Chapter 8 - Future work

Although the required operation of the instrument was achieved, there are possibilities for its further development. First, the electronics developed could be assembled using a dedicated PCB, and the size of the whole board would decrease by more than 50%. At present, the signal to trigger the ultrasound instrument is supplied via a coaxial cable. If a wireless system were employed to send these data wirelessly, this would increase mobility and safety of the patient. Possible RF interference can be overcome by careful design and by using wireless communications other than RF, e.g., infrared.

As discussed in the previous chapter, the back wall of the CCA could not be identified as easily as the front wall, due to the ultrasound attenuation. By applying the AGC (Automated Gain Control) to the received signal, it is possible to compensate for this extra attenuation and to enhance the back echo. This will improve the presentation of the echo, but will not improve its SNR.

Another improvement could be extension of ECG triggering to ultrasonic B-scans. In this case, a transducer array will be required and collection of many echoes requires many excitations. On the positive side, B-scan images allow for easier detection of front and back walls compared to A-scans. Finally, when the above refinements are completed, the instrument can be tested in a hospital, using the CVD protocol described in the last part of chapter 6.

Chapter 9 - Appendix

Appendix A: Questionnaire form being sent to the specialist in cardiology department to get more information about ECG



Omer Faruk Bener
School of Electrical and Electronic Engineering,
University of Nottingham,
University Park,
Nottingham,
NG7 2RD
UK

Email: eexofb@nottingham.ac.uk

Mob: +447818241464

Tel: +441158451146

11 October 2007

Dr. Wafer Dabdoub
Department of Cardiology
Hamad Medical Corporation,
P.O. Box 3050,
Doha, Qatar
Email: wdabdoob@yahoo.com
Mob: +974 536 9902
Fax: +974 439 2454

Subject: Questionnaire Form – Information about ECG related to IMT

Dear Dr. Wafer Dabdoub,

With reference to above subject, this letter is to learn more about the ECG. There are a few questions that was come across while designing the new ECG machine that will be used inter linked with the ultrasound machine to take IMT scans. If you could kindly fill out the questions below and return it to me. This will be really helpful in evaluating the right solution for the ECG machine.

- Do you know the manufacturer and model of the electrode pads and machine being used when taking the ECG of the patient?

- How many electrode pads are used when taking an ECG and what is each one used for? Would it make accurate if more are added?

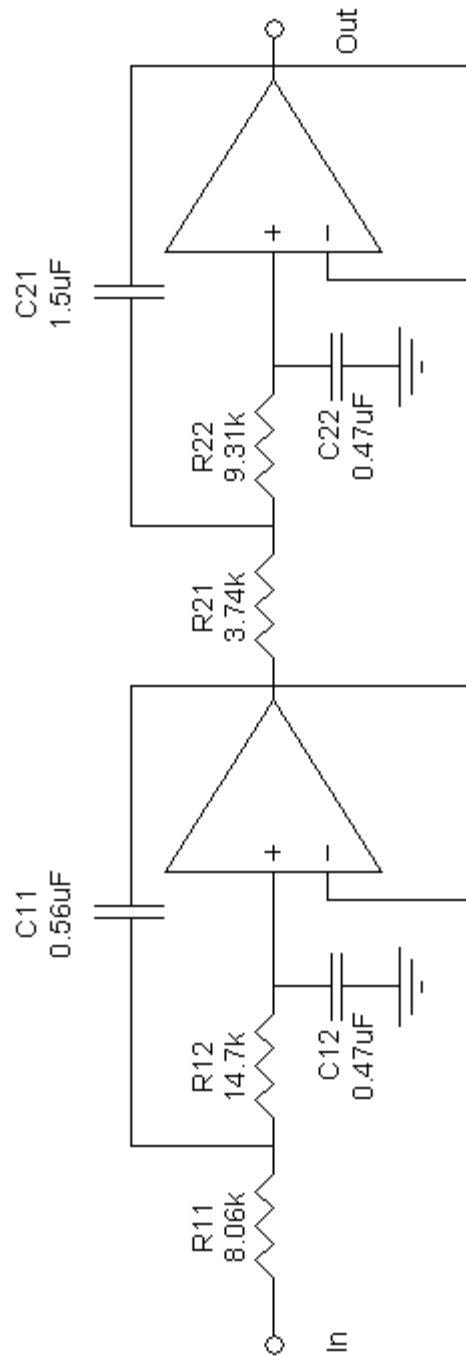
- Are the pads being used for taking the ECG of the patient disposable or reusable pads? If it is reusable then what are the procedures to apply to the pads before use for another patient? Also how many ECG tests can be read with a single ECG pad set?

- There are different waves P, Q, R, S, T, which wave would be the best when looking at the ECG when wanting to obtain the best result for IMT? If so why this choice? Could you specify any particular part of this wave? Does the device on the age/sex etc?

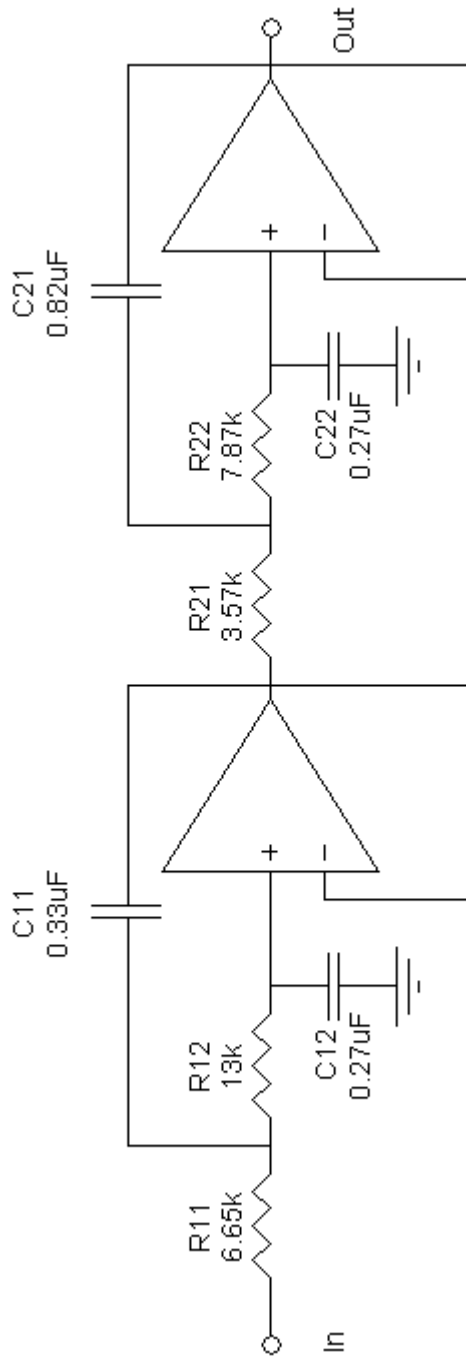
Should you have any queries and questions, which I failed to address, please do not hesitate to contact me at any time. Looking forward to hearing from you. Thanking you in anticipation. Kindest Regards.

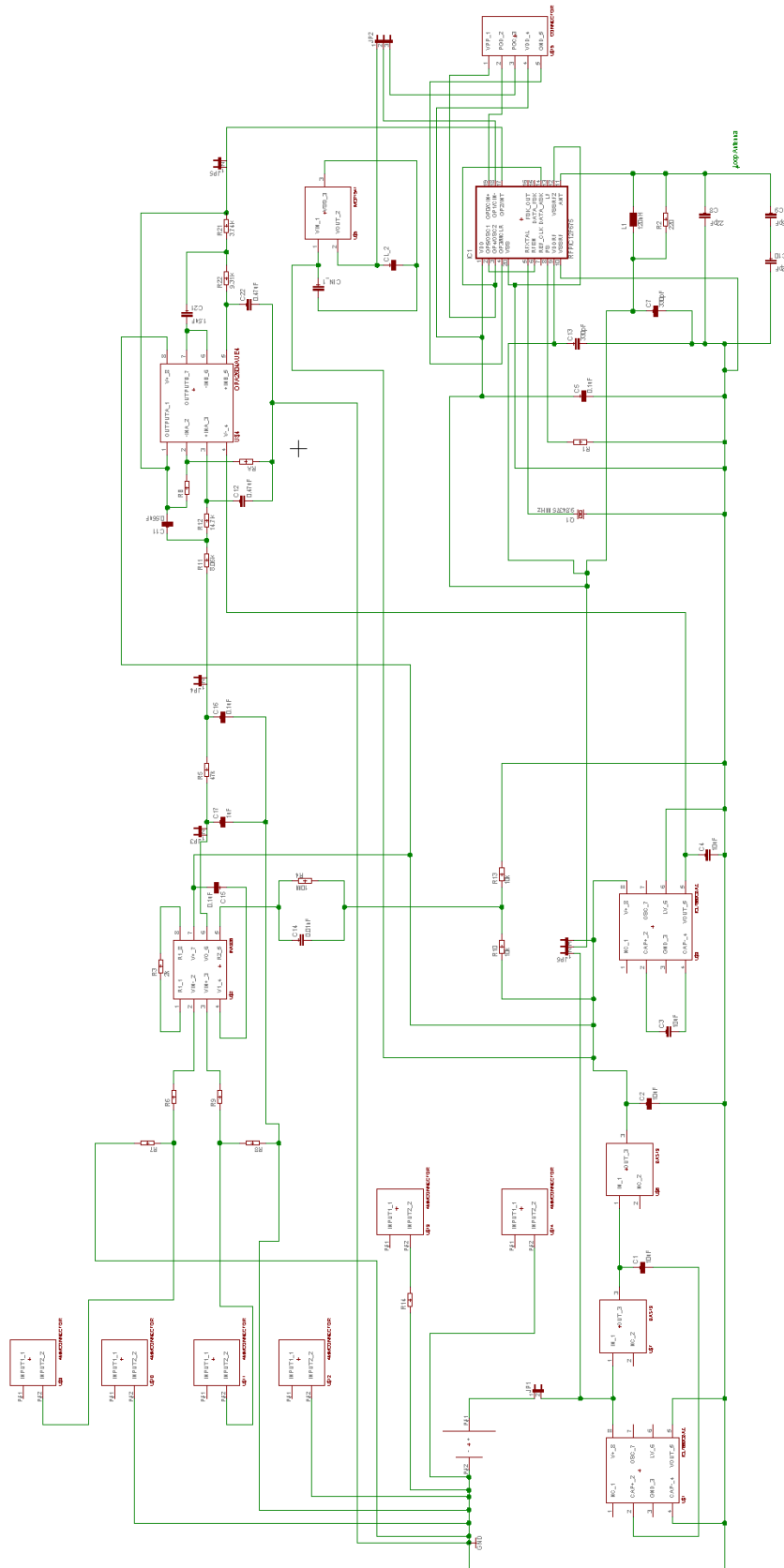
Yours Sincerely

Omer Faruk Bener



Appendix B: Schematic of the 4th order Bessel 20Hz Low Pass Filter created using FilterLab

Appendix C: Schematic of the 4TH order Bessel 40Hz Low Pass Filter created using FilterLab



Appendix D: Schematic of the front end which will be used to design the PCB

Appendix E: Error Rule Check Report for the schematic design for the front end

EAGLE Version 4.16r2 Copyright (c) 1988-2006 CadSoft

Electrical Rule Check for C:/vero/ecg4.sch at 01/10/2008 21:20:36

WARNING: Sheet 1/1: unconnected Pin: U\$9 INPUT1_1

WARNING: Sheet 1/1: unconnected Pin: U\$10 INPUT1_1

WARNING: Sheet 1/1: unconnected Pin: U\$11 INPUT1_1

WARNING: Sheet 1/1: unconnected Pin: U\$12 INPUT1_1

WARNING: Sheet 1/1: unconnected Pin: U\$13 INPUT1_1

WARNING: Sheet 1/1: unconnected Pin: U\$14 INPUT1_1

WARNING: Sheet 1/1: POWER Pin IC1 VDDRF connected to N\$33

WARNING: Sheet 1/1: POWER Pin IC1 VSS connected to GND

ERROR: Sheet 1/1: unconnected INPUT Pin: IC1 DATA_FSK

WARNING: Sheet 1/1: POWER Pin IC1 VSSRF connected to GND

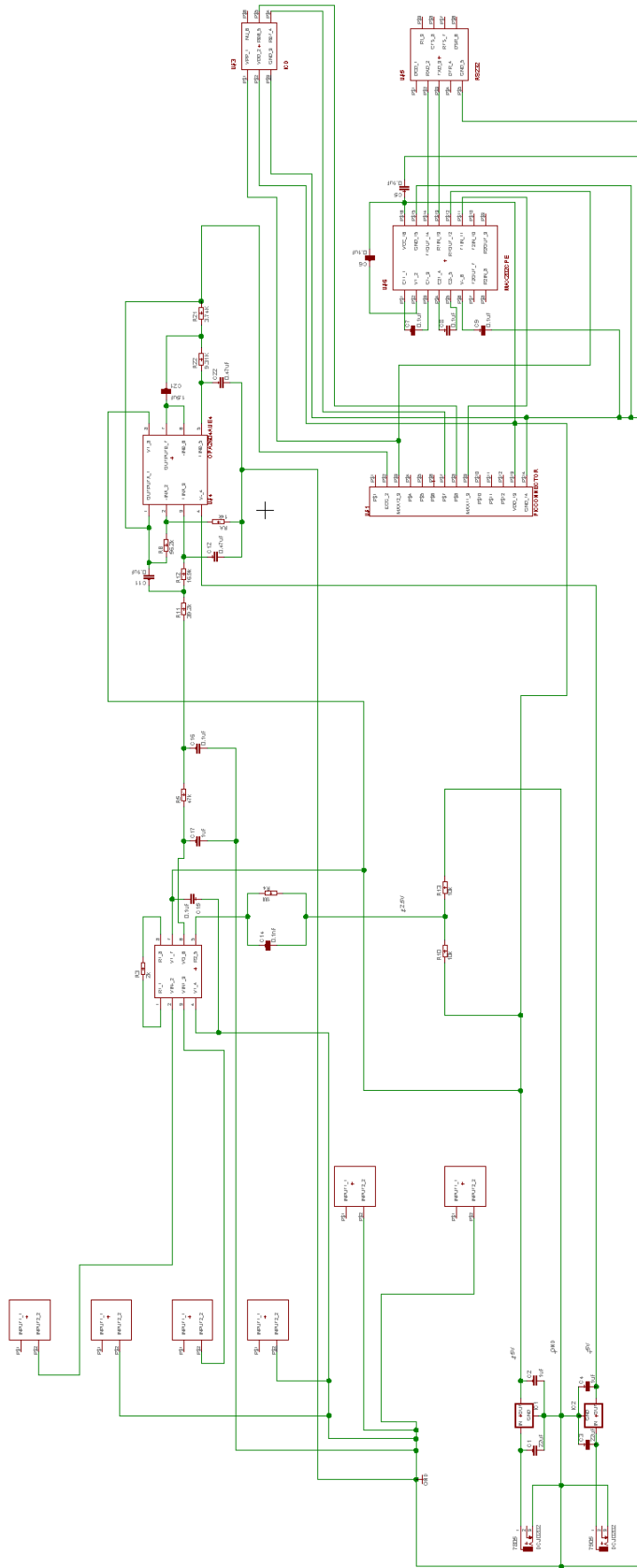
WARNING: Sheet 1/1: POWER Pin IC1 VDD connected to N\$33

WARNING: Sheet 1/1: POWER Pin IC1 VSSRF2 connected to GND

Board and schematic are consistent

1 errors

11 warnings



Appendix F: Schematic of the front end which will be used to design the veroboard

Appendix G: Glossary

(taken from <http://medical-dictionary.thefreedictionary.com>)

Attenuation is the reduction in amplitude and intensity of a signal. Signals may attenuate exponentially by transmission through a medium, in which case attenuation is usually reported in dB with respect to distance travelled through the medium. Attenuation can also be understood to be the opposite of amplification. Attenuation is an important property in telecommunications and ultrasound applications because of its importance in determining signal strength as a function of distance. Attenuation is usually measured in units of decibels per unit length of medium (dB/cm, dB/km, etc) and is represented by the attenuation coefficient of the medium in question.

Attenuation coefficients are used to quantify different media according to how strongly the transmitted ultrasound amplitude decreases as a function of frequency. The attenuation coefficient (α) can be used to determine total attenuation in dB/cm in the medium using the following formula:

$$\text{Attenuation[dB]} = \alpha[\text{dB}/(\text{MHz} * \text{cm})] \cdot l[\text{cm}] \cdot f[\text{MHz}]$$

As this equation shows, in addition to the medium length and attenuation coefficient, *attenuation is also linearly dependent on the frequency of the incident ultrasound beam.* Attenuation coefficients vary widely for different media. In biomedical ultrasound imaging however, biological materials and water are the most commonly used media. The attenuation coefficients of common biological materials at a frequency of 1 MHz are listed below:

Material	α (dB / MHz * cm)
Lung	41
Bone	20
Kidney	1.0
Liver	0.94
Fat	0.63
Blood	0.18
Brain	0.85
Water	0.0022

Acoustic energy losses occur in two general ways: absorption and scattering. Ultrasound propagation through homogeneous media is associated only with

absorption and can be characterised with absorption coefficient only. Propagation through heterogeneous media requires taking into account scattering.

Acoustic impedance,

Interference with the passage of sound waves by objects in the path of those waves. It equals the velocity of sound in a medium multiplied by the density of the medium. The acoustic impedance of bone may be nearly five times as great as that of blood.

Axial resolution,

The ability of an ultrasound system to separate two objects lying along the axis of an ultrasound beam.

Beam diameter (beam width)

(although the article uses electromagnetic waves for discussion, the same statements apply to ultrasound waves)

The diameter along any specified line perpendicular to an electromagnetic beam axis and intersects it. Since beams typically do not have sharp edges, the diameter can be obtained in many different ways. Five definitions of the beam width are in common use: $D4\sigma$, 10/90 or 20/80 knife-edge, $1/e^2$, FWHM, and D86.

Beam diameter usually refers to a beam of circular cross section, but not necessarily so. A beam may, for example, have an elliptical cross section, in which case the orientation of the beam diameter must be specified, for example with respect to the major or minor axis of the elliptical cross section. The term "beam width" may be preferred in applications where the beam does not have circular symmetry.

Beam divergence

(although the article uses electromagnetic waves for discussion, the same statements apply to ultrasound waves)

An angular measure of the increase in beam diameter, with distance from the optical aperture or antenna aperture, from which the electromagnetic beam emerges. The term is relevant only in the "far field", away from any focus of the beam. Practically speaking, however, the far field can commence physically close to the radiating aperture, depending on aperture diameter and the operating wavelength.

Beam divergence is often used to characterize electromagnetic beams in the optical regime, for cases in which the aperture from which the beam emerges is very large with respect to the wavelength. That said, it is also used in the Radio Frequency (RF) regime for cases in which the antenna is operating in the so-called optical region and is likewise very large relative to a wavelength.

Lateral resolution

The resolution of objects in a plane perpendicular to the axis of an ultrasound beam. It is a measure of the ability of the system to detect closely separated objects, such as adjacent blood vessels.

Penetration depth

(although the article uses electromagnetic waves for discussion, the same statements apply to ultrasound waves)

A measure of how deep light or any electromagnetic radiation can penetrate into a material. It is defined as the depth at which the intensity of the radiation inside the material falls to $1/e$ (about 37%) of the original value at the surface. When electromagnetic radiation is incident on the surface of a material, part of it is reflected and part transmitted into the material. This EM Wave interacts with the atoms and electrons inside the material. Depending on the nature of the material, the EM Wave might travel very far into the material, or on the other hand die out very quickly. For a given material, penetration depth can vary for different wavelength of EM Wave, and usually, is not a fixed constant.

Reflection and transmission coefficients

Coefficients used in physics and electrical engineering when wave propagation in a medium containing discontinuities is considered. A reflection coefficient describes either the amplitude or the intensity of a reflected wave relative to an incident wave. A transmission coefficient describes either the amplitude or the intensity of a transmitted wave relative to an incident wave. Different specialties have different applications for the term. (quantitative formulae and demos are available from

<http://paws.kettering.edu/~drussell/Demos/reflect/reflect.html>)

Tables of ultrasonic data:

Ultrasound physics <http://www.drgdiaz.com/tables.shtml>

Acoustic properties of common materials http://www.advanced-ndt.co.uk/Velocity_Chart.html